

STUDIES OF RADIO WAVE PROPAGATION  
IN THE LOWER IONOSPHERE

Presented

by

SUBHAS CHANDRA CHAKRAVARTY

for

the degree of

DOCTOR OF PHILOSOPHY

of

THE GUJARAT UNIVERSITY

043



B4915

NOVEMBER 1972

PHYSICAL RESEARCH LABORATORY

AHMEDABAD

: i :

to all those

who have

inspired me

with or without their

consciousness

## P R E F A C E

The thesis contains six chapters and consists of two parts. Part I - Chapters I to V deal with the propagation of low frequency radio waves ( 30 - 300 kHz ) by reflection from the D-region of the ionosphere ( 60 - 95 km ) at low latitudes. The study of the intensities of these radio waves reflected at oblique incidence provide an efficient method for exploring the D-region of the upper atmosphere.

The amplitudes of 164 kHz radio waves transmitted from Tashkent have been recorded at Ahmedabad since 1960. Similar receiving equipments were set up at Poona ( period 1963 - 1964 ) and at Gulmarg ( for a short period in 1971 ) in order to study the effect of changing the distance between the transmitter and receiver. The author modified the receiving equipment at Ahmedabad in 1969 by using a loop antenna and set up an identical unit at Gulmarg in 1971.


The thesis contains the results of a study of the above observations. (1) The radio data have first been analysed to obtain the variations during quiet day conditions. (2) The effect of solar X-ray flux enhancements during solar flares on the propagation of these radio waves has then been studied. (3) Night-time radio signal attenuations have been found to be

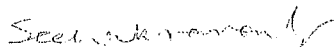
related to X-ray emissions from galactic X-ray sources. Theoretical estimates of this effect have been made and compared with the observations.

II. An associated D-region study has been made by the analysis of the lunar tidal variations of D-region absorption of medium frequency radio waves ( 1 - 3 MHz ) at the equatorial and the mid-latitude stations.

The author expresses with deep gratitude his indebtedness to Professor K.R.Ramanathan for introducing him the subject and guiding him during the entire period of investigation.

The author with great pleasure wishes to express his heartiest gratitude to Professor R.G.Rastogi for his guidance and supervision throughout the course of work.

  
R.G.RASTOGI  
PROFESSOR-IN-CHARGE

  
S.C.CHAKRAVARTY  
AUTHOR



## SCOPE OF THE THESIS

Brief descriptions of the present study contained in the six chapters of the thesis are given below:

### CHAPTER I - Formation of the low-latitude D-region ionosphere and propagation of low frequency radio waves

(a) Formation of daytime D-region during quiet solar conditions has been assessed by considering the production and loss processes using the most recent information about the ionising sources and atmospheric constituents.

(b) The experimental set-up at Ahmedabad for receiving the 164 kHz signal intensities transmitted from Tashkent is described. Theoretical calculations of the reflection coefficients of these radio waves have been made by using a method given by Sheddy (1968). The estimated reflection heights during different seasons from these computations have been used as providing guidelines for the propagation characteristics of these radio waves.

### CHAPTER II - General behaviour of 164 kHz radio signal strengths during quiet day conditions

(a) The diurnal and seasonal variations of the signal intensities of 164 kHz radio waves at Ahmedabad, Poona and

Gulmarg are compared. The general pattern of the radio signal variations at Ahmedabad during years of different solar activity are presented with their possible interpretation in the light of the heights of reflection and the variation of solar X-ray background flux.

(b) The possible candidates for the negative ions in the D-region arising from photo-dissociation and photo-ionization of molecules at sunrise and their effect in the radio signals observed at Ahmedabad are discussed.

(c) Some cases of abnormally large signal intensities during winter have been studied in relation to the possible role played by stratospheric temperatures.

### CHAPTER III - Effect of solar flares on 164 kHz radio propagation

(a) A statistical study of the solar flare effects observed at Ahmedabad in the 164 kHz signal intensities is presented with respect to the X-ray flares observed in satellites Explorer 35 and Explorer 37. A few flare effects during October - November, 1968 have been studied with the detailed X-ray flux data published by Kreplin (1970). The three types of effects produced in the radio field strength have been explained in terms of the total intensity of X-ray flux in the wavelength band  $1 - 8 \text{ \AA}$  during the flare.

(b) Electron density variations in the D-region have been computed during different stages of a moderately strong flare by solving the continuity equation. The continuation of the effect at 164 kHz radio intensity after the end of the X-ray flare is supported by these calculations.

#### CHAPTER IV - Nighttime variations of 164 kHz radio signal intensities

(a) The nighttime electron density profiles in the D-region are summarised and it is found that the possibility of the existence of free electrons below about 80 km is almost nil. The usefulness of the observations on LF radio waves in studying the nighttime D-region is considered. The seasonal variation of the nighttime field strength of 164 kHz field strength at Ahmedabad has been explained in terms of a simple electron density model after sunset and the ionization caused by scattered Lyman $\alpha$  radiation.

(b) Pronounced depressions in the nighttime radio waves amplitudes have been observed. These are related to the sidereal times of the transit of X-ray source Sco X-1. The possible effects of other X-ray sources, Tau X-1, Cyg X-1 and Cyg X-2 have been explored.

#### CHAPTER V - Theoretical estimates of the radio attenuation produced by the non-solar X-ray sources

The electron production rates in the D-region due to

Sco X-1 and Tau X-1 are theoretically estimated by using the available X-ray spectra of these sources. The possible enhancement over the nighttime ambient electron densities have been computed by using the maximum and minimum probable values of the loss coefficients. The attenuation of 164 kHz radio waves for the Tashkent-Ahmedabad path is estimated using the full wave technique of Barron and Budden (1959). The calculated values are compared with the observed ones. The calculated electron density profiles due to Sco X-1 are adjusted so that the theoretical and experimental results match. The values of nighttime effective loss rates in the D-region are then estimated.

## CHAPTER VI - Lunar tides in the D-region ionosphere

Lunar tidal oscillations in the ionospheric absorption at the equatorial station Colombo, Singapore and at a middle latitude station Kokubunji have been computed to determine the control of latitude on the phase of the tide. Also the tidal effects in the ionospheric absorption parameter,  $f_{\min}$  (minimum frequency recorded on ionograms) for the stations Huancayo, Chimbote, Talara and Panama are deduced to find the influence of the electrojet on the tidal amplitudes.

### ACKNOWLEDGEMENTS

Dr.S.Ananthakrishnan was associated with the work presented in this thesis during its initial stages; his keen interest, help and collaboration, the author gratefully acknowledges.

The author expresses his sincere thanks to Professor U.R.Rao and Professor J.S.Shirke for their helpful suggestions at various stages of the work.

Thanks are due to Dr.Harish Chandra, Dr.R.P.Sharma, Dr.K.Kasturirangan and Dr.V.R.Rao for many stimulating discussions.

The theoretical calculations presented in this thesis were carried out with the IBM-1620 computer facility at Physical Research Laboratory. The author wishes to thank Mr.S.R.Tahkore and the staff of the computing centre in general and Dr.D.Patel and Mr.P.S.Shah in particular for their kind cooperation.

Thanks are also due to Mr.S.S.Deshikachar for the help in writing some of the computer programmes, to Miss.B.M. Shah for occasional computational assistance and to Mr.P.Raghavan for the neat job with the typewriter.

The work presented in this thesis was carried out with the financial support from the Ministry of Education and the Department of Atomic Energy of the Government of India, the author acknowledges the assistance.

  
S.C. CHAKRAVARTY

## PUBLICATIONS

The following papers published by the author contain some of the main results based on the work presented in this thesis:

A : Propagation of low frequency radio waves (164 kHz) in the ionosphere

- 1 The propagation of low-frequency radio wave in low-latitudes  
S.Ananthakrishnan and S.C.Chakravarty  
Proc. Third International Symposium on Equatorial Aeronomy, Vol.I-A, 251 (1969).
- 2 Ionospheric effects of X-ray from Scorpio X-1 and Taurus X-1 (Crab)  
S.Ananthakrishnan, S.C.Chakravarty and K.R.Ramanathan  
Proc. Ind. Acad. Sci., 71A, 69 (1970).
- 3 Ionospheric effects of X-ray from discrete galactic sources  
S.Ananthakrishnan, S.C.Chakravarty and K.R.Ramanathan  
Non-Solar X- and Gamma-Ray Astronomy, L.Gratton (Ed.)  
p.146 (1970).
- 4 Nocturnal absorption of radio waves due to the ionisation produced by X-ray from Sco X-1 and Tau X-1 in the lower ionosphere  
S.C.Chakravarty  
Proc. Ind. Acad. Sci., 74A, 99 (1971).
- 5 Possibility of continuous monitoring of celestial X-ray sources through their ionisation effects in the nocturnal D-region ionosphere  
D.P.Sharma, A.K.Jain, S.C.Chakravarty, K.Kasturirangan, K.R.Ramanathan and U.R.Rao <sup>17</sup>, 409  
Astrophysics and Space Science (~~in press~~) (1972).
- 6 A comparison of field-strengths of 164 kHz radio waves transmitted from Tashkent and received at Ahmedabad with flare-time solar X-ray emissions measured in satellites  
S.C.Chakravarty and K.R.Ramanathan  
Proc. Ind. Acad. Sci., 75, 249 (1972).

B : Lunar tides in the D-region ionosphere

- 7 Lunar tides in the lower regions of the equatorial ionosphere  
R.G.Rastogi and S.C.Chakravarty  
Proc. Third International Symposium on Equatorial Aeronomy, Vol.II, 384 (1969).
- 8 Lunar oscillations in the D-region absorption at Singapore  
S.C.Chakravarty and R.G.Rastogi  
Nature, 223, 939 (1969).
- 9 Lunar tide in D-region of the ionosphere near the magnetic equator  
S.C.Chakravarty and R.G.Rastogi  
Journal of Atmospheric and Terrestrial Physics, 32, 945 (1970).
- 10 Lunar oscillations in the ionospheric absorption  
S.C.Chakravarty and R.G.Rastogi  
Indian Journal of Pure and Applied Physics, 8, 541 (1970).
- 11 Lunar effects in ionospheric absorption at Kokubunji  
S.C.Chakravarty and R.G.Rastogi  
Indian Journal of Radio and Space Physics, I(2), 158 (1972)

C : E-region ionosphere

- 12 Disappearance of equatorial Es and the reversal of electrojet current  
R.G.Rastogi, H.Chandra and S.C.Chakravarty  
Proc. Ind. Acad. Sci., 74A, 62 (1971).



C O N T E N T S

	<u>Page</u>
Dedication	i
Preface	ii
Scope of the thesis	iv
Acknowledgements	viii
Publications	x
Contents	xii

CHAPTER - I : FORMATION OF LOWER IONOSPHERE DURING  
QUIET-DAY CONDITION AND PROPAGATION OF  
LONG RADIO WAVES

1.1	Introduction	1
A :	<u>Electron densities in the D-region ionosphere during quiet solar conditions</u>	
1.2	Measured electron density profiles	1
1.3	Ionising sources and their production functions	4
1.4	Loss coefficients	11
B :	<u>Radio observations at 164 kHz</u>	
1.5	Identical experimental set up at Ahmedabad and Gulmarg	16

	<u>Page</u>
1.6 Propagation characteristics of LF radio waves	19
1.7 Conclusion	34
CHAPTER -II : STUDIES ON THE GENERAL BEHAVIOUR OF 164 kHz RADIO SIGNAL STRENGTH VARIATIONS DURING QUIET-DAY CONDITIONS	
2.1 Introduction	35
2.2 Typical diurnal and seasonal variations at Ahmedabad, Poona and Gulmarg	36
2.3 Average hourly variation of signal intensity at Ahmedabad	41
2.4 Effect of quiet sun background X-rays in the control of radio signal amplitudes	48
2.5 Interpretation of the results on the general variation of 164 kHz radio signal amplitudes	53
2.6 Derivation of dominant negative ions from the sunrise effects in 164 kHz signals received at Ahmedabad	58
2.7 Effect of stratospheric temperature variations in the radio propagation during winter	69
2.8 Conclusion	70
2.9 Discussion	73
CHAPTER - III : EFFECT OF SOLAR FLARES ON 164 kHz RADIO PROPAGATION	
3.1 Introduction	77

	<u>Page</u>
3.2 The effects observed on 164 kHz field strengths and their association with their ionospheric disturbances	79
3.3 A direct comparison of radio intensities at 164 kHz with flare time solar X-ray emissions measured in satellites	84
3.4 Occurrence of flare effects with respect to the X-ray flare events during 1968-71	91
3.5 Interpretation of the results on occurrence of solar flare effects in 164 kHz radio strengths	98
3.6 Electron production by X-rays in the 1-8 Å region	100
3.7 Electron density variations in the D-region during the course of X-ray flares	104
3.8 Conclusion	111
3.9 Discussion	114

#### CHAPTER - IV : POSSIBILITY OF CONTINUOUS STUDY OF NOCTURNAL D-REGION IONOSPHERE BY LF AND VLF PROPAGATION TECHNIQUE

4.1 Introduction	117
4.2 Observations of electron densities in nocturnal D-region by rocket borne experiments	118
4.3 General pattern of variation of radio intensity at Ahmedabad during night-time	122
4.4 Effects observed in 164 kHz radio amplitudes during the transit of a strong X-ray source Sco X-1	128

	<u>Page</u>
4.5 Effects observed in the 164 kHz radio intensity during the transit of other galactic X-ray sources	135
4.6 Other observational evidence supporting the effect of galactic X-rays on LF and VLF propagation during night	140
4.7 Conclusion	143
4.8 Discussion	145
 CHAPTER - V : THEORETICAL ESTIMATES OF LF RADIO ATTENUATION DUE TO THE IONISATION PRODUCED BY NON-SOLAR X-RAY SOURCES	
5.1 Introduction	147
5.2 Electron production rates by Sco X-1 and Tau X-1	150
5.3 Electron densities of the night-time D-region during the passage of Sco X-1 and Tau X-1	154
5.4 Wave-admittance method of Barron and Budden	156
5.5 Calculation of the attenuation suffered by LF radio waves passing through the excess ionisation produced by Sco X-1 and Tau X-1	163
5.6 Review of all possible night-time ionising sources and their production rates in the D-region	171
5.7 Enhancement in the electron densities caused by Sco X-1, Tau X-1 and Galactic Centre(G.C) over the background ionisation and the corresponding absorption of LF radio waves	177

	<u>Page</u>
5.8 Summary and conclusion	182
5.9 Discussion	184

## CHAPTER - VI : LUNAR TIDES IN THE D-REGION IONOSPHERE

6.1 Introduction	187
6.2 Data and method of analysis	189
6.3 Lunar tide in the D-region absorption at Singapore	194
6.4 Solar cycle variation of lunar tides in ionospheric absorption at Colombo	196
6.5 Lunar effects in ionospheric absorption at Kokubunji during 1957-68	199
6.6 Lunar tides in fmin close to the magnetic equator during IGY-IGC	205
6.7 Variation of normal absorption and the amplitude of semi-monthly tide in absorption with the magnetic latitude	210
6.8 Conclusion	215
6.9 Discussion	216

## REFERENCES

## CHAPTER I

### FORMATION OF LOWER IONOSPHERE DURING QUIET-DAY CONDITION AND PROPAGATION OF LONG RADIO WAVES

#### 1.1 Introduction

The thesis deals with the results of low frequency radio wave propagation studies through the D-region of the ionosphere. The objective of this first chapter is to summarise the results of electron density measurements in the D-region at low latitudes during quiet solar conditions. The observed electron density profiles are then explained in terms of electron production rates due to different ionising agencies and their effective loss coefficients because of various recombination processes.

The experimental set up for receiving the Tashkent 164 kHz radio signals at Ahmedabad and Gulmarg is described. The average heights of reflection during different seasons have been estimated from the calculation of reflection coefficients by using Sheddy's method for sharply bounded anisotropic ionosphere. These results have been used for the interpretation of the results obtained in the subsequent chapters.

#### A. ELECTRON DENSITIES IN THE D-REGION IONOSPHERE DURING QUIET SOLAR CONDITIONS

#### 1.2 Measured electron density profiles

The region covering the height range from 55 to 90 km of the upper atmosphere is generally known as the D-region of

the ionosphere. The measurement of electron density profiles in the D-region is difficult because of the low electron densities. There are however a few rocket observations, from which some informations can be obtained. The long series of ground-based observations in the 16 to 127 kHz radio frequencies for distances varying from 90 to 535 km (BRACEWELL ET AL., 1951; BELROSE, 1957) have yielded electron density profiles in the D-region during different hours of the day, season and sunspot activity. DEEKS (1966) has estimated the electron density profiles from these long-wave propagation experiments by suitably changing some postulated electron density profile so as to match them with observations.

In figure 1.1(a) and 1.1(b) a few electron density profiles obtained from rocket observations are shown. Figure 1.1(a) shows the electron density profiles in the D-region of the equatorial region whereas in figure 1.1(b) similar profiles at mid-latitude stations are shown. The profiles obtained by AIKIN ET AL. (1964) and by HALL and FOOKS (1965) are from rocket observations at Wallops Island, Virginia ( $37.8^{\circ}\text{N}$ ,  $75.5^{\circ}\text{W}$ ) and Woomera, Australia respectively whereas the profile due to BELROSE ET AL. (1966) is from ground-based partial reflection method. It can be noted that the electron densities at the equatorial stations for the high sunspot years are in general higher than those in middle latitude stations during low sunspot years.

There are very few rocket measurements giving the diurnal variation of electron densities in the D-region. However,

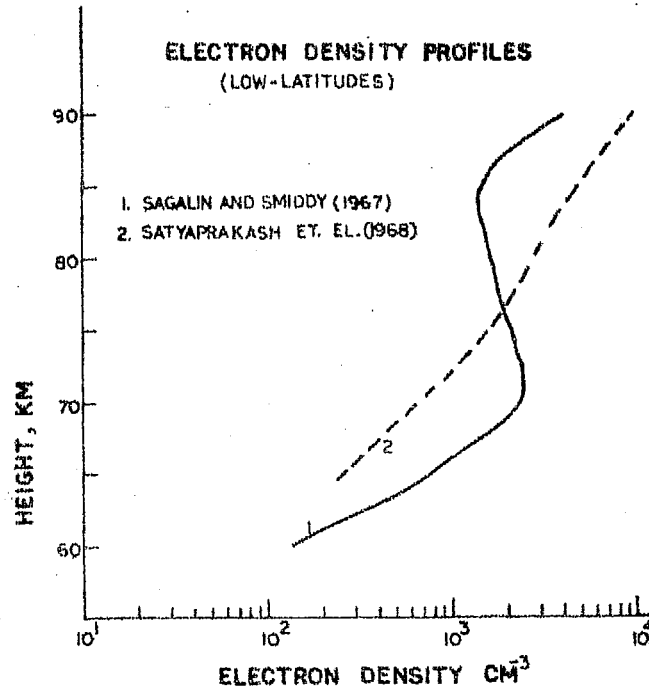


FIGURE 1.1(a) : Electron density profiles in the D-region at equatorial latitudes during quiet day time:  
1. Sagalin and Smiddy - 20 March 1965; 1204 EST, Peru, South America.  
2. Satyaprakash et al. - 29 August 1968; 1415 IST, Thumba, India.

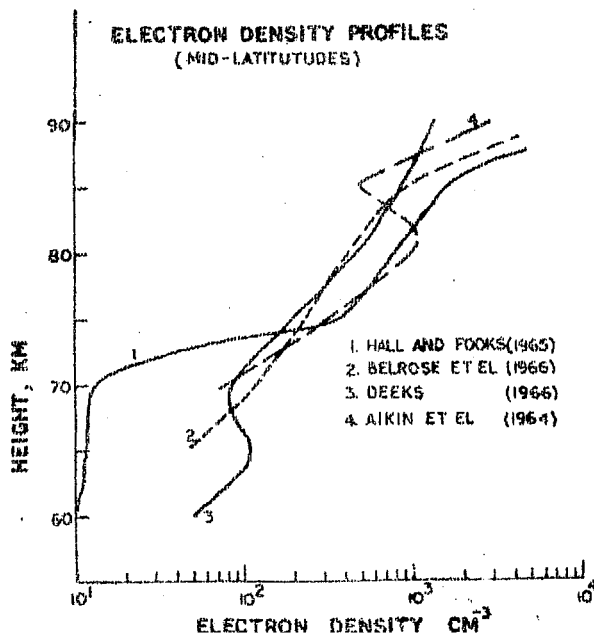


FIGURE 1.1(b) : Electron density profiles in the D-region at mid-latitudes:

Curve 1 : Hall and Fooks, 29 May 1963, 1456 LMT, Rocket flight at Wallops Island.

Curve 2 : Belrose et al. - Partial reflection experiment - 1200 LMT, Ottawa.

Curve 3 : Deeks - VLF and LF radio observations (OMEGA navigation system).

Curve 4 : Aikin et al. - 8 March 1963, 1430 EST - Rocket flight at Wallops Island.



from Deeks' estimates using low frequency reflection technique a diurnal variation of ~~6 to 40 el cm<sup>-3</sup>~~ <sup>the order of 4-5</sup> above 75 km can be seen from figure 1.2(a).

The seasonal variation of electron densities in the D-region has been studied by MECHTLY and SMITH (1967) from a series of rocket observations in 1967 for a constant solar zenith angle of 60°. The results are summarised in figure 1.2(b). It can be seen that the electron densities during summer are higher than in the other seasons. During the winter months the electron densities are lower by a factor of about 3. A sharp ledge in the electron density occurs between 80 - 85 km in the middle latitudes. An explanation of this sharp increase in electron density has been given in terms of higher recombination of electrons with water vapour cluster ions below about 85 km (REID, 1970).

### 1.3 Ionising sources and their production functions

In this section we will consider the sources responsible for the production of electron densities in the D-region. During quiet solar conditions the main ionising sources below 90 km are as follows:

- (a) Galactic cosmic rays
- (b) Lyman $\alpha$  (ultraviolet radiation at  $\lambda = 1216 \text{ \AA}$ )
- (c) Solar X-rays ( $\lambda < 10 \text{ \AA}$ )

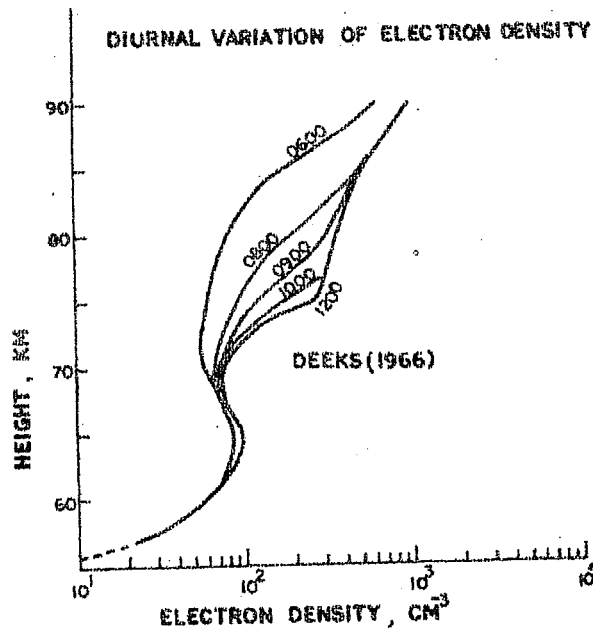


FIGURE 1.2(a) : Diurnal variation of electron density in the D-region estimated from VLF and LF radio observations of OMEGA navigation system by Deeks (1966).

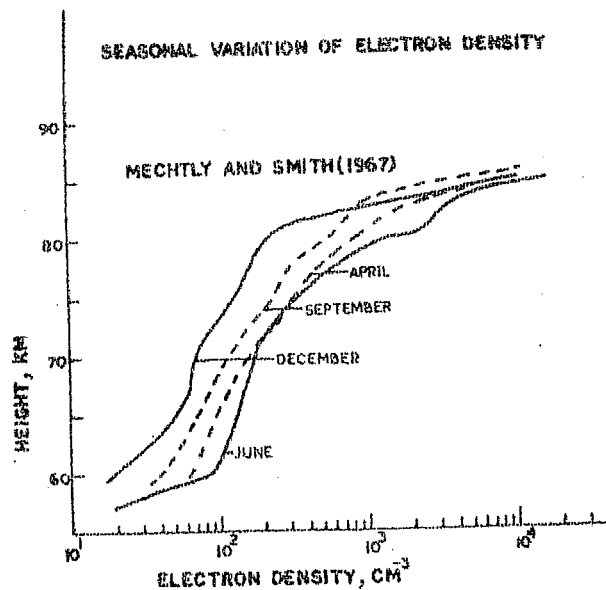


FIGURE 1.2(b) : Seasonal variation of electron density in the D-region from a series of rocket observations at Wallops Island ( lat. 38° ) for a constant solar zenith angle of 60° by Mechtly and Smith (1967)

(a) Galactic cosmic rays

BRACEWELL and BAIN (1952) investigated the propagation of very low frequency (VLF) radio waves ( 16 kHz) over distances ranging from 90 to 535 km, and in order to explain their results postulated the existence of an ionospheric layer between 60 - 70 km. Ionisation at these heights can be produced by galactic cosmic rays because of their penetrating characteristics. The presence of a cosmic ray layer ( also referred to as the C-layer) was confirmed by measurements using other experimental techniques (BARRINGTON ET AL., 1962; DEEKS, 1966; VELINOV, 1966a). Recently, VELINOV (1968) has made extensive computations of the electron production by cosmic rays, including the effect of particles of higher charge numbers. His analysis gives the electron production rates during high and low sunspot years for the geomagnetic latitudes of 0°, 30°, 41° and 55°. The variation of this production rate with season and changes in atmospheric density (SPENCER ET AL., 1964; STROUD and NORDBERG, 1963) has also been estimated. Figure 1.3 shows the electron production rates due to galactic cosmic rays during different solar activity periods at the geomagnetic latitudes 0°, 30° and 41° (VELINOV, 1968). The maximum production rates take place during the summer of minimum solar activity years (cosmic ray intensity decreases with increasing solar activity) and the production increases with decreasing altitude.

(b) Lyman $\alpha$  - radiation

Lyman $\alpha$  radiation from the sun having a quantum

energy of 10.2 eV remains quite intense even at a height of 90 km. The minor constituent Nitric Oxide NO at these heights require about 9.2 eV for its ionisation. NICOLET (1945) pointed out that the ionisation of NO by Lyman  $\alpha$  is a major contribution to D-region electron densities. Due to the presence of an absorption band of  $O_2$  around the wavelength of 1216 Å (WATANABE, 1958), Lyman  $\alpha$  flux gets attenuated by atmospheric  $O_2$  before it reaches 90 km. Hence a realistic evaluation of ionisation by Lyman  $\alpha$  requires the knowledge of Lyman  $\alpha$  flux above the ionosphere and also the concentrations of  $O_2$  and NO below 100 km. Lyman  $\alpha$  flux is quite accurately known by satellite observations (NEUPERT, 1963; WEEKS and SMITH, 1968). It is reasonable to conclude from the available satellite data that the Lyman  $\alpha$  flux is fairly constant with the changes in solar activity. At altitudes below about 120 km the molecular oxygen densities given by all atmospheric models compare well with those estimated by direct rocket measurements (SUBBARAYA ET AL., 1971). The difficulty in the evaluation of the Lyman  $\alpha$ -caused ionisation arises because of the uncertainties involved in the concentrations of Nitric Oxide. The rocket observations using spectroscopic techniques by BARTH (1964) and PEARCE (1969) yielded orders of magnitude higher concentrations of NO compared to those estimated by NICOLET and AIKIN (1960) and MITRA (1969) from ionospheric and photochemical methods. The recent experiment by MEIRA (1971) shows considerably lower values compared to those given by Barth and Pearce. More

elaborate theoretical estimates of NO concentration by HESSTVEDT (1969) and STROBEL ET AL. (1971) and the revised values of Pearce (THOMAS, 1971) seem to be supporting the values obtained by Meira. The NO density profiles due to different experimental and theoretical results are given in figure 1.4. The ionisation rates due to Lyman  $\alpha$  using different NO densities of Nicolet and Aikin, Meira, Barth and Pearce ( curves 2, 3, 4 and 5 respectively) are shown in figure 1.5. The following relationship has been used in the calculation of ion production  $q(h)$  by Lyman  $\alpha$

$$q(h) = 2\pi n_1(h) I \sigma_i \int \exp[\sigma_a \sec \chi \int n_2(h) dh] \sin \chi d\chi \dots (1.1)$$

where $h$	= any particular height
$n_1(h), n_2(h)$	= densities of NO and $O_2$ at height $h$
$I$	= intensity of Lyman $\alpha$ at height $h$
$\sigma_a$	= absorption cross-section of $O_2$
$\sigma_i$	= ionisation cross-section of NO
$\chi$	= zenith angle

It may be noted from figure 1.5 that the ionisation due to Lyman  $\alpha$  has peak production around 75 km ( curves 2 and 4 ).

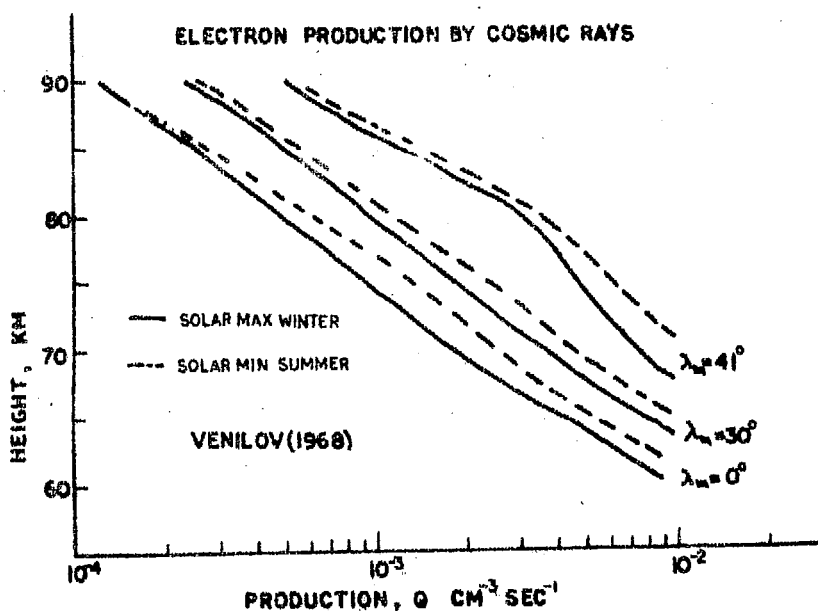


FIGURE 1.3 : Electron production rates due to cosmic rays at geomagnetic latitudes  $0^\circ$ ,  $30^\circ$  and  $41^\circ$  for solar maximum and solar minimum activity conditions.

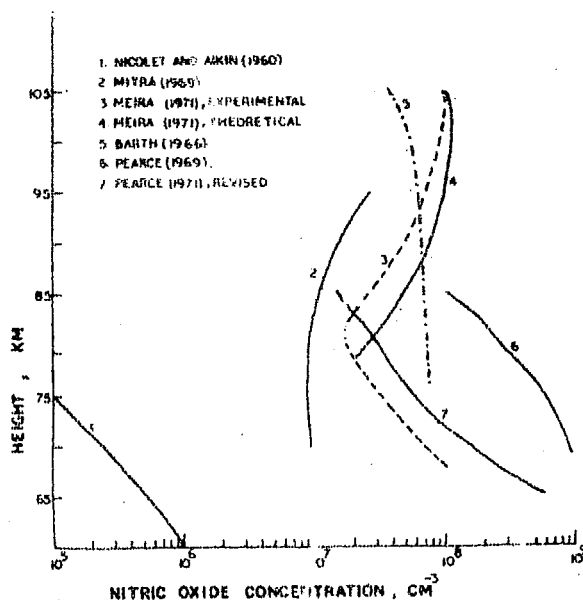


FIGURE 1.4 : Nitric oxide densities in the lower ionosphere taken from various experimental and theoretical results.

(c) X-rays ( $\lambda < 10 \text{ \AA}$ )

Solar background (ie. nonflare ) X-radiation in the spectral range below  $10 \text{ \AA}$  is the most influential agent for ionisation in the D-region. MULLER (1935), RAWER (1952), CHAMBERLAIN (1961), and WHITTEN and POPPOFF (1962) by estimating the electron production from the available spectral distribution of X-rays below  $10 \text{ \AA}$  demonstrated the importance of X-radiation in controlling the electron density in the D-region. The actual physical process by which X-rays interact with the atmosphere resulting in ion-electron production will be discussed in Chapter III. There is some difficulty in the proper appraisal of this effect due to the variable nature of the X-ray flux. From rocket and satellite observations of solar X-ray flux under non-flare conditions, it is difficult to define a quiet solar condition. Solar X-ray flux is highly variable in nature, however, increasing with increase of solar activity by atleast a factor of 100, between minimum and maximum solar active years. The ionisation rates due to quiescent solar X-ray fluxes are  $6 \times 10^{-3} \text{ ergs}/(\text{cm}^2 \cdot \text{sec})$  and  $0.5 \times 10^{-3} \text{ ergs}/(\text{cm}^2 \cdot \text{sec})$  respectively in maximum and minimum sunspot periods ( figure 1.5). It may be noted that electron production due to X-rays becomes important above the level of peak production due to Lyman  $\alpha$  (  $\approx 75 \text{ km}$  ). The production rate due to galactic cosmic rays for low latitudes has also been included in the figure in order to have the relative levels and orders of ionisation by different agencies.

Besides the production due to the above mentioned sources, the production due to the ionisation of excited molecular oxygen  $O_2$  ( $^1\Delta_g$ ) may also be important in the D-region (HUNTEN and McELROY, 1968). Meteors can produce sporadic ionisation in the upper D-region and the relevant magnitudes of such ionisation however are quite low (THOMAS, 1971).

We have seen above that in low latitudes, the main ionising agencies in the D-region are Lyman $\alpha$  and X-radiation ( $\lambda = 1-8 \text{ \AA}$ ). Proper assessment of the production rate due to Lyman $\alpha$  becomes difficult owing to uncertainties in our knowledge of NO concentration. The solar cycle variation of the rate of electron production due to X-rays is not fully known. If we consider Barth's values of NO density the production due to X-rays even during the maximum sunspot years becomes dominant only above 75 km (figure 1.5) whereas if we consider Meira's values of NO concentration the production due to X-rays become important above 75 km only. during low and medium sunspot activity periods. X-ray production dominates over all other ionising sources during maximum solar activity periods if Meira's NO densities are accepted. We may conclude that electron production due to X-rays will dominate over the production due to Lyman $\alpha$  above 75 km, during a large part of the solar cycle.

#### 1.4 Loss coefficients

From the values of production functions and the actual



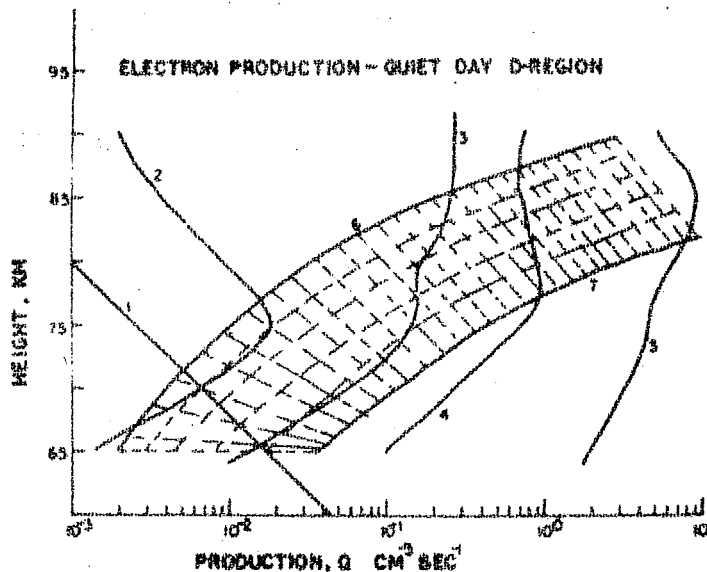


FIGURE 1.5 : Electron production rates in the D-region during quiet conditions:

Curve 1 : due to cosmic rays

Curve 2 to 5 : due to Lyman $\alpha$  and NO concentrations of Nicolet and Aikin, Meira, Barth and Pearce

Curve 6 to 7 : due to X-rays ( 1-8 Å ) for low and high sunspot years.

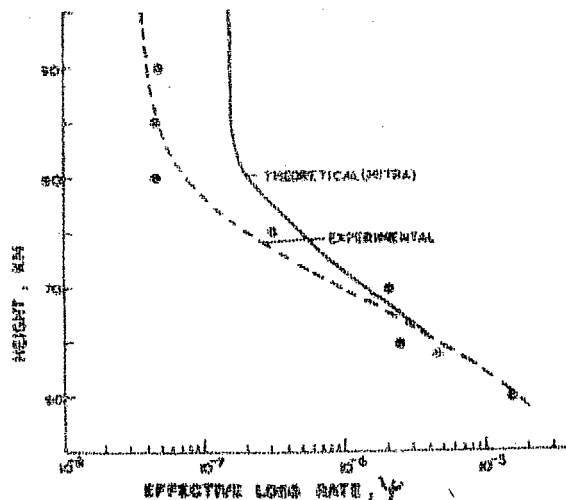


FIGURE 1.6 : Effective recombination coefficient in the D-region ionosphere:

Dots represent experimental points compiled by Mitra (.968), continuous curve represents the theoretical values.

numbers of free electrons in the ionosphere it can be noted that there exists a considerable difference between the two at all heights. This can be explained in terms of the loss processes which have to be considered alongwith the production rates. In general the following continuity equations for electrons and positive ions have to be considered for lower region of the ionosphere ( neglecting loss due to diffusion as it will be small compared to other loss processes ):

$$\frac{\partial N_e}{\partial t} = q - \alpha_D N_e N^+ - \beta N_e m + \delta N^- n + \rho N^- \quad \dots(1.2)$$

$$\frac{\partial N^+}{\partial t} = -\alpha_L N^- N^+ + \beta N_e m - \delta N^- n - \rho N^- \quad \dots(1.3)$$

and also assuming that the ionosphere is electrically neutral

$$N^+ = N_e + N^-$$

where  $N_e$  = electron density

$N^+$  = positive ion density

$N^-$  = negative ion concentration

$m$  = molecular oxygen concentration

- $n$  = neutral atmospheric concentration
- $q$  = total electron production
- $\alpha_D$  = ion-electron recombination
- $\alpha_i$  = ion-ion recombination
- $\beta$  = electron attachment coefficient
- $\gamma$  = negative ion collisional detachment coefficient
- $P$  = negative ion photo-detachment rate

From equations (1.2) , (1.3) and (1.4), defining a quantity

$\lambda = N^-/N_e$  and assuming  $\frac{\partial \lambda}{\partial t} = 0$ , we have the following relationship

$$\frac{\partial N_e}{\partial t} = \frac{q}{1+\lambda} - (\alpha_D + \lambda \alpha_i) N_e^2 \quad \dots (1.5)$$

Under equilibrium conditions for a particular height this reduces to

$$\frac{q}{N_e^2} = (1+\lambda)(\alpha_D + \lambda \alpha_i) = (1+\lambda) \alpha_{eff} = \psi \quad \dots (1.6)$$

where  $\alpha_{eff}$  = effective recombination coefficient.

It can be noted that  $\alpha_{eff}$  becomes equal to  $\Psi$  for small values of  $\lambda$ . During day-time  $\lambda$  becomes appreciably high only below about 70 km. The most effective way by which the  $\Psi$  has been estimated is by comparing the actual measurements of electron densities with the theoretically estimated total value of production function. MITRA (1968) has determined the values of  $\Psi$  at different heights by using five electron density profiles (DEEKS, 1966; AIKIN ET AL., 1964; BOURPEAU ET AL., 1964; 1965 and PIGGOTT and THRANE, 1966) and the corresponding total production rates. The average values of  $\Psi$  at different heights from these five measurements are plotted in figure 1.6 as dark circles. The theoretical values of  $\Psi$  derived from the following formula are also included in the figure.

$$\Psi = \alpha_D + (\lambda_0 \alpha_i) \frac{n^2(O_2)}{n_0^2(O_2)} \quad \dots(1.7)$$

where  $n_0(O_2)$  refers to the molecular oxygen concentration at a reference level of 70 km.

The dotted curve gives the average variation of loss coefficient  $\Psi$ , with height in the lower ionosphere. It can be noticed that below about 75 km the loss coefficients show rapid increase because of the increased values of  $\lambda$  due to larger concentrations of negative ion formed by attachment to neutral molecules.

B RADIO OBSERVATIONS AT 164 kHz

1.5 Identical experimental set up at Ahmedabad and Gulmarg

The field strength recording of the 164 kHz radio waves (CW) as received at Ahmedabad started in the middle of the year 1960. The transmitter used for the general communication purposes is situated at Tashkent, USSR. The initial experimental set up using a Beverage or wave antenna terminated in the direction of the <sup>transmitter</sup> receiver has been described by ALURKAR (1965). An identical experiment was installed at Poona by ANANTHAKRISHNAN (1967) in 1963 to study the effect of increasing the radio path on LF propagation. In order to reduce the background noise in the reception the Beverage antenna was replaced by a 6 square feet air-core loop antenna and a preamplifier. This antenna has a single layer of 50 turns with the spacing of about  $\frac{1}{2}$ " between two turns. The inductance associated with the loop antenna was calculated by using the following relation:

$$L = 0.885 k D n^2 \times 10^{-6} \quad \dots (1.8)$$

where the inductance L is in henrys

k = inductance factor

D = coil diameter in meters

n = total number of turns

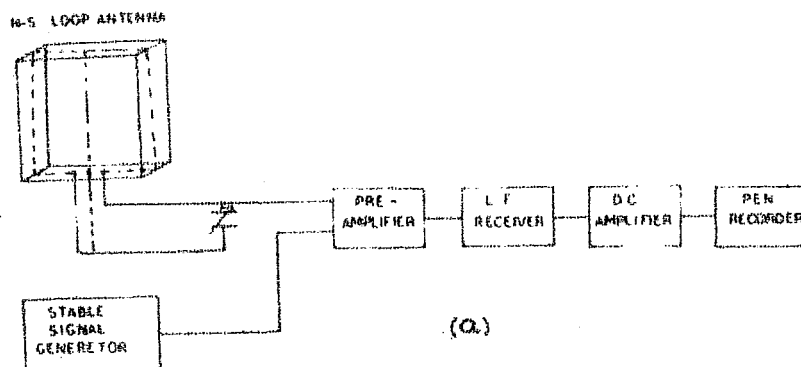
Value of k as a function of D/W, where W is the width of the loop has been given by WATT (1967a).

A tuned ( 164 kHz ) preamplifier having a gain of about 50 dB was connected in the output of the loop taken through a tuning capacitor. The centre and one of the terminals of the loop were grounded, so that effectively only half of the loop was used to neutralise the noise picked up in the two halves. The whole set up of the antenna and preamplifier was tuned for maximum reception at 164 kHz by varying the tuning capacitor of the loop. The loop antenna and preamplifier combination was put at the top of an isolated hut. The output of the preamplifier was taken to a receiver through a matched radio frequency cable. The receiver is suitably chosen for recording the field strength of LF radio waves. Figure 1.7 gives the block diagram and antenna preamplifier combination circuit for the set up.

The use of loop antenna makes the system perfectly tuned for the wanted signal reducing the noise of reception and also the orientation of the antenna can be arranged to receive the normal and abnormal components of the sky wave in two orthogonal directions.

The recording of the normal component of the signal of 164 kHz radio waves by the modified set up started in 1968 and an identical set up was put in operation at Gulmarg in the middle of 1971.

# BLOCK DIAGRAM OF LOW FREQUENCY RECEIVING UNIT



## ANTENNA EQUIVALENT AND PRE-AMPLIFIER CIRCUITS

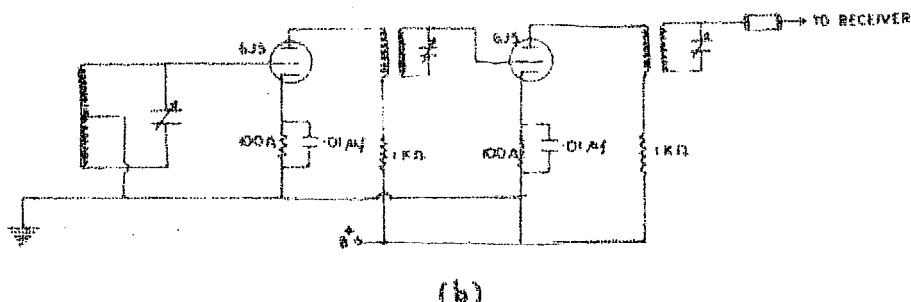


FIGURE 1.7 : Experimental set up for receiving 164 kHz radio waves transmitted from Tashkent.

## 1.6 Propagation characteristics of LF radio waves

In this section we shall examine the various propagation characteristics of LF radio waves with special reference to the 164 kHz waves transmitted from Tashkent and received at Ahmedabad. The study made is from the theoretical considerations involving the estimation of the reflection coefficients of the lower ionosphere. This study will furnish a picture of the general behaviour of these radio waves as expected from theoretical stand point.

### (a) Ground wave propagation

The geographical coordinates of the different receiving stations and their distances from the transmitter at Tashkent are given in Table 1.1. It will be noticed that although the stations differ significantly in latitude, they differ little in longitude, hence we will be mostly concerned with the N-S propagation of 164 kHz radio waves. The intensity of the vertical electric field due to the ground wave is given by the following relation (WATT, 1967b):

$$|E_z| \text{ (db, 1 mV/m)} = 109.54 + 10 \log P_r \text{ (kilo watts)} \dots (1.9) \\ - 20 \log d \text{ (km)} + 20 \log |W_s|$$



Table 1.1

Geographic coordinates of transmitting and  
receiving stations

Station	Latitude (Geographic)	Longitude (Geographic)	Distance from Tashkent in km
Tashkent	42°N	69°E	0
Gulmarg	34°N	74°E	800
Ahmedabad	23°N	72°E	2150
Poona	18°N	74°E	2560

where  $P_r$  = Transmitter power

$d$  = Transmitter - receiver separation

$W_s$  = Surface wave factor according to Norton's surface wave relation

By putting a value of 100 KW for the transmitter power, the intensity was calculated at different receiver distances. It was found that the ground wave intensity would become negligible after a distance of 800 km. Hence it can be concluded that there is almost no possibility of 164 kHz ground signals to be received at Ahmedabad or Poona though at Gulmarg the intensity due to ground propagation may be present to some extent. A loop antenna at the receiving end of Ahmedabad or Poona will only pick up the sky wave of 164 kHz radio signals from Tashkent.

(b) Angle of incidence

The angle of incidence of radio waves for a particular fictitious reflection height can be calculated from single geometry of the propagation. But for very long distances the correction due to the curvature of earth has to be taken into account. Following formulations can be used for the calculation of the angle of incidence:

$$\theta = \tan^{-1} \left( \frac{d}{2h} \right) \quad \dots(1.10)$$

$$\theta^* = \tan^{-1} \left[ \frac{R \sin \left( \frac{d}{2h} \right)}{h + R \left\{ 1 - \cos \left( \frac{d}{2h} \right) \right\}} \right] \quad \dots(1.11)$$

where  $\theta$  is the angle of incidence without the correction due to earth's curvature

$\theta^*$  is the angle of incidence with the correction of earth's curvature

$d$  = transmitter-receiver distance

$h$  = height of reflection

$R$  = Radius of earth

Figures 1.8(a) and 1.8(b) show the variation of the angle of incidences  $\theta$  and  $\theta^*$  with the receiver-transmitter distance for different heights of reflections. The effect of the inclusion of earth's curvature can be noticed at distances larger than about 500 km. The angle of incidence becomes almost constant with any reflection height between 60 km - 100 km for distances greater than about 1250 km is also brought out by the figure. For the propagation of 164 kHz radio waves upto Ahmedabad we will consider an angle of incidence of  $80^\circ$  in our further theoretical calculations.

### (c) Reflection coefficients

The reflection coefficient matrix of the ionosphere

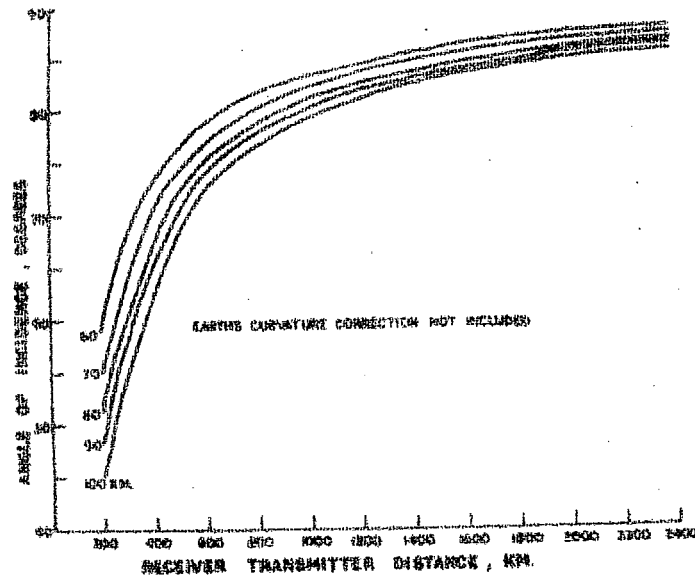


FIGURE 1.8(a) : Variation of angle of incidence of radio waves with the transmitter-receiver separation (when correction due to earth's curvature is not included )

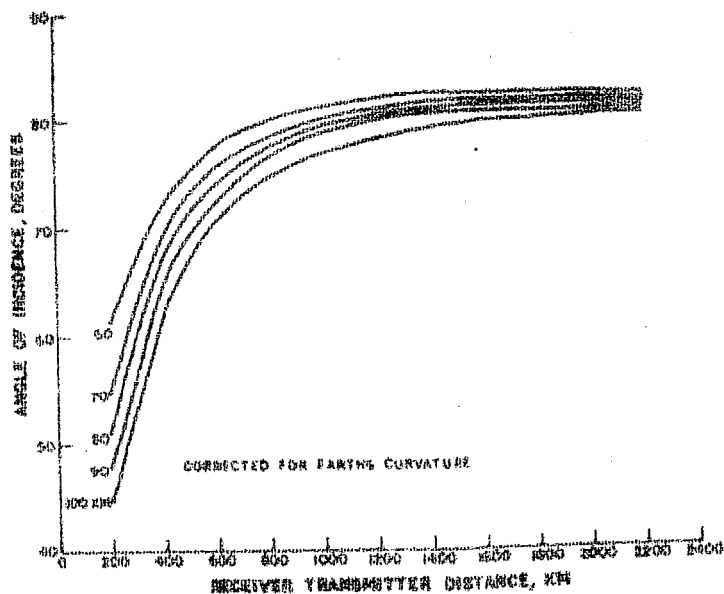


FIGURE 1.8(b) : Variation of angle of incidence with the transmitter-receiver separation (when correction due to earth's curvature is included ).

for an incident wave of any polarisation can be expressed as:

$$[R] = \begin{pmatrix} R_{||||} & R_{||\perp} \\ R_{\perp||} & R_{\perp\perp} \end{pmatrix} \quad \dots (1.12)$$

where the subscripts refer to propagation with the electric vector in the plane of incidence ( $||$ ) or perpendicular to it ( $\perp$ ). The subscript corresponds to the polarisation of the incident wave and the second to that of the reflected wave.

When oblique radio waves enter the ionosphere in the presence of the earth's magnetic field, they split up into two polarised components, which propagate independent of each other. The refractive index of each of them depends on the altitude and also on the angle of reflection ( $\Theta_r$ ) in a complicated way, so much so, Snell's law with  $\Theta_r = \pi/2$  does not give the reflection level. The true level of reflection is the level where the group velocity and not the phase velocity is horizontal. In **figure 1.9(a)** and **(b)** the continuous lines represent the ray paths (both for group rays and phase rays) and the arrows superimposed on the ray paths show the direction of wave normals. For frequencies below the gyro frequency, in the case of ordinary wave the wave normal becomes horizontal after the reflection takes place and in case of extra-ordinary wave, the wave normal becomes horizontal before reflection (**figure 1.9(a)** and **(b)**). For oblique radio

waves in the presence of earth's magnetic field, the refractive index satisfies a quartic known as the BOOKER's quartic (1938) instead of the quadratic given by Appleton and Hartree ( for the case of normal incidence). Hence there are four roots of Booker quartic equation; e.g.  $q$ 's ( $= \mu \cos \theta_r$ ), corresponding to upgoing ordinary and extraordinary and downgoing ordinary and extraordinary waves. The propagation of the components of the wave through the atmosphere can be represented by plotting  $q$  as a function of a parameter  $X$ , dependent on the electron density, while keeping other parameters; wave frequency, the earth's magnetic field and the angle of incidence constant. Such a plot is shown in figure 1.9(c). The continuous curve corresponds to the ordinary wave and the broken curve corresponds to the extraordinary wave.  $X_B$  and  $X_C$  represent the critical electron densities for the ordinary and extraordinary components above the levels of which the wave will not penetrate. It can be noted that the reflection of the waves take place at the points B and C where  $\partial q / \partial X \Rightarrow \infty$  and not at A and D where  $q = 0$  or  $\theta_r = \pi/2$ , as in the case of an isotropic ionosphere. To understand the propagation characteristics of the radio waves in the anisotropic ionosphere, the solutions of the Booker quartic equation will be necessary, the roots of which are related to the reflection coefficients of the ionosphere.

By assuming a sharply bounded model of the anisotropic ionosphere, the derived reflection coefficients can be used as

rough approximation to reflection from the real inhomogeneous ionosphere. These can also be used as the exact starting solutions to an integration of the reflection coefficient matrix through an ionosphere of arbitrary electron density distribution (BUDDEN, 1955). The reflection coefficient matrix for the above mentioned ionosphere has been computed by various workers for the general and various special cases of propagation (JOHLER and WALTERS, 1960; CHROMBIE, 1961; and DE LISLE, 1967). Recently SHEDDY (1968) has given a comparatively simple method by selecting a suitable coordinate system resulting in simpler boundary conditions. The Booker's quartic in  $q$  is expressed as:

$$B_4 q^4 + B_3 q^3 + B_2 q^2 + B_1 q + B_0 = 0 \quad \dots(1.13)$$

where the coefficients are functions of the component of the susceptibility matrix, arising from the constitutive relations of the ionosphere. The roots of this equation are obtained from the closed solution given by BURNSIDE and PANTON (1904). The two roots corresponding to the positive real and negative imaginary parts are chosen for the upgoing waves and then using the boundary conditions simple relations of reflection coefficients in terms of the two quartic roots are obtained.

In the present calculations we have used the method of Shetty by considering the coordinate system of figure 1.10 appropriate for the propagation of 164 kHz radio waves over the

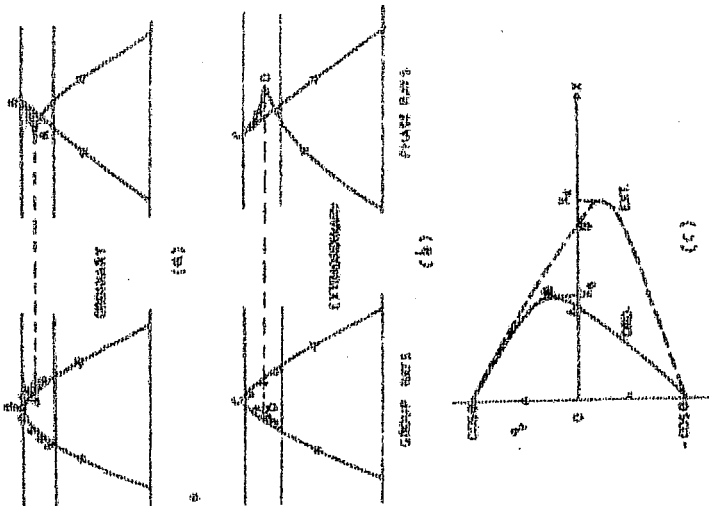


FIGURE 1.9: (a) Group and phase rays of the ordinary wave for an anisotropic collisionless ionosphere, (b) Group and phase rays of the extra-ordinary wave for an anisotropic collisionless ionosphere, (c) the Booker quartic root  $q$ , plotted against  $X$  (a function of electron density)

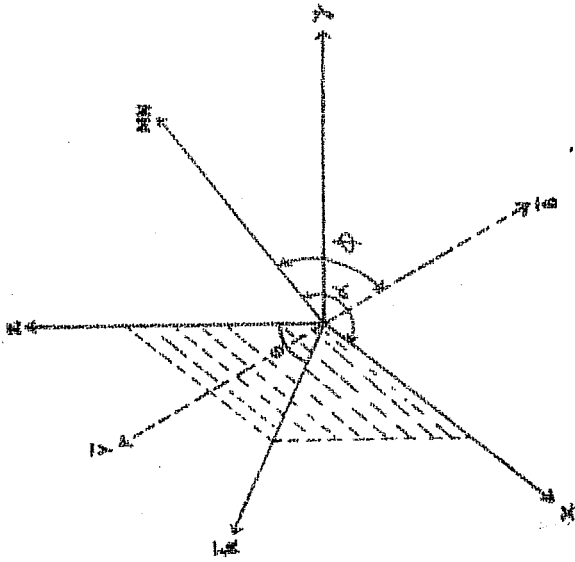


FIGURE 1.10: The coordinate system for the transmitter at Tashkent. The wave vector  $\vec{K}$  lies in  $xz$  plane,  $z$  is vertically up.  $\vec{Y}$  is in the plane of magnetic meridian.  $\vec{MN}$  is the direction of magnetic north.  $\phi$  is the magnetic dip angle measured down from the horizontal.  $\theta$  is the angle of incidence of the radio waves in the ionosphere measured from the vertical and  $\alpha$ , the azimuthal angle east of magnetic north.



longitude of  $72^\circ\text{E}$ , in the N-S direction. Here we assume that the wave vector  $\vec{k}$  lies in the x-z plane and z is the vertical direction.

$\theta$  and  $\phi$  are the angle of incidence and magnetic dip angle corresponding to the midpoint of propagation.  $\alpha$  is the azimuthal angle east of magnetic north in the horizontal plane (denoted as MN). The magnetic field vector  $\vec{B}$  and the gyromagnetic field vector  $\vec{Y}$  are also shown in the figure.

A computer programme for calculating the reflection coefficient matrix for the general case was made, suitable for processing in a IBM 1620 computer at Physical Research Laboratory, Ahmedabad. The quantities in Sheddy's formulae are complex and hence could not be directly handled by the available computer. All the formulae were rewritten by separating the real and imaginary parts. The correctness of the programme was checked by feeding the data for 21.4 kHz of VIERTEL and SECHRIST (1969) and comparing with their results. The reflection coefficient matrix at any height of the ionosphere was determined by feeding the input data which consists of the angle of incidence, dip angle, azimuth, radio frequency, electron density, collision frequency and magnetic field intensity. All the data are in standardised MKS units.

In receiving the 164 kHz radio signals the main lobe of the antenna lies in the plane of incidence, hence the variation of only  $||R_{11}||$  will be considered important in signifying the

propagation properties. In literature  $_{||}R_{||}$  and  $_{\perp}R_{\perp}$  are called the reflection coefficients whereas  $_{||}R_{\perp}$  and  $_{\perp}R_{||}$  are called the conversion coefficients. In our calculations we have used the modified collision frequency profile given by Deeks (1966). Figure 1.11(a) shows the variation of the reflection and conversion coefficients (  $_{||}R_{||}$  and  $_{||}R_{\perp}$  ) with the angle of incidence of the 164 kHz radio waves for a fictitious reflection height of 65 km. The value of electron density was taken from the curve of Sagalin and Smiddy of figure 1.1(a). It can be seen that the reflection coefficient (  $_{||}R_{||}$  ) is almost zero upto about  $60^{\circ}$  from where it starts increasing and reaches a value of .5 at  $80^{\circ}$ . The low values of angle of incidences will amount to small receiver transmitter separation, which means that the reflectivity of an ionisation layer at 65 km will decrease with decrease in propagation path of 164 kHz signals. The conversion coefficient shows a steeper rise after 60 degrees. Figure 1.11(b) shows the variation with the radio frequency. It can be noticed that for a constant value of angle of incidence, the reflection coefficient at a height of 65 km decreases with the increase in frequency whereas the conversion coefficient remains almost constant with a small rise. Hence the reflectivity of the layer at 65 km will be more for smaller frequencies at a particular angle of incidence. Figure 1.12(a) shows that the effect of different values of dip angle is insignificant for the reflection coefficient. The reflection and conversion coefficient height profiles for 164 kHz radio waves received at Ahmedabad are

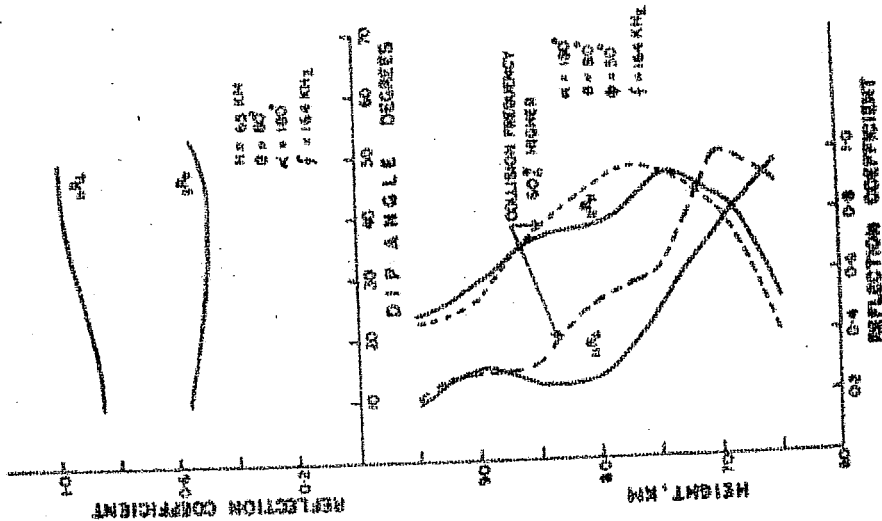


FIGURE 1.11 : Variation of reflection coefficient and conversion coefficient (a) with angle of incidence of 164 kHz radio waves (received at Ahmedabad) (b) with frequency.

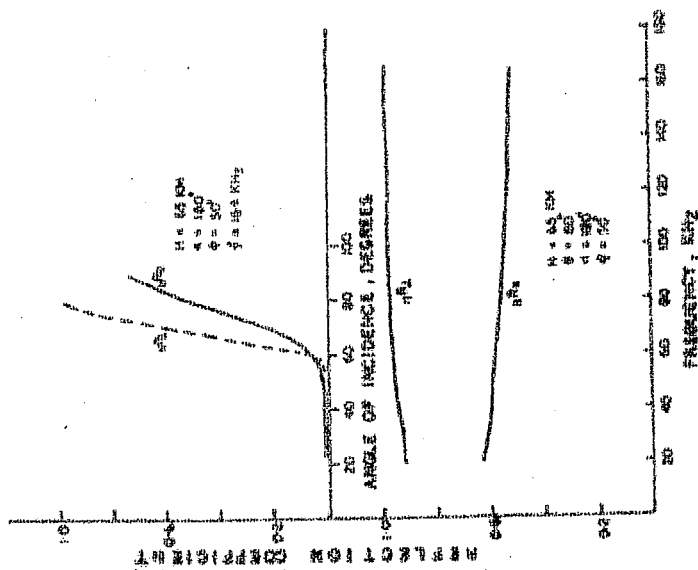


FIGURE 1.12 : Variation of reflection coefficient and conversion coefficient (a) with dip angle (b) with height for different collision frequencies profiles.

given in figure 1.12(b). Here again we have used the electron density profile due to Sagalin and Smiddy of figure 1.1(a). The profile of the reflection coefficient shows a peak around 74 km whereas the profile due to the conversion coefficient show a lower peak. Hence it can be concluded that the 164 kHz radio waves received at Ahmedabad will be reflected roughly from a height of about 74 km if we assume the particular electron density profile of Sagalin and Smiddy. In the figure are also included the effect of changing the collision frequency by 60 percent on the reflecting properties. PIGGOT and THRANE (1966) has suggested an increase of collision frequency by about 60 percent from winter to summer. It is noticed from the figure that though the changes in the corresponding curves are not much nevertheless there is indication that the height of reflection could be elevated. The increase of height of reflection will be actually less than what has been shown if the 60 percent increase on the winter profile of the collision frequency is considered. The reduction of the reflecting property of a particular layer with the increase in collision frequency can be interpreted as the layer becomes more diffused due to the increased absorption of the radio waves. Figure 1.13(a) shows two reflection coefficient height profiles at frequencies of 50 kHz and 164 kHz for identical paths of propagation. It is noticed from the figure that the dominant reflection height of 50 kHz is about 70 km whereas that of 164 kHz is about 75 km, which suggests that for the identical ionospheric

and propagation conditions lower frequencies are reflected from the lower heights.

In these calculations we have used the electron density profile due to Satyaprakash given in figure 1.4(a). Figure 1.13(b) shows that the components of the reflection coefficient matrix will have small values upto the height of about 84 km for 164 kHz radio propagation during night, when the electron densities become very small at lower heights. Hence the radio waves received at Ahmedabad from Tashkent will be reflected from a height of about 85 km during the nocturnal propagation. Here we have used the night-time electron density profile given by SMITH (1961).

In order to get the expected seasonal daytime variation of the reflection heights of 164 kHz signals received at Ahmedabad we have used the winter and summer electron density profiles at mid-latitudes by Metchly<sup>t</sup> and Smith shown in figure 1.5(b). The possible variation of collision frequency from summer to winter has not been considered. The results are shown in figure 1.14(a) and 1.14(b). It is noticed from the figures that during winter the reflection of 164 kHz radio waves will take place from a height of about 80 km whereas during summer from a height of about 68 km. In interpreting our studies on the experimental results of 164 kHz field intensities we will consider the reflection heights during summer and winter as  $70 \pm 2$  km and  $78 \pm 2$  km respectively. The reflection height during the equinoxes will

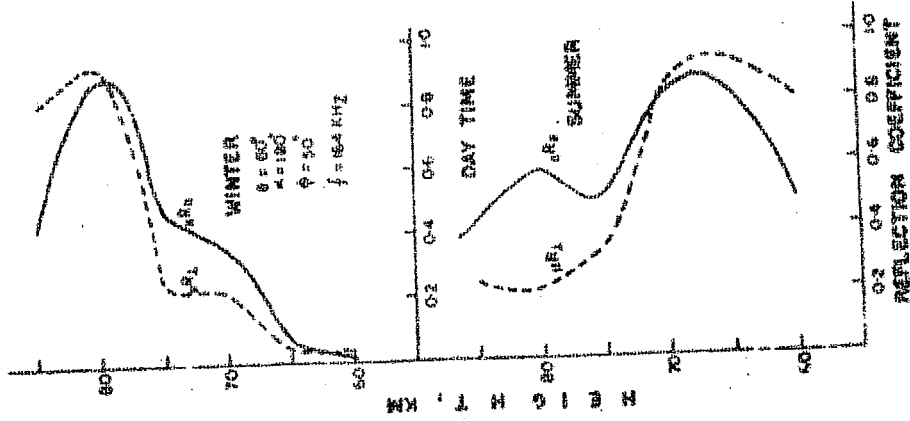


FIGURE 1.14 : Height profile of reflection and conversion coefficient of 164 kHz radio waves during winter and summer.

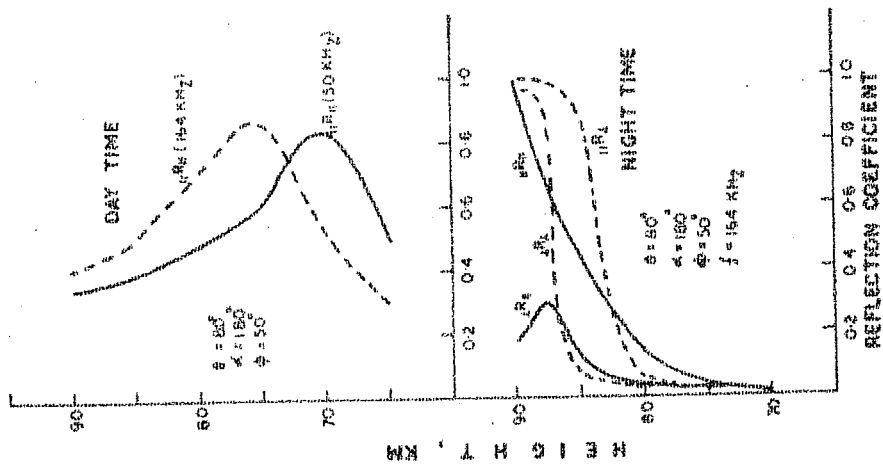


FIGURE 1.13 : Variation of reflection and conversion coefficients with height during day and night time conditions for radio frequencies of 164 kHz and 50 kHz.

lie near to the winter values ( about  $76 \pm 2$  ). During certain winter anomaly days the reflection heights may come down considerably.

#### 1.7 Conclusion

The characteristics of 164 kHz radio waves received at Ahmedabad from Tashkent can be summarised as follows:

- (1) The ground wave intensity becomes negligible at a distance of about 800 km from the transmitter
- (2) The angle of incidence of these waves is about  $80^\circ$ .
- (3) The heights of reflection of these radio waves are about 70 and 76 km during summer and winter seasons respectively.

CHAPTER - II

STUDIES ON THE GENERAL BEHAVIOUR OF 164 kHz RADIO  
SIGNAL STRENGTH VARIATIONS DURING QUIET DAY CONDITIONS

2.1 Introduction

The diurnal and seasonal variations of the 164 kHz signal intensity <sup>transmitted from Tashkent and</sup> during the period 1960 - 61 received at Ahmedabad have been discussed by ALURKAR (1963). From the simultaneous observations of these radio signals at Ahmedabad and Poona a comparative study of the diurnal and seasonal variation for the years 1963 - 64 has been presented by ANANTHAKRISHNAN (1967). A possible control of the daytime value of field strength by the background solar X-ray (  $1 - 8 \text{ \AA}$  ) has been suggested by ANANTHAKRISHNAN and RAMANATHAN (1967). The present study deals with the diurnal and seasonal changes during low, medium and high sunspot years at Ahmedabad. An explanation of these variations is attempted in terms of changes in the reflection coefficients and of ionizing radiations responsible for the formation of the quiet D-region. Information about the photo detachment of electrons, from dominant negative ions during sunrise has been derived from the effective ozone screening heights. Some cases of anomalous signal intensities during winter have been studied in relation to sudden changes in stratospheric temperatures.



2.2

Typical diurnal and seasonal variations at Ahmedabad, Poona, and Gulmarg

A pair of typical summer records of 164 kHz radio intensity observed at Ahmedabad during a moderately high solar activity year, 1970 is shown in figure 2.1. The signal intensity starts falling from the high night-time values at about 0505 hr which is 40 minutes earlier than the ground sunrise time. The atmosphere below the nighttime level of reflection of 164 kHz radio waves will begin to be irradiated by sunlight when the sun is 8° 9' below the horizon and the absorption is increased. The drop in intensity continues and a minimum value is reached a little after ground sunrise time; from this point the signal strength starts increasing. The absorption of the radio waves decreases because the waves start getting reflected from a lower layer of ionisation. The reflectivity of the layer improves with the enhanced ionisation and we get a maximum signal strength around local noon. The situation is reversed after local noon and the field strength starts decreasing till it reaches a minimum around 1845 hr. Thereafter because of sunset the ionising radiations are cut off resulting in the fast disappearance of electron density, hence signal intensity slowly increases reaching a nighttime level. This increase in intensity after sunset is very rapid in the record of 13 July 1970 whereas it is gradual in the 9 August 1970 records. A small peak in the intensity before finally getting into night-conditions can be seen in both

days records. It can be inferred from these records that throughout the day the signal intensities are fairly regular with a variation which arises due to the zenith angle changes of the sun. This type of systematic variation of signal strengths are observed from the month of June upto about the second week of October. For the rest of the year the amplitudes of radio waves are more variable showing oscillatory features specially after sunrise and before sunset.

Figure 2.2 shows two records of daytime field intensities registered at Ahmedabad during local winter. A marked difference between these records and those during summer can be observed. On 1 February 1969 after the sunrise drop in intensity there are two prominent peaks around 0755 hr and 0840 hr and one peak around 1700 hr before sunset. Though the signal intensities are higher during noon hours, there is no systematic variation of intensity from 1100 hr to 1500 hr as could be ascribed to solar zenith angle changes. The observations on 15 January 1970 show that the peaks after sunrise are present at around 0735 hr and 0810 hr with a less prominent peak before sunset. The signal intensity after increasing upto 1000 hr starts decreasing showing a low value during local noon. Though there is some solar zenith angle control on the post sunrise and pre-sunset maxima, there is no set pattern of variation during the rest part of the day.

So far as the variation of field amplitudes of 164 kHz radio waves at Ahmedabad and Poona are concerned we will define

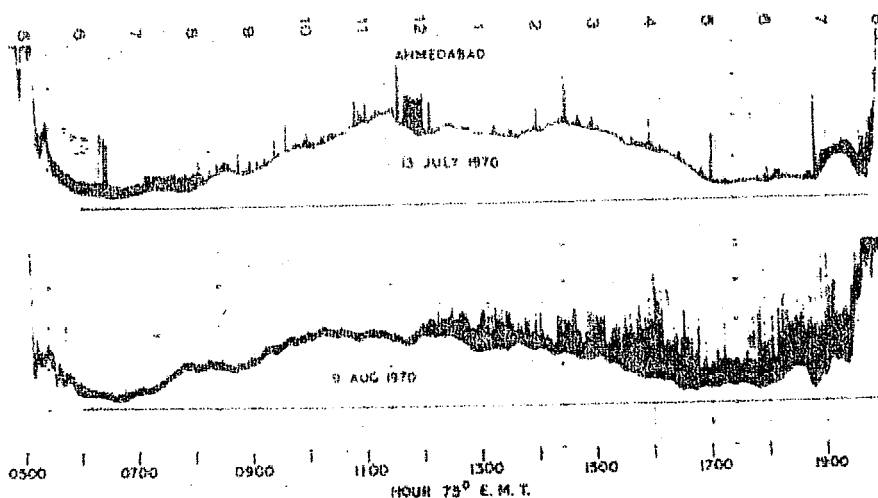


FIGURE 2.1

Two typical daytime summer records of 164 kHz radio intensity received at Ahmedabad during 1970.

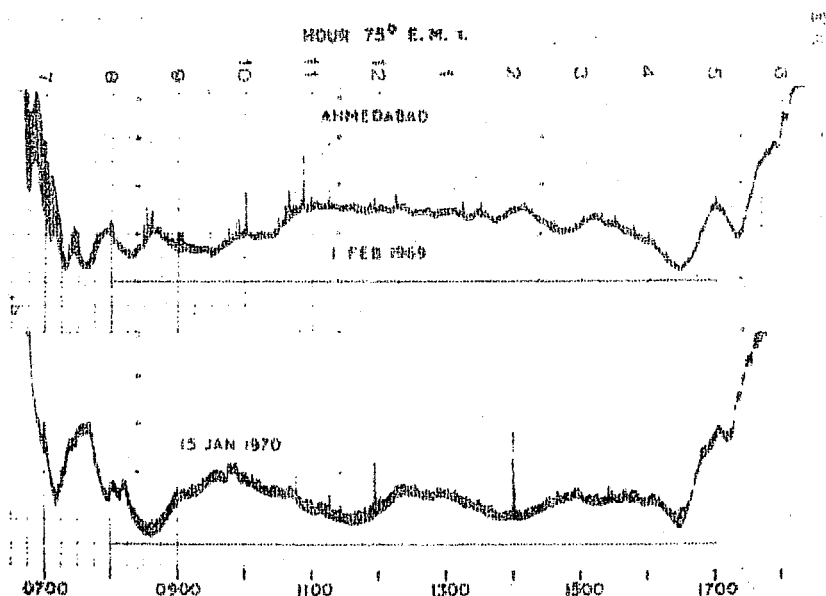


FIGURE 2.2

the equinoctial months as March and April only, because the summer type of variation continues upto October. Nevertheless some features of equinoctial variations would be seen in the second half of October. Field strength observations for two days in March are shown in figure 2.3. It can be noticed that after the occurrence of the post sunrise oscillatory features, radio signal intensity shows a rise upto around 0900 hr. Thereafter some change in the ionosphere takes place which inhibits further enhancement of the signal. Rest of the features are similar to those of winter conditions but there are some shorttime irregular variations. These can be seen from the record on 23 March 1970 also.

In order to demonstrate the effect of increasing the radio-path we have selected two records taken simultaneously at Ahmedabad and Poona which are shown in figure 2.4. The marked similarity in the nature of variation of 164 kHz radio signals at the two stations can be seen from the figure. From a detailed study of these simultaneous observations, ANANTHAKRISHNAN (1967) has shown that the amount of absorption from the non-peak to the minima on either side is about 5 dB less in Poona than at Ahmedabad during summer months. During the rest of the year the intensities at Poona also show large variability.

Simultaneous records of the radio intensity observations at Ahmedabad and Gulmarg ( nearer to the transmitter ) are shown

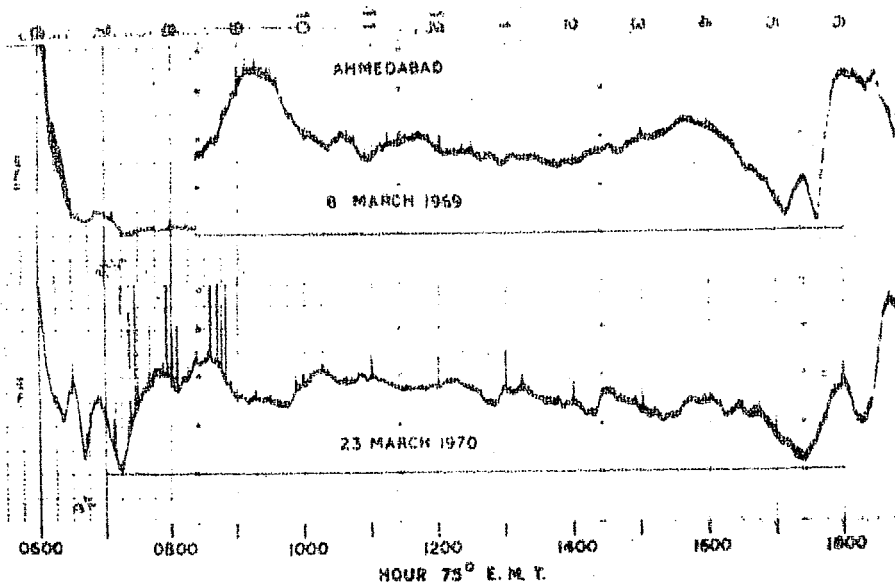
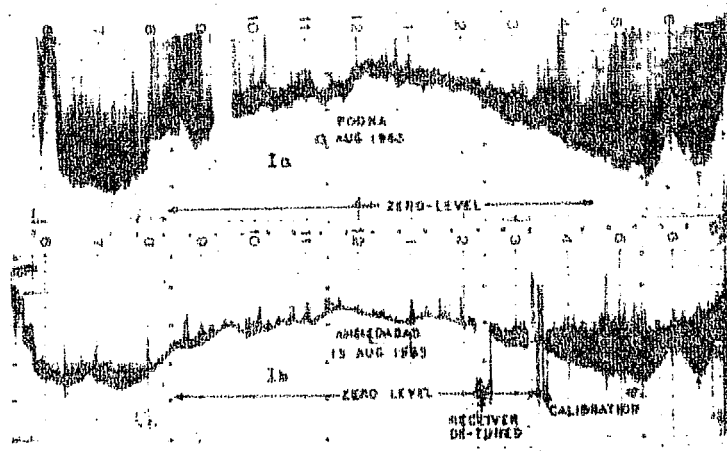


FIGURE 2.3

Field-strength observations of 164 kHz radio waves received at Ahmedabad during two equinoctial days of 1969-70.



Records of 164 kHz radio amplitudes received simultaneously at Poona and Ahmedabad on 13 August 1963.

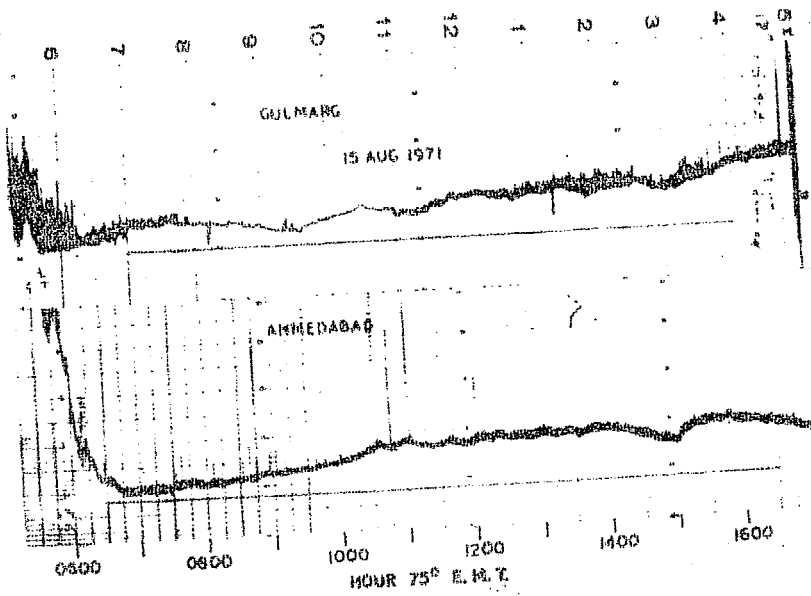
FIGURE 2.4

in figure 2.5. It can be noticed that the variations at the two places are similar except during the period 1- 2 hrs earlier than the sunset time. During this period the signal amplitude increases at Gulmarg whereas it decreases at Ahmedabad.

### 2.3 Average hourly variation of signal intensity at Ahmedabad

We have seen that the signal strength of 164 kHz radio waves at Ahmedabad shows systematic variation from June to September ( summer months ), The intensity change are irregular during the rest of the year, so much so, that it becomes highly variable during March - April ( equinoctial months ). However some features of the variations even during the non-summer months occur systematically. It has been observed that the prominent post-sunrise peak occurs when the solar zenith angle is between  $55^{\circ}$  to  $59^{\circ}$  at Ahmedabad. Similarly the pre-sunset peak occurs for zenith angles between  $67^{\circ}$  -  $71^{\circ}$ . Hence these peaks will shift from month to month according to the changes in solar declination.

In order to understand the variation of signal intensity from month to month the average hourly values starting from the end of sunrise effect to the beginning of sunset effect are computed for each month. The hourly values affected by solar flares are excluded from this analysis. In figure 2.6 we have plotted the hourly average values for the different months of 1969.



Simultaneous observations of 164 kHz radio waves at Gulmarg and Ahmedabad on 15 August 1971.

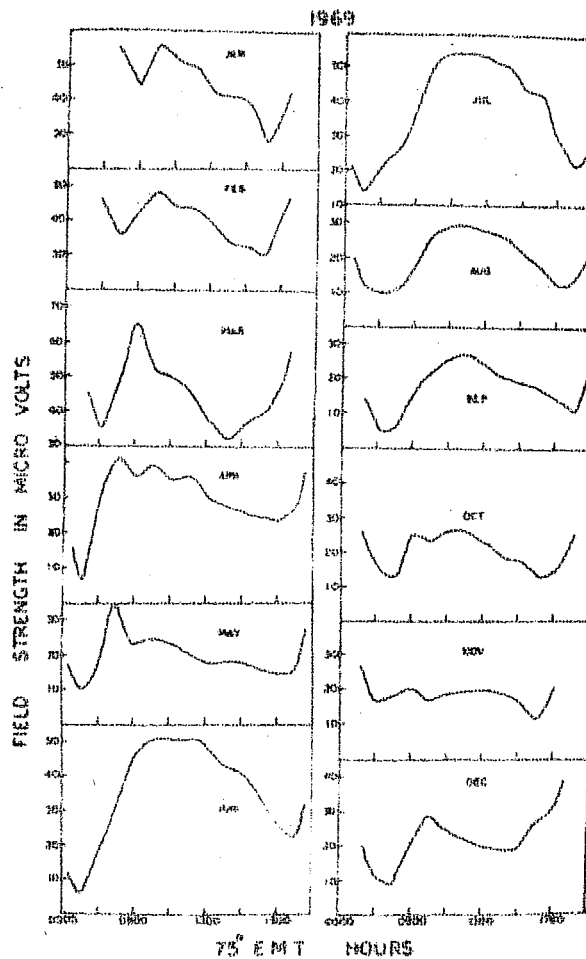
FIGURE 2.5

It can be noticed that during the summer months ( viz. June to September ) the amplitude variations follow a  $\text{Cos}^n \chi$  law, value of  $n$  lying between .95 to 1.50. During the rest of the months the post sunrise peaks show systematic shifts from January to May and October to December. The radio amplitude variations after this post sunrise peak do not follow any set pattern. The relative amplitudes of signal strength during the months September to December are lower than the values for the remaining months.

Figure 2.7 shows similar variations of signal intensities for the year 1970. The morning peaks during March to May are very distinct. The peak is not clear for the month of January because a maximum has appeared around local noon time. For the month of February the signal intensities are very high just after sunrise hence the peak is not clear. Other features compare well with the variation during 1969.

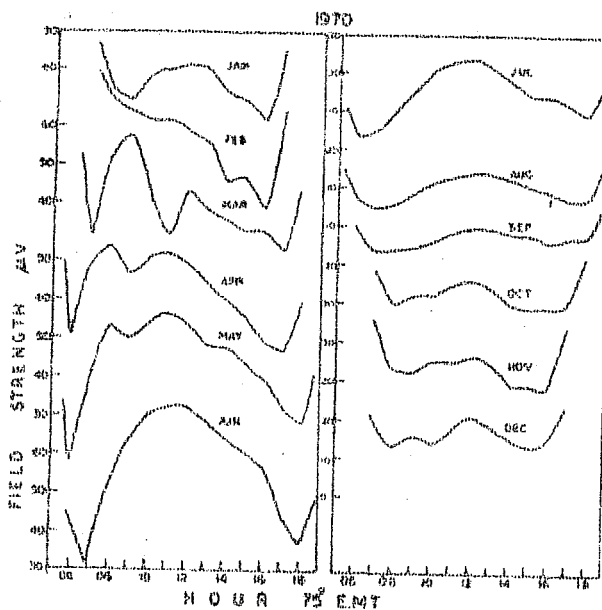
In order to investigate whether the general pattern of variations changed with the change in solar activity the whole data of 164 kHz field strength at Ahmedabad from 1960 to 1970, covering a sunspot cycle, were scrutinised. It was observed that every year the same types of variation repeated. In order to have some comparison of the respective amplitudes in relation to the local noon values, the average hourly values for each month were divided by the corresponding noon time values, i.e., the





Hourly average field strength of 164 kHz radio waves for different months of 1969.

FIGURE 2.6



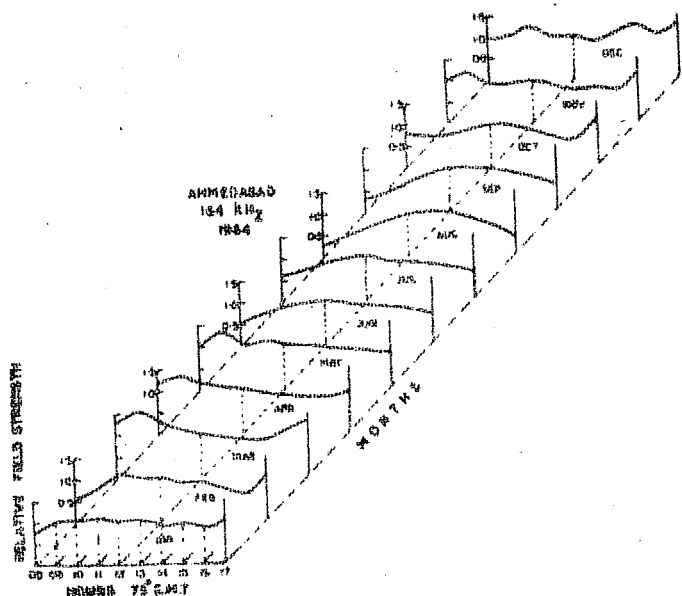
Hourly average field-strength of 164 kHz radio waves for different months of 1970.

relative field strength values of each hour were computed normalised to the 1200 hr values. In figures 2.8 and 2.9 we show the variations of these relative field strengths for all the months during 1964, and 1969 corresponding to low and high solar activity years, respectively. The data from August 1964 - December 1964 has been taken from the intensity measurements at Poona since the experiment was not in operation for that period at Ahmedabad. This is justified because the variation trends are similar for the two places.

It is interesting to find that the summer and non-summer type of variations do not change with the solar activity. The minimum value of signal intensity occurs around noon for the summer months and at the post sunrise peak for the other months.

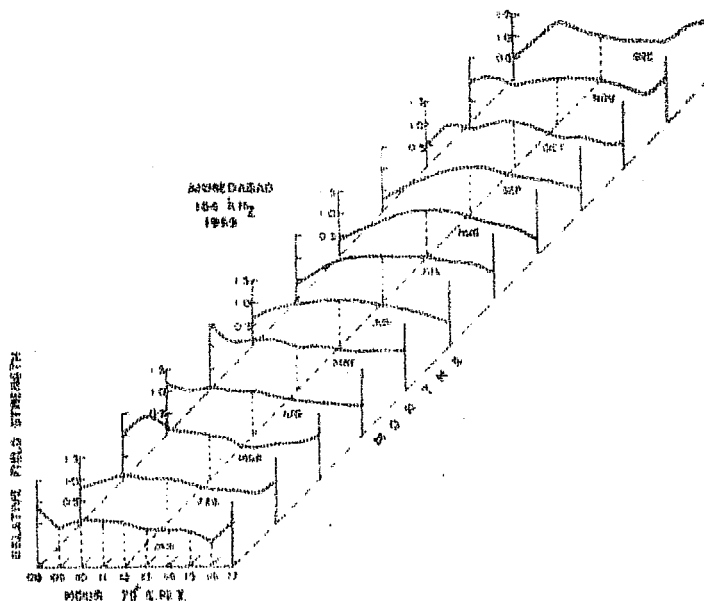
Figures 2.10 and 2.11 are presented to demonstrate that the relative amplitudes during different months varies with the change in solar activity. The increase in the signal strength for the month of June - July in relation to other months is clearly brought out from these figures.

It can be concluded that the general system in which the 164 kHz radio signals intensities vary from month to month remains almost unaltered by the different conditions of solar activity.



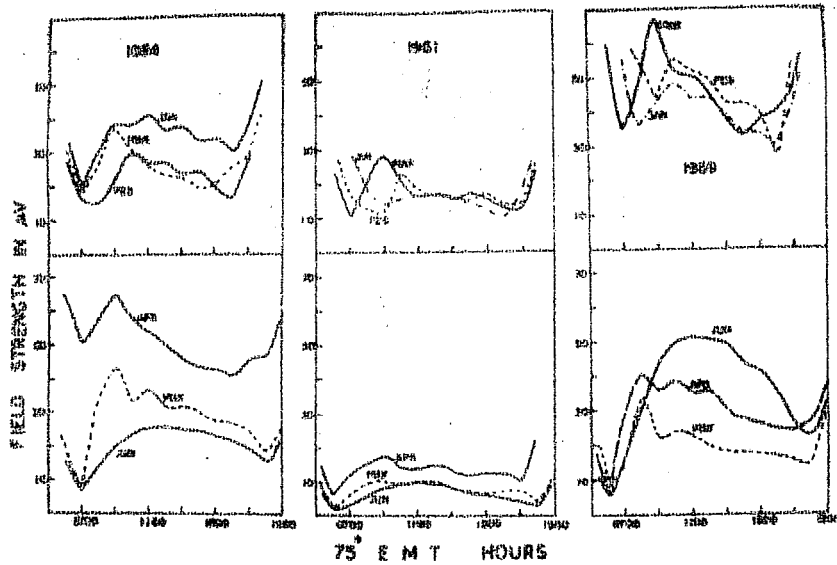
Average hourly field strengths for different months normalised to the noontime values for a low sunspot year 1964.

FIGURE 2.8



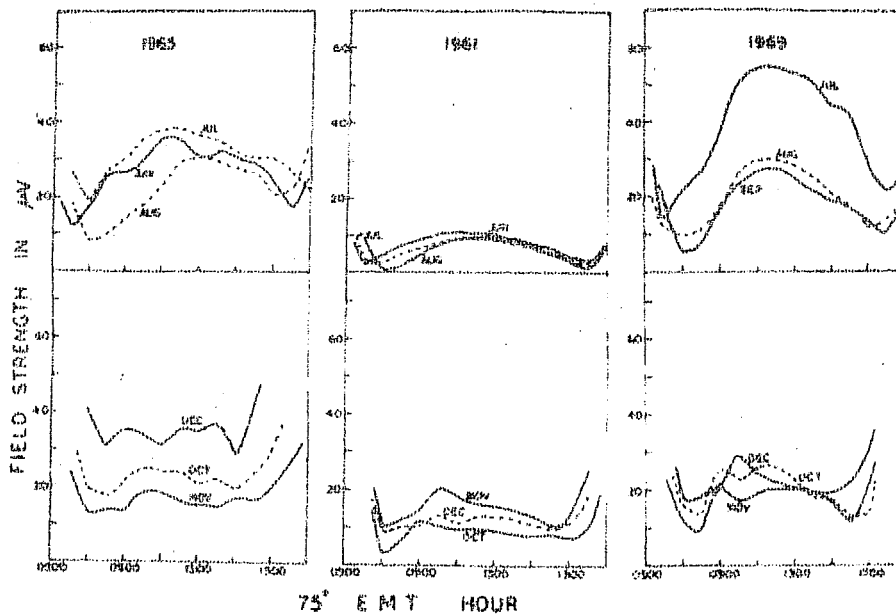
Average hourly field strengths for different months normalised to the noontime values for a high sunspot year 1969.

FIGURE 2.9



Relative amplitudes of radio intensities averaged over the months January-June for low, medium and high sunspot years (1964, 1961, 1969).

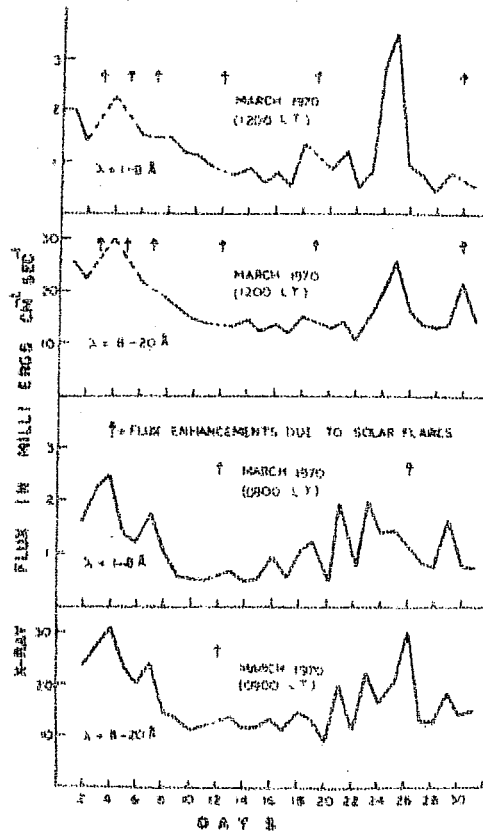
FIGURE 2.10



Relative amplitudes of radio intensities averaged over the months July - December for low, medium and high sunspot years (1965, 1961, 1969).

2.4 Effect of quiet sun background X-rays in the control of radio signal amplitudes

It has been shown that solar background X-ray flux ( $1 - 8 \text{ \AA}$ ) is important so far as the formation of upper D-region is concerned. Hence the study of the signal strength variation with respect to the corresponding changes in X-ray flux will be appropriate. The hourly average values of X-ray fluxes in the wavelength bands between  $1 - 8 \text{ \AA}$  and  $8 - 20 \text{ \AA}$  published in Solar Geophysical data bulletins as measured from the satellite SOLARD-9, are utilised for the present comparative study. It is known that the softer X-rays above the wavelength of about  $10 \text{ \AA}$  will be more influential in producing the effect above 90 km. Also it has been found that the average hourly values of the fluxes in the two above mentioned bands vary in a similar manner. This fact is presented in figure 2.12 by plotting the average hourly data for 1200 hr and 0900 hr local time during March 1970. The true nature of the covariation of the fluxes in the two bands is quite clear. Hence for our purpose it will be sufficient to consider only the fluxes in the  $1 - 8 \text{ \AA}$  wavelength band. The data of 164 kHz field strength changes during 1969-70 are studied with respect to the highly variable solar X-ray fluxes integrated for the wavelengths of  $1-3 \text{ \AA}$ . Some very interesting results have emerged which will be illustrated in this section. The midday values of signal intensities and the average X-ray fluxes ( $1 - 8 \text{ \AA}$ ) for one hour centred around the noon are plotted against all the days of a



Comparison of the variations of solar X-ray flux in the wavelength bands 1-8 Å and 8-20 Å separately for March 1970 ( 1200 hr L.T.) and March 1970 (0900 hr L.T.)

FIGURE 2.12

particular month to have a day to day comparison. Fig.2.13 shows the parallel variations of field strengths and X-ray fluxes during April 1969. A close inspection of the figure reveals that the field intensities increase with the decrease in X-ray flux and vice versa. The maxima in X-ray flux variation are associated with the simultaneous minima in the signal strength. The larger enhancements of X-ray fluxes on 11 and 26 April have been rise to bigger depressions. Almost all the maxima and minima of X-ray fluxes are anti-correlated with the maxima and minima of 164 kHz radio amplitudes. Similar correlation has been found for the variations during other equinoctial months.

Figure 2.14 shows similar diagram during the winter month January 1970. Though there is an anti-correlation, it is not very clear. From similar such comparison of field strength data and X-ray fluxes during other winter months it becomes definite that the variations in the opposite senses is not as definite as that for the equinoctial months ( March, April and November ).

In order to show the correlation during summer months we have plotted the radio amplitudes together with X-ray fluxes during June 1969 in figure 2.15. It can be noted that the signal intensities do not vary in a opposite way compared to that changes in X-ray fluxes. It is interesting to find that the intensities of radio waves are higher between 3 to 15 June 1969

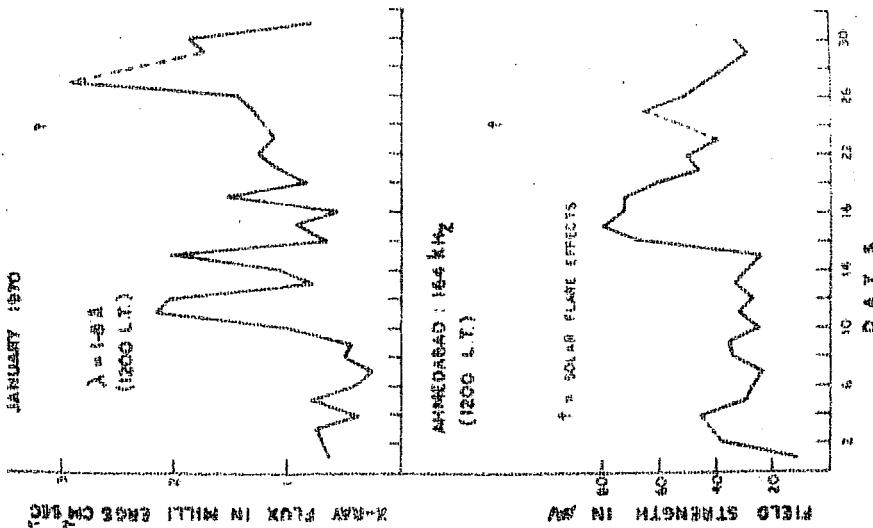


FIGURE 2.14

Variations of solar X-ray flux ( 1-8 Å) and field strength of 164 kHz radio waves during April 1969 (1200 hr L.T.).

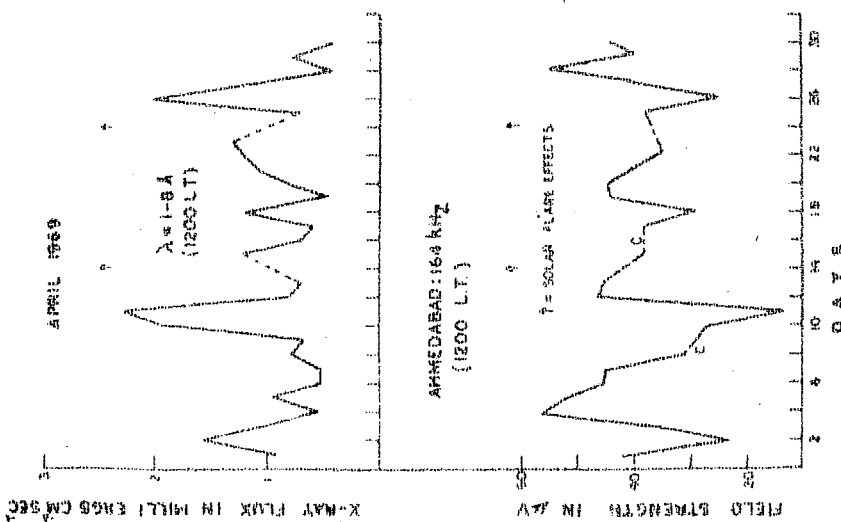
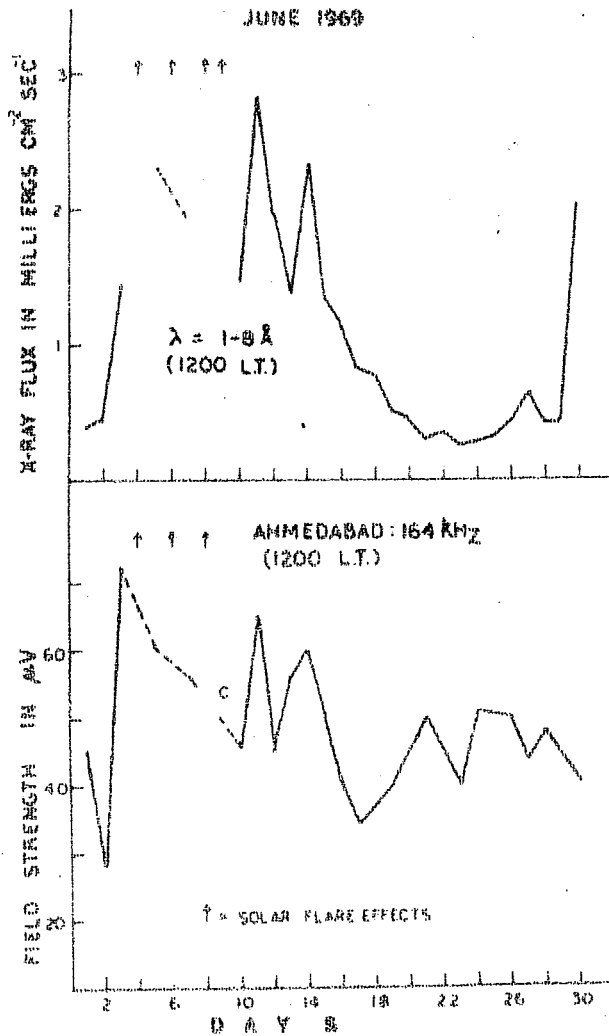


FIGURE 2.13

Variations of solar X-ray flux ( 1-8 Å) and field strength of 164 kHz radio waves during January 1970 (1200 hr L.T.).





Solar X-ray flux ( 1-8 Å ) variations  
alongwith 164 kHz radio intensity variations  
during June 1969.

FIGURE 2.15

inspite of the higher values of X-ray fluxes during the same period. Also, the field strengths do not show any enhancement during the period when the X-ray fluxes were low. In other words the signal intensities do not vary in opposite senses as observed during other seasons. From similar observations during other summer months it is found that the behaviour of signal intensities are similar to those of X-ray fluxes indicating a positive correlation in contrast to the negative correlation found in non-summer months. It can be mentioned that ANANTHAKRISHNAN and RAMANATHAN (1967) also noticed that during June 1966, the large X-ray enhancements in the background solar X-ray flux did not give rise to low values of field intensities of 164 kHz radio waves received at Ahmedabad. The values of correlation coefficient calculated for different months are collected in Table 2.1. It can be seen that during summer months there is a positive correlation whereas during other months it is negative. Also it can be observed that during March 1970, the anti-correlation is clear between 1300 - 1500 hr whereas the behaviour is reversed for morning hours ( viz. 0900 hr ). During summer months no marked change in the behaviour for the morning hours has been noticed.

## 2.5 Interpretation of the results on the general variation of 164 kHz radio signal amplitudes

We will attempt to explain the results described so far on the variation of signal intensities of 164 kHz radio waves. For this purpose, as computed in chapter I we will assume the

Table 2.1

Correlation coefficients of the variations  
of 164 kHz signal strength and quiet solar  
X-ray ( 1 - 8 A )

Year	Month	No. of obs.	Time (L.T)	Correlation coefficient
1969	April	25	1200	-0.84
1969	November	23	1200	-0.33
1969	December	25	1200	-0.20
1970	January	25	1200	-0.10
1970	March	24	0900	+0.28
1970	March	26	1300	-0.67
1970	March	24	1500	-0.39
1970	April	27	1200	-0.63
1969	June	23	1200	+0.53
1970	June	22	1200	+0.55
1970	July	25	1200	+0.10

reflection heights of these radio waves to be about 70 km and 78 km during summer and non-summer months respectively for their reception at Ahmedabad. The similar kind of variation at Ahmedabad and Poona will arise because the angle of incidence will not change appreciably for an increase of about 400 km in the radio-path, so that the heights of reflection will roughly be same for the two places.

At 70 km in the ionosphere the main ionising source will be Lyman $\alpha$  for getting free electrons from the atmospheric constituent Nitric Oxide. Since the Lyman $\alpha$  flux does not change much from day to day, the electron densities at these heights will be fairly constant except for the diurnal variation which can be expected by the variation of solar zenith angle. If the radio waves are reflected from 70 km height during summer months, the signals after sunrise effect will grow with the growth of electron density around this height. The reflectivity of the layer will go on improving because of increase in production of electron densities by Lyman $\alpha$ . After the maximum electron densities are attained around noon the reverse processes will start acting and the signal intensity will reduce until sunset. Hence the regular summer variations are quite satisfactorily explained by assuming that Lyman $\alpha$  is the dominant source of ionisation around 70 km. X-ray fluxes which are more variable compared to Lyman $\alpha$  are not able to produce significant changes of ionisation below the reflection level during summer months.

But sometimes it may be possible that they add a little to the electron densities of the reflecting layer near 70 km thus improving the reflection coefficient. Hence the signal strength level may be increased slightly because of enhancement of X-ray fluxes.

The situation is quite different for the higher reflection height of 78 km during winter months. The ionisation around these heights will be controlled both by Lyman  $\alpha$  and X-rays ( 1 - 8 Å). After sunrise the signal intensity increases because the reflectivity of the layer goes on increasing due to the electron densities caused by Lyman  $\alpha$  and X-rays. After the radio wave amplitudes attain a maximum value some time before noon, the X-rays become the dominating ionising agency and because of increasing influence of X-rays, producing more electrons below the level of reflection, this gives rise to the decrease in field intensities. The signal intensities thereafter will vary depending on how X-ray fluxes are changing. An increase in flux will be associated with the attenuation of the signal

strength and vice versa. The X-ray fluxes vary with the zenith angle and with the different radiating conditions in the sun. In most of the cases the zenith angle dependence will be masked by the large hour to hour changes. Also the general level of the signal intensities after the pre-noon peak will depend upon the average values of X-ray fluxes for any particular hour. Hence during winter months the signal intensities for most of the day varies in a way opposite to that of X-ray. For heights between 70 -78 km the variations can be a mixture of both summer and winter types. From the observations, the anti-correlation between the radio amplitudes and X-ray fluxes seem to be better during March - April and November as compared to the other non-summer months.

2.6 Sunrise effects on 164 kHz signals transmitted from Tashkent and received at Ahmedabad and their interpretation

It is found that there is a large and sudden decrease in the amplitude of the 164 kHz radio waves transmitted from Tashkent and received at Ahmedabad commencing at a time when the sun is below the horizon. A systematic study of this has shown that in general the signal intensity undergoes a rapid drop in intensity, beginning at a time when the value of the solar zenith angles is between  $99^\circ$  and  $96^\circ$  and that this decrease continues until the intensity reaches a low value near the time of ground sunrise (ALURKAR, 1963). In this section we shall examine the variation of this time with season during the period 1968-70 and attempt to explain them.

During the sunrise period, the photodetachment of electrons from negative ions results in a rapid increase in D-region electron densities. H<sup>U</sup>OLTQVIST (1966) from various techniques of observation has shown that the changes in electron density of the D-region can be explained if we assume that the D-region sunrise and sunset effects are mainly controlled by the shadow of the ozone sphere

rather than by that of the solid earth. The pre-sunrise rocket measurements and the simultaneous ground data of VLF observations as analysed by SECHRIST (1968) show that the time when VLF intensities show a marked decrease during sunrise, is associated with the rocket electron density profiles showing larger electron densities between 80 - 90 km height region. From the calculations of zenith angles, it has been concluded that the VLF sunrise effect will mostly be due to the photodetachment of electrons from negative ions by solar ultraviolet radiation. From this point of view,  $O_3^-$ ,  $NO_2^-$  have been suggested to be the dominant negative ions in the D-region (REID, 1961; WHITTEN and POPPOFF, 1964; BOWHILL and SMITH, 1966).

Considering the geometry of the pre-sunrise photodetaching radiation on the absorption of 164 kHz radio waves the solar depression of  $99^\circ$  at the time of the sunrise effect can be understood. As the photodetachment of electrons from the negative ions around 85 km will give rise to enhanced electron production and will result in the absorption of 164 kHz waves starting at a time when solar zenith angle is about  $99^\circ$ . The effect which is observed at  $99^\circ$  can not be explained in this way as the heights <sup>at</sup> where the photodetaching radiations will reach are much



lower than the normal reflection heights of these radio waves.

The possibility of the recombination of these photodetached electrons is larger for these lower heights owing to higher recombination coefficients.

Hence in order to explain the sunrise effects for  $\chi < 99^\circ$ , the concept of the ozonosphere shadow height has been introduced.

The pre-sunrise geometry will then be modified as shown in figure

2.16b, where  $Z$  is the height at which the ray crosses the zenith

before ground sunrise and  $h$  is the height of maximum atmospheric

density while the photodetaching radiation passes through before

reaching the height  $Z$ . The relation between  $h$  and  $Z$  is given

by

$$h = Z \cos(\chi - 90^\circ) - R [1 - \cos(\chi - 90^\circ)]$$

here the refraction of the ray in the earths atmosphere has been neglected.

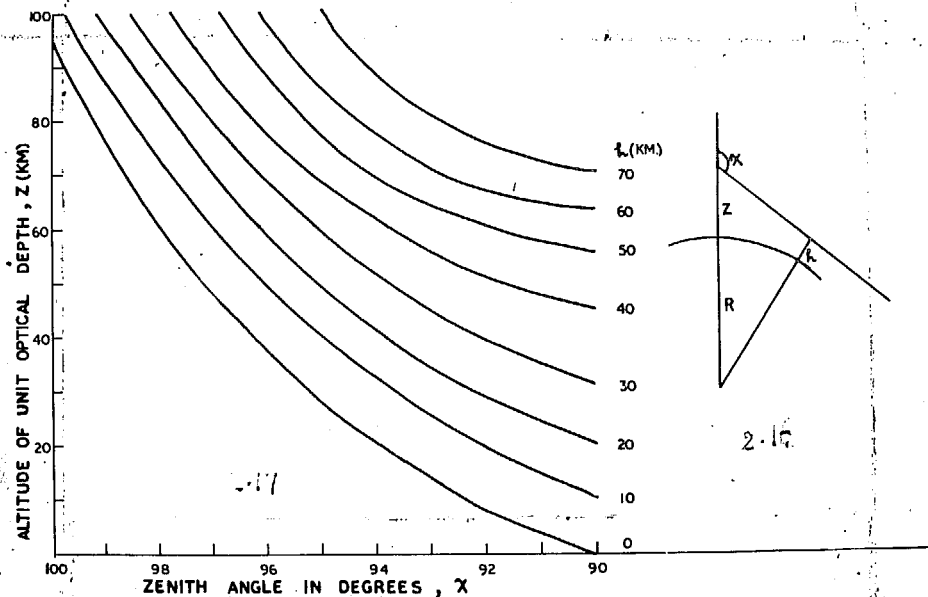
$R$  = radius of the earth

Following Sechrist, the variation of  $z$  and  $\chi$  ( $90^\circ - 100^\circ$ ) for different values of  $h$  has been plotted in figure 2.16a. Here the height of unit optical depth  $z$  is defined as the height where the intensity of the photodetaching radiation is 1% of the intensity outside the earths atmosphere.

We assume that absorption of the low frequency signal intensities begins when a significant amount of electrons is produced below 90 km, which is taken to be the reflection level of these radio waves during night (Chapter I).

The time (corresponding to  $72^\circ\text{E}$  and  $32^\circ\text{N}$ ) of the start of the sunrise drop observed at Ahmedabad in the radio signal intensity for each month during 1968-70 have been studied.

Figures 2.17 and 2.18 show the plots of these times for the months of February and March. Open circles denote the times of



Variation of the amplitude of unit optical depth of solar photodetaching radiation with zenith angle with the minimum ray height as a parameter. The unit optical depth is defined to be the altitude where the intensity of the photodetaching radiation is 1% of the intensity outside the earth's atmosphere.

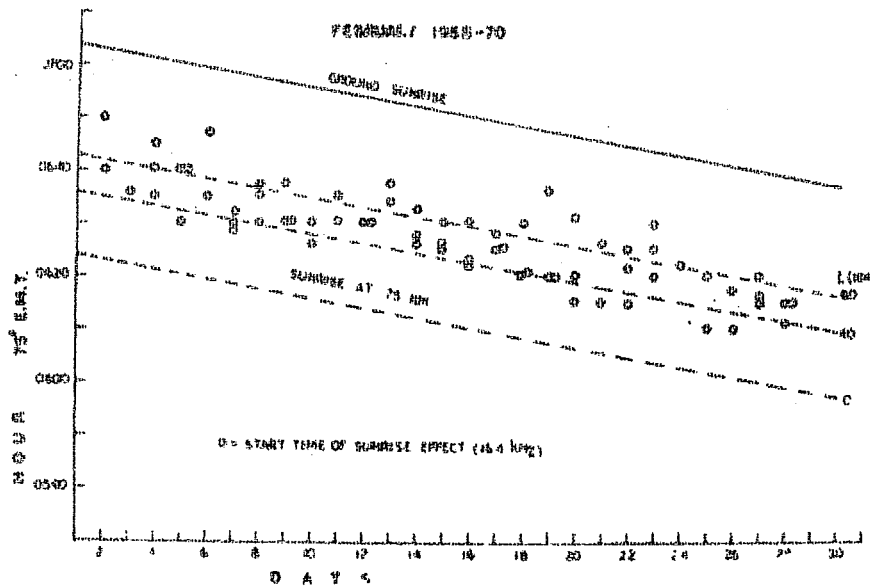
Table 2.2

Electron affinities and corresponding maximum  
wavelengths for photodetachment of negative ions

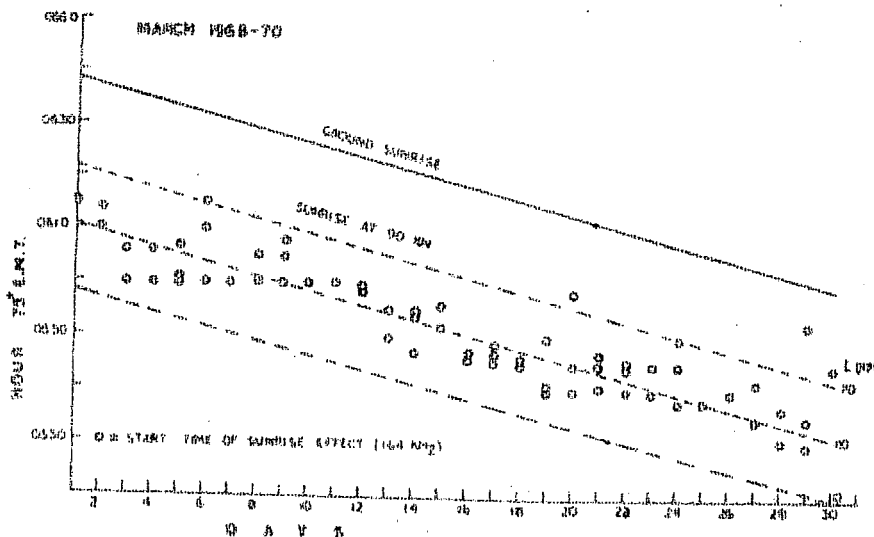
Molecule	Electron Affinity (eV)	$\lambda_{\text{max}}$ (Å)	Reference
O	1.465 $\pm$ 0.005	11,800	Branscomb et al. (1958)
	1.47	11,850	Edlen (1960)
O <sub>2</sub>	1	12,400	Whitten and Poppoff (1965)
O <sub>3</sub>	3.0	4,150	Branscomb(1964)
	1.9	6,500	Wood and D'Orazio (1965)
NO <sub>2</sub>	4.0	3,100	Farragher et al. (1964)
	3.8	3,260	Curran (1962)
NO <sub>3</sub>	3.9	3,180	Freshenfeld et al.(1967)
CO <sub>3</sub>	Still uncertain		

start of the sunrise effect in the radio signal intensity. In these figures the ground sunrise line and the 90 km layer sunrise line for different values of  $h$  are also plotted corresponding to the local time of the latitude and longitude of the mid-point between Tashkent and Ahmedabad ( $32^{\circ}\text{N}, 72^{\circ}\text{E}$ ). It can be noticed that during the month of February the points lie nearly parallel to the 90 km sunrise line with  $h$  values of about 60 km. During the month of March this value is about 55 km. In figure 2.19a and b similar plots for the months of May and December are shown. It can be noticed that the sunrise points lie mostly near the line with the values of  $h$  about 50 km<sup>and 60 km</sup> for the months of May and December respectively. Hence from the start time of the sunrise effects for all the months it can be concluded that the effect starts at the 90 km level over ( $72^{\circ}\text{E}, 32^{\circ}\text{N}$ ) when the minimum ray height lies between 50 - 60 km.

The vertical profiles of ozone and their variations with latitude are known. The ozone concentrations are quite low above

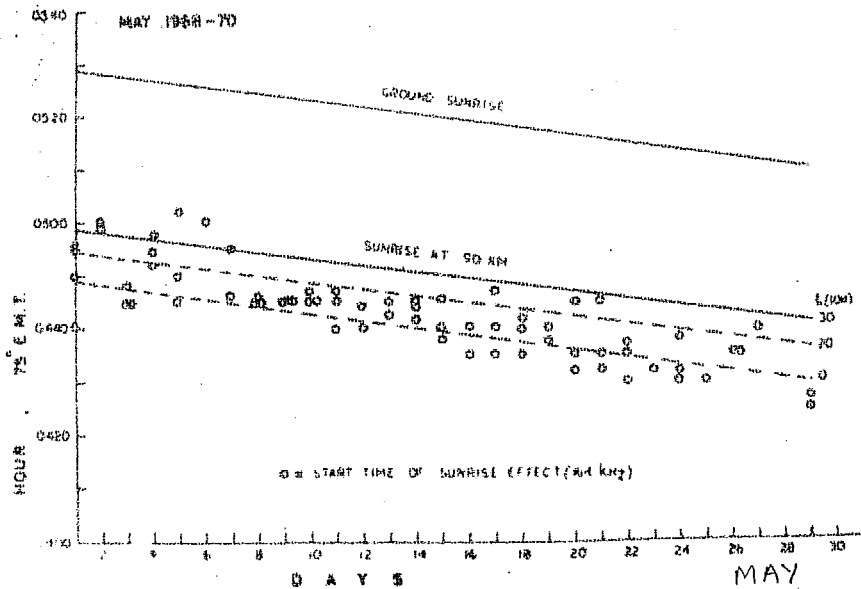


Plot of the start time of the sunrise effect in 16.4 kHz radio amplitudes for different days of February during 1968-70. Solid straight line denotes the ground sunrise times and dotted lines denote the sunrise times at 90 km for different minimum ray heights of 60, 40 and 0 km respectively.



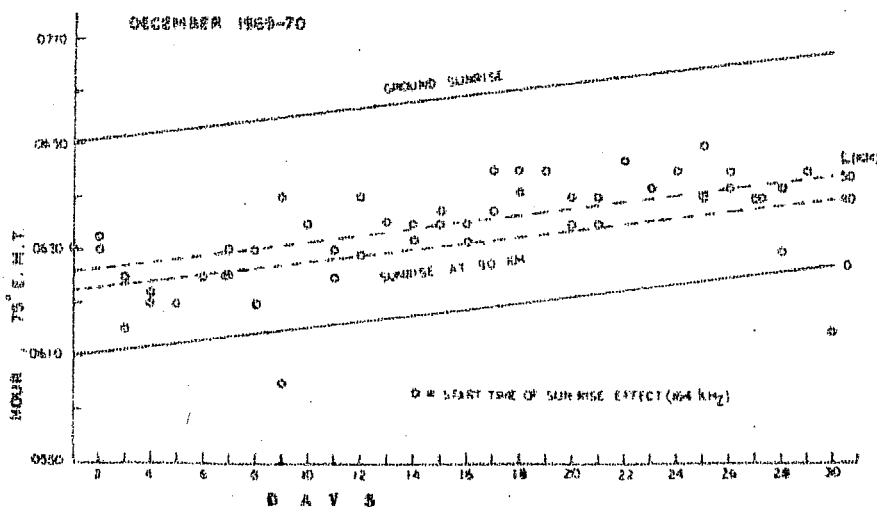
Sunrise time plot for the month of March 1968-70. Broken lines represent sunrise times at 90 km for different minimum ray heights of 60, 50, 40 and 0 km.

FIGURE 2.18(b)



Sunrise time plot for the month of December during 1969-70. Broken lines represent sunrise times at 90 km for different minimum ray heights of 60, 40 and 0 km.

FIGURE 2.19(a)



Sunrise time plot for the month of December during 1969-70. Broken lines represent sunrise times at 90 Km for different minimum rayheights of 60, 40 and 0Km.

FIGURE 2.19(b)

50 km, although there is a small increase during night between 60 and 70 km. Hence it has been suggested that the sunrise effect on low frequency radio propagation starts when the solar ultraviolet radiation of wave lengths of about 2500 Å at which the ozone absorption is maximum reaches the zenith and produces ionisation by the process of photodetachment of negative ions of  $O_3^-$ ,  $NO_2^-$  or  $NO_3^-$ . Table 2.2 lists the different molecules, their electron affinities and the corresponding wavelength of the radiation which can detach electrons from the negative ions. From the table it can be noted that solar ultraviolet radiations produce the photodetachment with maximum efficiency for the negative ions  $O_3^-$ ,  $NO_2^-$ ,  $NO_3^-$  and  $CO_3^-$ .

A comparison of the calculated and experimentally observed (mass spectrometer rocket flights) densities of different negative ion species in the night time D-region has been carried out by ARNOLD and KRANKOWSKY (1971). They have found that the negative ions  $O_2^-$  and  $O^-$  dominate above about 80 km whereas the concentra-



tions of  $\text{CO}_3^-$ ,  $\text{NO}_3^-$  and  $\text{NO}_2^-$  are more below 80 km.

TURCO and SECHRIST (1972) from a series of investigations about the D-region during the sunrise have found that the photodetachment of the terminal ion,  $\text{NO}_3^-$  could contribute largely in the development of the D-region.

In the light of the above investigations our observations of the sunrise effect in the 164 kHz field-strengths can be explained. It can be concluded that the drop in intensity during the sunrise period must be taking place because of the ionisation produced around 80 - 90 km due to the photodetachment of the terminal negative ion,  $\text{NO}_3^-$  by the solar ultraviolet radiation.

~~ionisation produced by the second species increases the reflectivity of the layer which causes the enhancement in the signal amplitude.~~

2.7 Effect of stratospheric temperature variations in the radio propagation during winter

The winter anomaly i.e., the higher electron densities in the D-region during winter against what is normally expected has been explained to some extent by the coupling processes between plasma and neutral gas. It has been shown that the existence of high absorption during some winter days are associated with certain warming events in the stratosphere (BEYNON and JONES, 1965; NESTOROV and TAUBENHEIM, 1965; LAUTER, 1959, 67; DIEMINGER ET AL., 1967 and GREGORY, 1965).

The effect observed in the 164 kHz field strength during winter months reveal that on about quite a few occasions there are groups of 3 - 5 days when the signal intensities are abnormally high compared to other days values. It was noticed that there is no definite change in the condition of solar activity during this period. It is noticed that the days of high field strength are associated with the sudden decrease in the temperatures in the stratosphere at 30 mb level (Free University of Berlin Weather Data is used). The examples are shown in figures 2.20 and 2.21. The temperature data corresponds to the 38° - 40°N, the northern-most reflection point for a two

hop transmission. Similar changes are observed at  $32^{\circ}\text{N}$ , also, though the overall temperature is about  $10^{\circ}\text{C}$  lower. The field strength values are the averages for 1100 - 1300 hr observations. From the figure 2.20, it can be noticed that during November 1963, the field intensity is high between 21st and 27th day and the corresponding stratospheric temperatures are appreciably lower than normal. The 10.7 cm flux variation represents that there is almost no change in the solar activity. In figure 2.21 similar kind of behaviour is shown during December 1965. Hence it can be concluded that during certain days in winter the absorption level of radio waves is considerably low compared to other days and these are associated with the reduction in stratospheric temperatures.

## 2.8 Conclusion

The results presented so far will be summarised in way of conclusions as follows:..

(1) The field-strength of 164 kHz radio signals received at Ahmedabad shows a smooth variation during summer months (June - September ), the intensity reaching a peak value during local noon and falling off on either side. During winter the signal intensities are more variable with the occurrence of one or more humps after sunrise and before sunset. During equinoxes (March - April ) the variations are similar to those

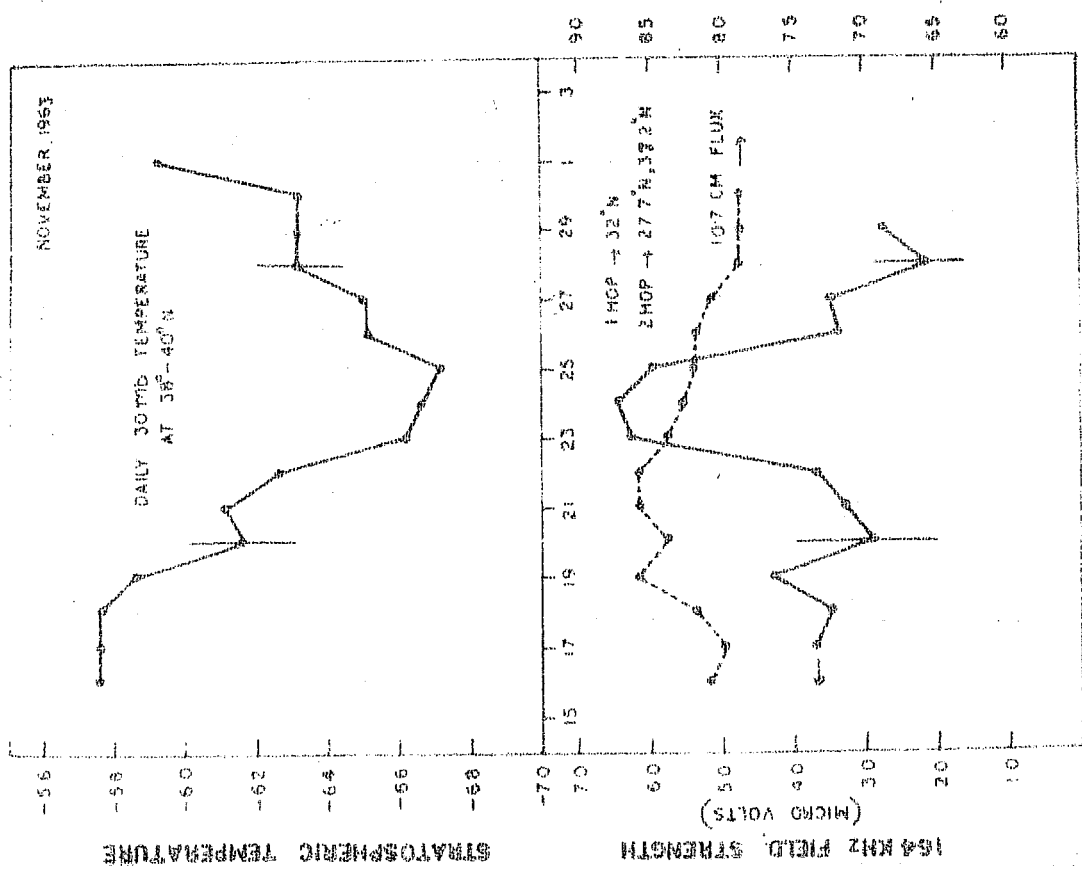


FIGURE 2.20

Variation of stratospheric temperatures and amplitudes of 164 kHz radio waves during November 1963.

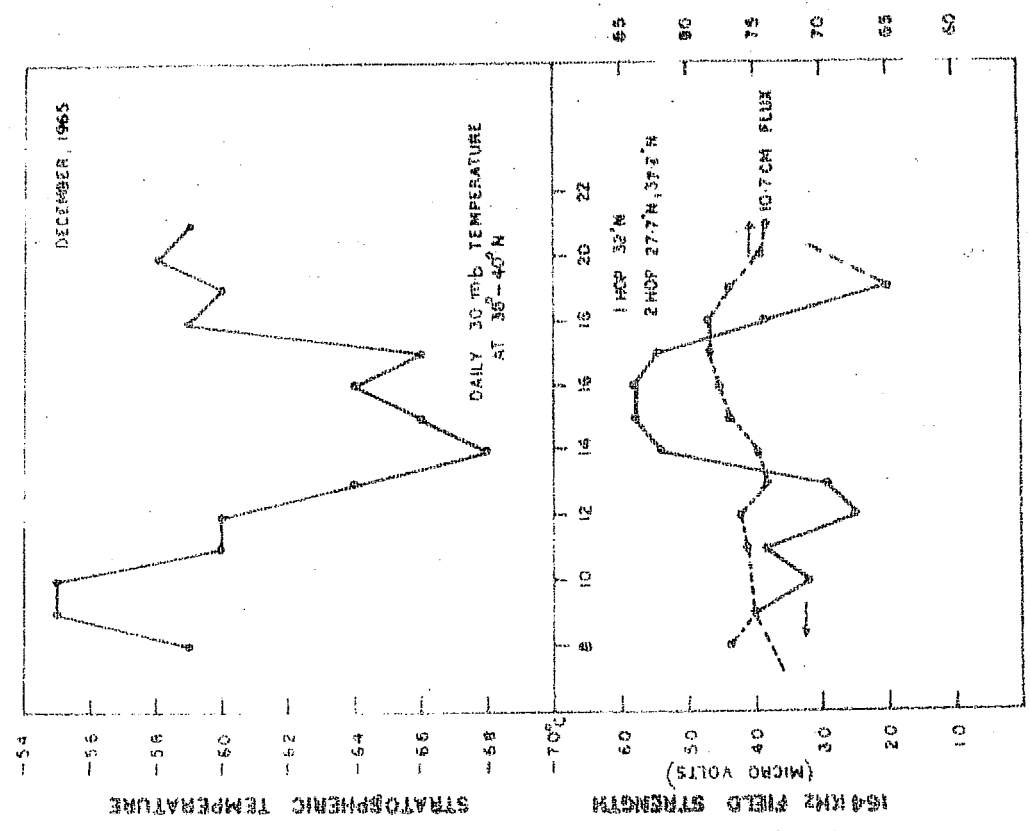


FIGURE 2.21

Variation of stratospheric temperatures and amplitudes of 164 kHz radio waves during December 1965.

during the winter months except for some more short time irregular fluctuations. At Poona the signal intensities show almost similar variation as observed at Ahmedabad. At Gulmarg during summer months the signal intensity shows a slow increase after the noon values.

(2) The general pattern of behaviour of the 164 kHz signal intensities at Ahmedabad during different months remain unaffected by the different conditions of solar activity.

(3) The relative amplitudes during the summer months, specially for June, are higher during a high sunspot year as compared to those during the low and medium sunspot years.

(4) The changes of the level of field intensity as well as the hour to hour variations are both affected by the flux alterations of solar background X-rays (  $1 - 8 \text{ \AA}^0$  ). During the non-summer months there is in general an anti-correlation between the two whereas during summer months either they show a positive correlation or no-correlation.

(5) The diurnal and seasonal variations can be interpreted by estimating a change in the general reflection heights with season. During summer the radio waves are reflected from a lower height of about 70 km where the ionisation is mainly governed by solar Lyman  $\alpha$  radiation. In winter season the radio waves are reflected from a higher level of about 78 km

in the ionosphere where solar X-ray fluxes are very influential. The whole pattern of these variations remaining unaffected by sunspot number changes is explained by the reason that the reflection heights of these radio waves do not change appreciably with the solar cycle.

(6) The sunrise effect in the field strength is observed as a drop in the intensity when the sun is below the horizon by about 6 - 8 degrees.

(7) The solar ultraviolet radiation controlled by a ozone screening height produces photo-detachment of the terminal ion  $\text{NO}_3^-$ . The ionisation produced by this effect gives rise to the sunrise effect in 164 kHz radio intensities.

(8) It has been observed that during the winter months, specially between December - February, there are quite a few cases of a group of days when there is considerably less absorption of the radio waves, these seem to be related with the appreciable reduction in stratospheric temperatures.

## 2.9 Discussion

The observations regarding the propagation of radio frequencies in the low and very low frequencies have been carried

out mostly at frequencies below 100 kc/s for short as well as very long distances. The references have already been given in chapter 1.5. On frequencies greater than 100 kHz the wave propagation for long distances (  $\approx 2000$  km ) have not been widely studied, except some experimental results given by LAUTER (1967). Very low frequency ( below 30 kHz ) propagation over very long distances have been found to show a steady picture as they are reflected from the C-layer of the ionosphere. It is expected that the propagation of very low frequencies over short distances may be equivalent to the propagation of low frequencies over large distances. Keeping this in view we have collected the midday reflection heights of LF and VLF radio waves along with the height changes from day to night based on some important observations all over the world; which is shown in Table 2.4. In this table we have also included the theoretical values as estimated for 164 kHz radio signals received at Ahmedabad. It can be noticed that during winter the reflection heights are in general higher by about 3 - 5 km compared to the summer values. It can also be noted from Lauter's results that the heights are maximum during the equinoxes. The winter reflection heights for 164 kHz radio waves have been computed by assuming a particular electron density profile due to METCHLY and SMITH (1967). Because of the effect of the winter anomaly the heights can be lowered and there is a possibility of getting an average higher reflection height during the equinoctial period. From the

Table 2.4

Apparent reflection heights deduced from  
short and long range observations of VLF  
and LF radio waves

Reference	Receiver-transmitter distance (km)	Midday reflection heights (km)	Height change from day to night (km)
Bracewell et al. (1951)	535 ( 16 - 100 kHz)	Summer $73 \pm 3$ Winter $77 \pm 3$	-
Bain et al. (1952)	535 ( 16 kHz)	Summer 74	18
Straker (1955)	90 ( 16 kHz)	70-74	13 - 17
Bracewell (1952)	190 ( 16 kHz)	Summer 65.5	14
Hopkins and Raynolds(1954)	108 ( 16 kHz)	-	15 - 17
Lauter (1966)	350 ( 155 kHz)	Summer 75 Equinox 79 Winter 77	-
Wait (1963)	1000 km (10 - 100 kHz)	70 - 80	10 - 20
Present study (1972)	2000 km ( 164 kHz)	Summer $70 \pm 2$ Winter $78 \pm 2$	10 - 18



table it can also be observed that the effect of the solar activity in changing the reflection heights can not be expected to be more than about 3 km.

In interpreting the amplitude attenuation of VLF measurements during sunrise SECHRIST (1968) has shown that the amplitude decreases near  $\chi = 94^\circ$  and  $\chi = 98^\circ$  are caused by the solar ultraviolet radiation whereas the occasional VLF amplitude decrease commencing near  $\chi = 99^\circ$  is caused by photodetachment by solar visible radiation. The signal intensity increase continuing for some group of days during winter has been associated with the decrease in stratospheric temperatures. This effect is slightly different from what has been observed at high latitudes which give an enhanced absorption corresponding to the increase in stratospheric temperature. Hence this suggests that for the 164 kHz signal intensities observed at Ahmedabad, the so called winter anomaly is almost present throughout the winter months except for some days when the absorption increases because of decrease in the stratospheric temperatures.

## CHAPTER - III

EFFECT OF SOLAR FLARES ON 164 kHz RADIO PROPAGATION3.1 Introduction

It is well known that the enhancement of ionisation in the D-region during solar flares gives rise to short and medium wave fade-outs, sudden cosmic noise absorption, sudden enhancement of atmospherics, sudden rise in the magnetic field component (crochet) and sudden changes in the intensity and phase of the low frequency radio propagation. The enhancement of ionisation progressively decreases with height from a factor of 5 - 10 or more around 70 - 80 km to about 50 - 100% in the E-region and about 1- 20% in the F-region. The D-region ionisation increase during flares has been measured by the high-power wave interaction (cross-modulation) technique (ROWE ET AL., 1970) and partial reflection technique (BELROSE and CENTINER, 1969). The enhancement of electron density between 100 to 300 km has been estimated by the incoherent scatter equipment at Arecibo (THOME and WAGNER, 1967) and two series of rocket flights during flare by SOMAYAJULU and AIKIN (1970). In the F-region the deviations in the electron density have been determined by N-h profiles at intervals of 15 minutes during a flare (BHATTACHARYA and BALAKRISHNAN, 1967).

If Lyman  $\alpha$  has to account for the D-region changes during flare, then the intensity of the radiation has to be

increased by a factor of  $10^6$ , which has not been observed. Recent rocket and satellite observations have led to the suggestion that the enhanced D-region ionisation during flares is due to the increase in X-ray flux mainly in the 1 - 8 Å wavelength band (FRIEDMAN ET AL., 1958; CHUBB ET AL., 1960a, 1960b; KREPLIN ET AL., 1962). It has been noticed that the direct measurement of electron density in the D-region during a flare (SOMAYAJULU and AIKIN, 1970) and the electron densities estimated by the spectral distribution of X-rays show an agreement within 20 - 25% upto about 85 km (ANANTHAKRISHNAN, 1971). Hence the studies of the sudden ionospheric disturbances should involve the knowledge of the X-ray flares taking place in the sun. A list of such events with the details of start, peak and end timings and the peak fluxes for the wave-length band .5 - 3 Å, 1-8 Å and 8-20 Å are regularly published in the Solar Geophysical Data bulletins by the observations made on the satellite Explorer 37. A study of the sudden ionospheric disturbances (SID's) in correspondence with the X-ray flares has revealed that a minimum flux below 8 Å required to produce an SID is about  $2 \times 10^{-3}$  ergs/cm<sup>2</sup>/sec (KREPLIN, 1962).

During solar flares, sudden changes in the field strength of 164 kHz radio waves transmitted from Tashkent and received at Ahmedabad have been recorded since 1962 (ALURKAR, 1963). A detailed study of such events by SHIRKE and ALURKAR (1963) showed that the type of variations of intensity due to

the flares depended on the time of the day and season. In the present study the effect of the solar flares on the field-strength at Ahmedabad has been scrutinized for the three years 1968-70 with respect to the solar X-ray events recorded by the satellites SOLRAD 9 (Explorer 37) and Explorer 35. Also the observed effects have been interpreted by the computations of electron densities during the various times of the flare.

### 3.2 The effects observed on 164 kHz field strengths and their association with other sudden ionospheric disturbances

In general the effects observed on 164 kHz field-strength at Ahmedabad during solar flares, fall under three following categories ( here all the timings are in terms of universal time : local time = universal time + 5 hrs ) :

(1) which start with a drop in the intensity followed by slow or quick recovery to the pre-flare condition. Figure 3.1A shows two such examples on the same day of 19 February 1969. The first flare starting at 0455 hr U.T., the maximum attenuation is observed on 0500 hr. Then the signal intensity starts increasing, it had almost reached the initial value at 0537 hr when another flare has taken place, and the intensity drops again reaching a maximum value at 0540 hr. The field-strength values are recovered to the normal values around 0630 hr. The drop in intensity can be very sharp or

slow ranging from 2 to 10 minutes. We term this kind of effect as Type I.

(2) which start with a drop in intensity followed by a rise ( the rise can be less, equal or more than the fall ), and after attaining the peak value the intensity decreases reaching a minimum value, then the recovery to the normal conditions begins. Figure 3.1B and 3.1C show the examples of such effects. On 7 February 1969 ( figure 3.1B), the signal suddenly falls at 0521 hr, then increases to a peak value at 0530 hr and then decreases to a low value at 0640 hr from where it starts reviving. The full recovery takes place around 0730 hr. Similarly on 20 February 1969 (figure 3.1C) the drop in intensity, the rise to peak value and then tapering off to a low value followed by recovery stage are clear. Here also the field strength is fully revived after about 45 minutes of the time of the post-peak low value. On 7 February the rise is higher than the initial attenuation but on 20 February 1969 it is lower than the initial fall. The other flare at 0806 hr on 20 February 1969 is of the kind of type I. Let us call this second kind of effect as Type II.

(3) which start with a rise in intensity and after attaining the peak value decrease to achieve a low value from where the phase of going back to normal begins. Figure 3.1D shows that the initial drop in intensity is missing and

the signal starts rising from the normal value at 0610 hr, reaches the peak at 0616 hr and the subsequent minimum at 0730 hr. The full normalcy is attained at 0800 hr, 1/2 an hour after the time of minimum. We call this as Type III.

In all the above three types of effect, the intensity before going back to normal value can attain an abnormally low value. In figure 3.2 a few more examples of flare effects have been shown. Figure 3.2A shows that in a quick run ( 3 inches/hour ) record the absence of initial drop is very clear. The effect starts with the sudden enhancement of signal. Also the normal low value of signal strength before recovering can be noted. Figure 3.2B shows an example of type II with the amount of initial drop and subsequent rise roughly same. Figure 3.2C shows a type II effect starting at 0610 hr. Before the signal has been able to reach the low value another flare has started and that has given a sudden enhancement of the signal. We cannot decide the type of the effect in this case for the second event. Figure 3.2D shows an example of the multiple flares. Because of consecutive flares occurring on the same day ( during a strong active period of sun ) the effect on the field-strength is highly complicated. From a statistical study of the occurrence of these effects during the period 1968-70, it is observed that Type I changes are very common during the equinoxes ( March - April - October ) less frequent during

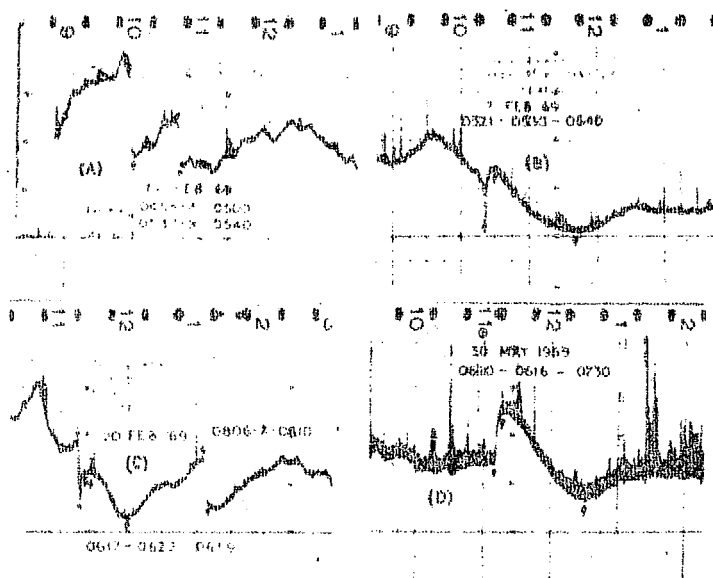
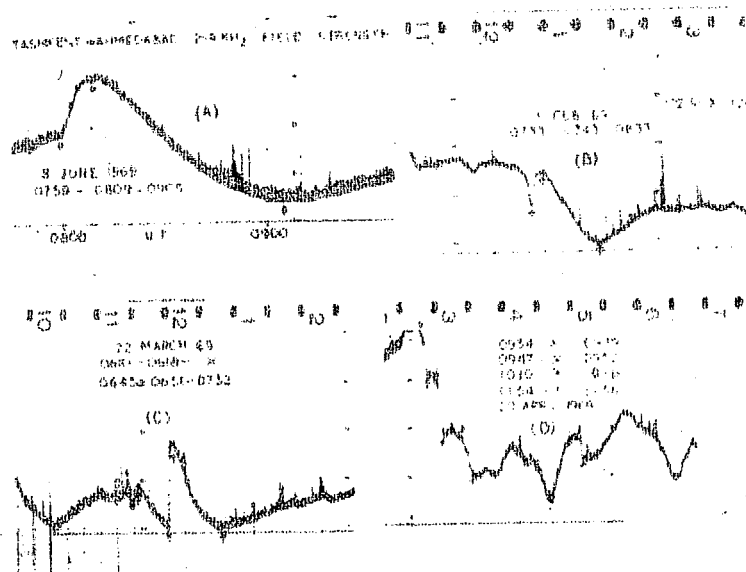


FIGURE 3.1

Some typical examples of solar flare effects on 164 kHz radio waves observed at Ahmedabad.



Some typical examples of solar flare effects on 164 kHz radio waves observed at Ahmedabad.

FIGURE 3.2

winter, and do not occur during summer. Type II effects are registered during winter and equinoxes whereas type III are observed only during summer months.

In figure 3.3 are presented two cases of the effect produced in the 164 kHz radio intensity on the same day 7 June 1969. The effects can be distinguished as type III. The difference between the two cases lies in the initial rise in the signal intensity. The first effect (A) has taken 11 minutes to reach the peak whereas the second effect (B) has taken only 3 minutes. By comparing the records of cosmic radio noise absorption ( representative of D-region absorption) and magnetic field measurements by proton precession magnetometer ( representative of the conductivity in the E-region) obtained at Ahmedabad we notice that the first effect (A) has given rise to neither a SCNA (Sudden Cosmic Noise Absorption) nor a crochet but the second one has given rise to both. It can be mentioned that the occurrences of SCNA and crochet are less frequent as compared to SEA and SPA's probably because they require a larger ionisation enhancement to get induced. Hence it can be suggested that the magnitude of ionisation enhancement in the D-region as observed in 164 kHz intensity, is governed by the sharpness of the effect rather than the total signal amplitude enhancement. It can be mentioned that the flare effect at 0809 hr (figure 3.3B) produced more ionisation in the D-region

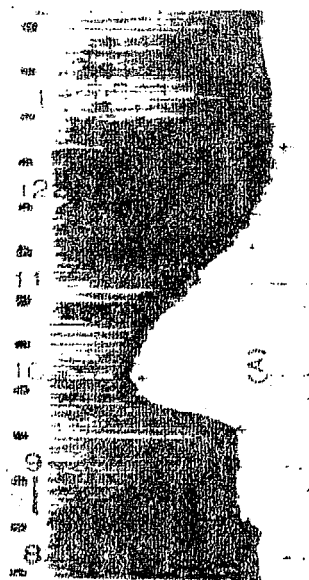


compared to the flare effect on 0948 hr ( figure 3.3A). The former produced a SCNA and crochet whereas the later did not.

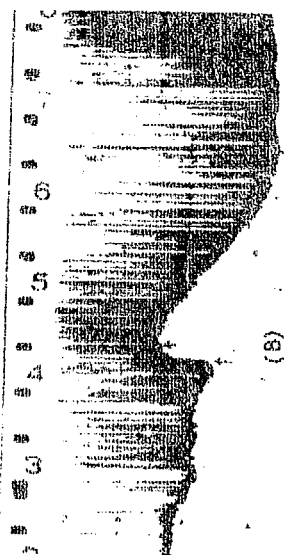
A comparison of the flare effects in 164 kHz radio signals at Ahmedabad and the horizontal component of the earths magnetic field at Kodaikanal ( dip  $3.5^{\circ}\text{N}$ ) revealed that only a few percent events were common in both. But in many events though the magnetic crochet is not observed there are, however , detectable short-time enhancements in the H-field. The simultaneous effect of solar flare in 164 kHz radio wave amplitudes and in the H component of magnetic field is shown in figure 3.4 which shows an example of magnetic crochet observed at Kodaikanal and the corresponding effect on 164 kHz field strength.

### 3.3 A direct comparison of radio intensities at 164 kHz with flare time solar X-ray emissions measured in satellites

In order to study the flare effects on 164 kHz radio intensities in relation to the X-ray flares we make a comparison of a few flare effects with the detailed X-ray flux data as measured in the satellites SOLRAD 9 (Explorer 37 ) and Explorer 35. The solar X-ray data of a few flares during October - November 1968 published by KREPLIN, VAN ALLEN and TESKE (1970) have been used in the present study. The times of the flares have been compared with the changes in the field intensity of 164 kHz radio waves received at Ahmedabad



7 JUNE 1969  
0909 - 0912 - 0855



7 JUNE 1969  
0909 - 0912 - 0855

FIGURE 3.3

Two solar flare effects observed on a typical summer day of 7 June 1969.

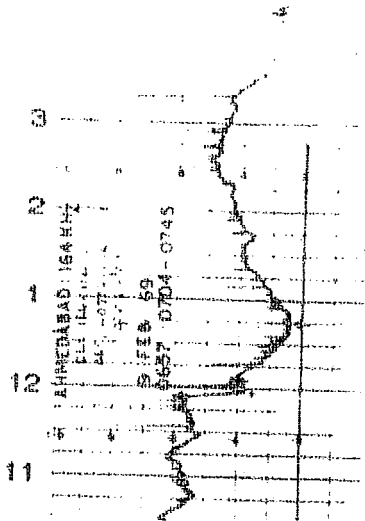
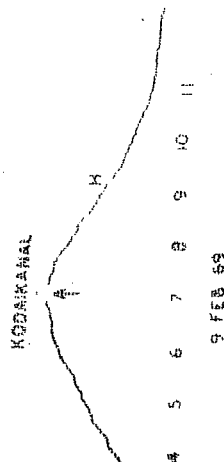


FIGURE 3.4

Simultaneous records of flare effects in the H-component of earth's magnetic field at Kodaikanal and in the 164 kHz radio intensity at Ahmedabad.

from Tashkent. The X-ray fluxes in the  $2 - 12 \text{ \AA}$  wavelength band measured by Explorer 35 are well suited for this comparison because of good time resolution during sudden changes. The SOLRAD 9 data ( $\lambda = 1 - 8 \text{ \AA}$ ) have also been used when data of Explorer 35 are not available. Table 3.1 gives the details of the data used. During the period 27 October - 3 November 1968, all the X-ray events observed during the hours 0200 - 1200 U.T. ( 07 - 17 hr L.T) and the corresponding X-ray flux changes in the  $2 - 12 \text{ \AA}$  region ( for Explorer 35 ) ;  $1 - 8 \text{ \AA}$  ( for SOLRAD 9 ) are also listed in table 3.1. It will be observed that all the observed X-ray events produced a simultaneous effect in the radio signal. The minimum X-ray flux which is able to induce a measurable effect shows a value of about  $4.5 \times 10^{-3} \text{ ergs/ (cm}^2 \cdot \text{sec)}$ . The starting time and time of peak intensity of the sudden ionospheric disturbance and of the X-ray flare agree well ; in general within a few minutes. The end time of the SID effect on the 164 kHz signal cannot be determined accurately and hence the end time mentioned in table 3.1 only indicates the time of the first minimum after the flare effect started. After reaching the minimum value, the field strength slowly recovers to its normal level. The reestablishment of the original signal level takes place about an hour or more after the X-ray flare has ended. There is less agreement between the end time ( as given in table 3.1) of changed signal intensity and the end time of the X-ray flare. In order to present the variations of radio intensity

Table 3.1

X-ray flares observed in satellites and the corresponding SID effects  
observed in the field strength of 164 kHz radio waves from Tashkent  
to Ahmedabad

Date	Satellite	Times of X-ray flares as recorded in satellite			Peak flux erg/(cm <sup>2</sup> . sec)	SID effect observed in 164 kHz field strength		
		Start time	Peak time	End time	2 - 12 Å	Start time	Peak time	End time
27-10-68	Exp.35	1102	1113	-	8 x 10 <sup>-3</sup>	1108	1114	-
	-do-	1130	1150	U1230	1 x 10 <sup>-2</sup>	1130	1149	1200
28-10-68	-do-	0200	0205	0300	8.5 x 10 <sup>-3</sup>	0200	0244	0320
	-do-	0500	0516	0555	1.0 x 10 <sup>-2</sup>	0502	0520	0530
	SOLRAD 9	0555	0600	0630	5.0 x 10 <sup>-3</sup>	0557	-	0602
	-do-	0650	0700	0715	4.5 x 10 <sup>-3</sup>	0702	-	0708
	-do-	0715	0725	0740	4.5 x 10 <sup>-3</sup>	0730	-	0740
	-do-	0828	0835	0845	5.0 x 10 <sup>-3</sup>	0835	-	0845
29-10-68	Exp.35	0330	0400	U-	6.2 x 10 <sup>-3</sup>	0330	U	0400
	-do-	0407	0421	0500	7.2 x 10 <sup>-3</sup>	0415	-	0430
	-do-	0545	0600	0630U	7.5 x 10 <sup>-3</sup>	0552	0600	0630
	-do-	C	C	C		0730	0748	U
	-do-	0858	0915	C	2 x 10 <sup>-2</sup>	0900	0915	-
	-do-	1000	-	1008	1 x 10 <sup>-2</sup>	1000	1004	1015
1-11-68	-do-	0545	0557	0620	7 x 10 <sup>-3</sup>	0545	-	0557
	-do-	0627	0640	0645	5 x 10 <sup>-3</sup>	-	0622	0630
	-do-	0825U	0910	1200	5 x 10 <sup>-2</sup>	0814	0900	1200
2-11-68	-do-	C	C	C	-	0330	0338	0355
	-do-	0600	0610	0637	7 x 10 <sup>-3</sup>	0600	0610	0655
	-do-	0915	1002	1200	1 x 10 <sup>-1</sup>	0915	1000	1045
3-11-68	-do-	0530	0537	0600	5.4 x 10 <sup>-3</sup>	0530	-	0537
	-do-	0708	0715	0730	7.0 x 10 <sup>-3</sup>	0712	0722	0800

and the corresponding changes of X-ray fluxes ( integrated flux between  $2 - 12 \text{ \AA}$  ; Explorer 35 ) some of the important events are reproduced.

Figure 3.5 shows examples of two flares on 3 November 1968 observed in 164 kHz intensity and the sudden enhancements of X-ray flux. The first X-ray flare around 0540 hr U.T. has given rise to a small drop in intensity of radio signal whereas the second bigger flare produces an enhancement in the signal. Figure 3.6 shows the big flare of November 2, 1968. The simultaneous changes in the field intensity of 164 kHz radio waves can be seen at every stage of the changes of X-ray spectrum. The X-ray flux starts increasing at 0915 hr and the rate of rise decreases at 0945 hr. From 0945 to 0952 hr flux increases only slightly, but from 0952 hr the X-ray flux increases sharply reaching a maximum at 1000 hr. After this the flux decreases to attain a constant low value. The corresponding field intensity decreases by about  $40 \mu\text{V}$  from 0915 to 0945 hr and then shows an enhancement upto 0952 hr. The increase in intensity continues with a conspicuous break at 0952 hr reaching a peak at 1000 hr. Hence the slow increase of X-ray flux between 0945 to 0952 hr gives rise to an enhancement in the signal of about  $35 \mu\text{V}$ . The change over point at 0952 hr are seen in both the observations. After the peak is reached in the signal strength it slowly recovers, the time of which cannot be clearly estimated.

Hence upto the time of peak flare the variations of signal intensity are truly simultaneous. Even the small details of X-ray flux changes are reflected in the sudden deviations of the signal strength. The second peak in field strength at 1245 hr is not a flare effect but in a normal sunset effect.

Figure 3.7 shows the occurrence of a complex of 6 flares during the period 0700 to 1400 hr of 28 October 1968. The remarkable point to be noticed is that even the small X-ray fluxes of average peak intensities of  $4.5 \times 10^{-3}$  ergs/(cm<sup>2</sup>.sec) have been able to produce detectable effects in the radio intensity at Ahmedabad in the form of small decreases. The Tashkent signal received at Delhi ( 1000 km from the transmitter) shows sudden changes due to the big flare at 0500 hr but does not show any change for the subsequent small flares. The absence of any effect of the small flare at 0600 hr at Delhi can be noticed in the figure. It has been studied that the flare effects produced in the field strength observations at Ahmedabad and Poona are exactly similar (ANANTHAKRISHNAN, 1967). One example of similar variations at Ahmedabad and Poona during disturbed conditions is shown in figure 3.8. It will be seen that the flares at 0325, 0715, 0954 and 1100 hrs produced similar impressions at both the stations. Returning to figure 3.7 it appears that the smaller flares do not produce an effect at short distances, but do show up in the records at larger distances. Hence it is suggested that the Tashkent -

### FIGURE CAPTIONS

Fig.3.5 : Variation of the amplitude of 164 kHz radio waves and X-ray fluxes (2- 12 Å) during the flares on 3 November 1968.

Fig.3.6 : Variation of the amplitude of 164 kHz radio waves and X-ray fluxes ( 2 - 12 Å) during the flares on 2 November 1968.

Fig.3.7 : Field strength changes of 164 kHz radio waves observed at Ahmedabad and at Delhi during a complex of X-ray flares on 28 October 1968.

Fig.3.8 : Simultaneous observations of flare effects in the radio intensity at Ahmedabad and at Poona on 29 March 1966.

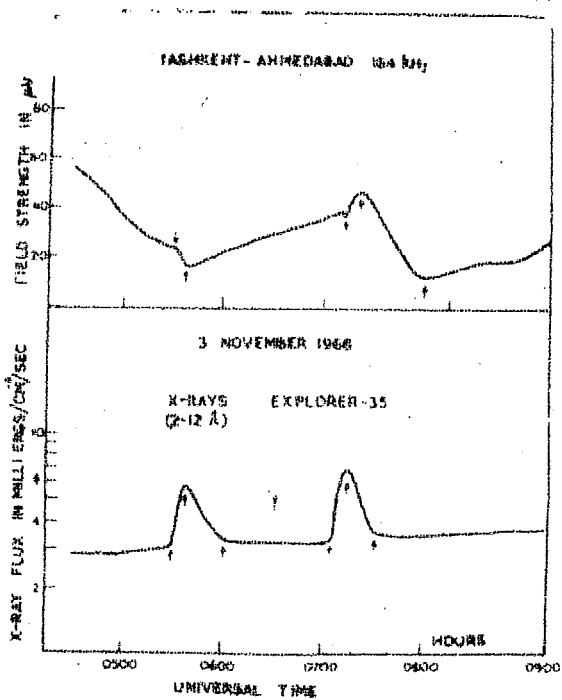


FIGURE 3.5

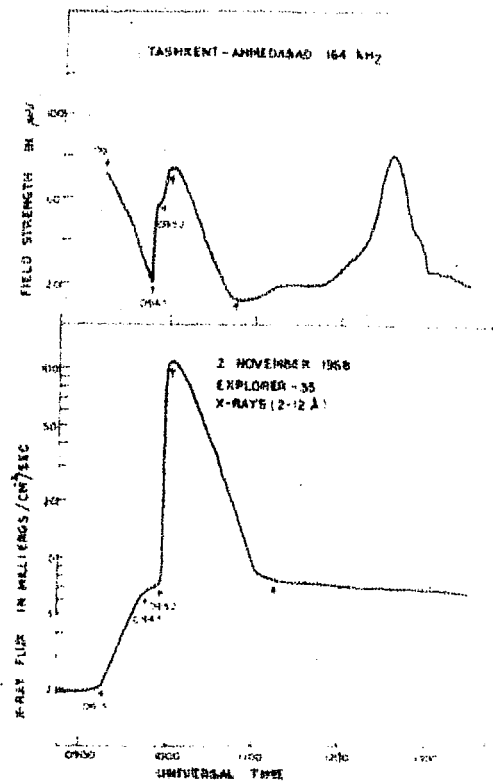
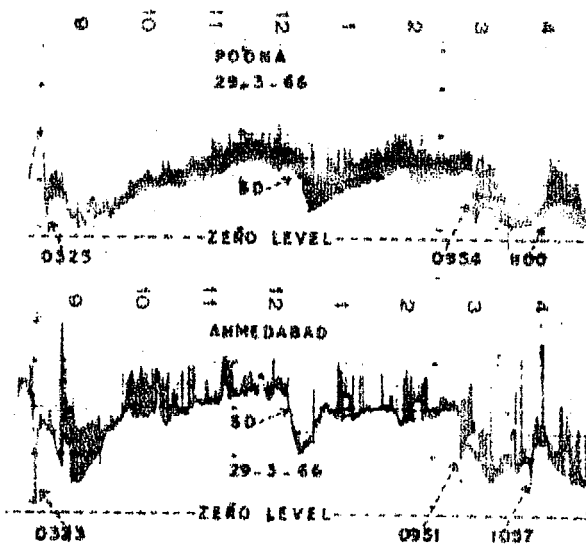
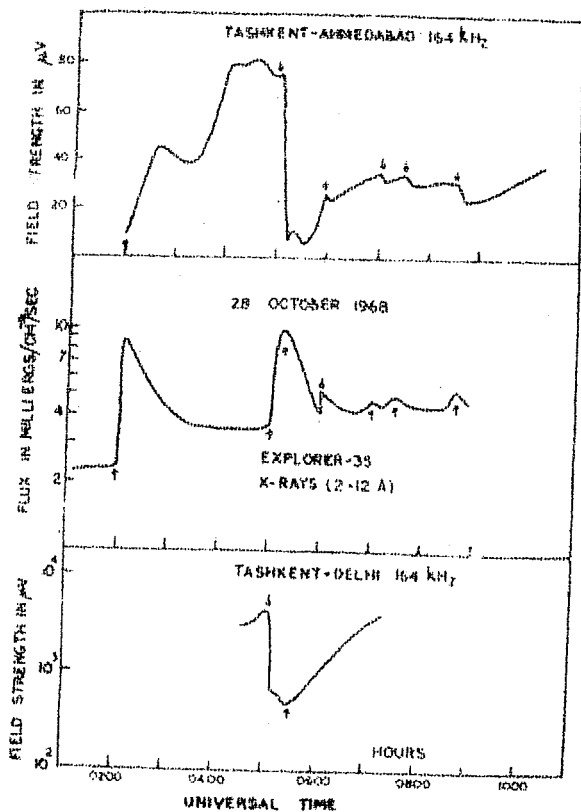


FIGURE 3.6





Ahmedabad or Tashkent - Poona radio paths are better suited for observing the effects of even the weaker X-ray flares. A thorough comparison of the effects at shorter and longer distances will be required before drawing any definite conclusion about the sensitivity in detecting the solar flares depending upon the receiver - transmitter separation.

Figure 3.9 shows a multiple flare on 27 October 1968. The X-ray flux starts increasing at 1102 hr; the effect on the radio intensity appears at 1108 hr when the X-ray flux reaches a value of  $4.5 \times 10^{-3}$  ergs/(cm<sup>2</sup>.sec). Before the first flare ends another begins at 1130 hr and this shows up in the signal by a change of slope in the recovery stage at 1130 hr. The peak corresponding to the second X-ray flare is quite small in the field strength records, presumably because of the existing high absorption due to the ionisation produced by the first flare. Similar results have been obtained by comparing all the X-ray flares and the flare induced effects on 164 kHz field intensity for the period 2 - 10 March 1970 and the data has been published in the special issue of Report UAG - 12 Part I of the World Data Center (1971).

#### 3.4 Occurrence of flare effects with respect to the X-ray flare events during 1968 - 71

For investigating the role of the type of spectrum of X-rays between  $1 - 8 \text{ \AA}$  in producing the radio effects at 164 kHz it will be necessary to have the details of the spectral

characteristics during the progress of a flare. The data giving such informations is quite scarce and hence a real statistical study cannot be possible. However, the X-ray flare events with the start, peak and end times as well as the values of peak fluxes integrated for three wavelength bands, namely 1-3, 1-8 and 8-20 Å are published regularly in the solar Geophysical Data Bulletins (Boulder, Colorado). Hence our study of the flare effects will be limited by this source of data.

For getting a picture of the statistical occurrence of the SID's observed on 164 kHz field strength, all the events registered during 1968 - 70 are tabulated between 7-18 hrs for different months. Figure 3.10 shows the occurrences of the solar flare effects with the time of the day and with months combined for the years 1968-70. It can be noticed that the maximum number of occurrences is around 10-11 hr local time. The number of occurrences become appreciably small close to the sunrise and sunset effects. It can also be noticed that during the equinoctial and winter months the number of occurrences is larger as compared to the number of events during the summer months ( June - September). Near the equinoxes ( March - April and October - November ) the occurrences are maximum. It has been observed that on the average all the X-ray events well suited for producing an SID effect on 164 kHz radio intensity do not do so. The estimate

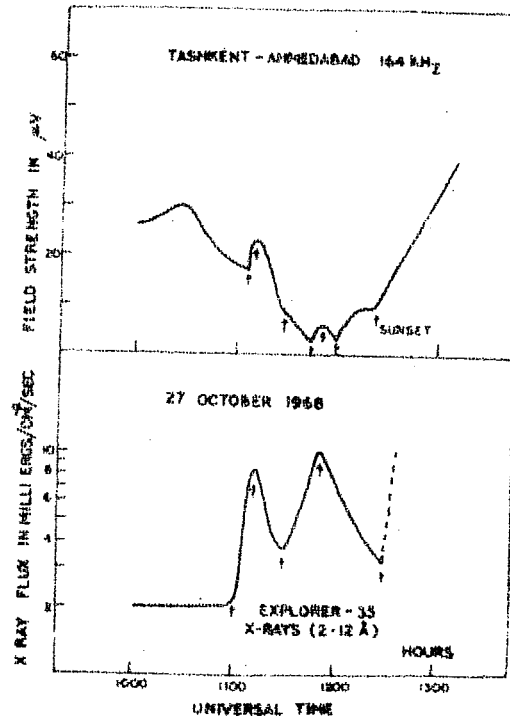


FIGURE 3.9

Changes in the field-strength of 164 kHz radio waves observed during the overlapping X-ray flares of 27 October 1968.

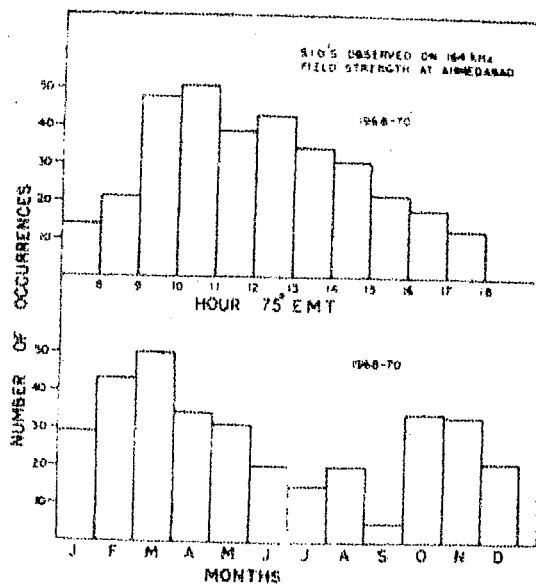


FIGURE 3.10

of as how many X-ray events have been able to induce the corresponding effect during 1969 can be availed from figures 3.11A and 3.11B. The histograms of X-ray events and SID's show that though the production of X-ray flares do not have any obvious dependence on a particular month, the occurrences of SID's are maximum during equinoxes and minimum during summer. It can be noticed that about 60-80% of the X-ray flares have given rise to the flare effects during the equinoxes, whereas it is only 20% during the summer months. Hence it is suggested that the most suitable periods of the observability of solar flare effects on 164 kHz field amplitudes at Ahmedabad are the non-summer months (January to May and October-December).

In view of the possible dependence of the three types of effects observed in the field intensity of 164 kHz radio waves, on the total X-ray fluxes during these events, the peak X-ray intensities in the wavelength bands  $1-3 \text{ \AA}$  and  $1-8 \text{ \AA}$  are considered. All the observed SID's during January -August, 1971 are studied with respect to the peak X-ray intensities in the two said bands. To have a proper appraisal of the effect of the relative magnitudes of the X-ray fluxes in the two bands, on the type of the SID produced, a hardness factor is defined as follows:

$$\text{Hardness factor (H.F.)} = \frac{\text{X-ray flux ( } \lambda = 1-3 \text{ \AA )}}{\text{X-ray flux ( } \lambda = 1-8 \text{ \AA )}}$$

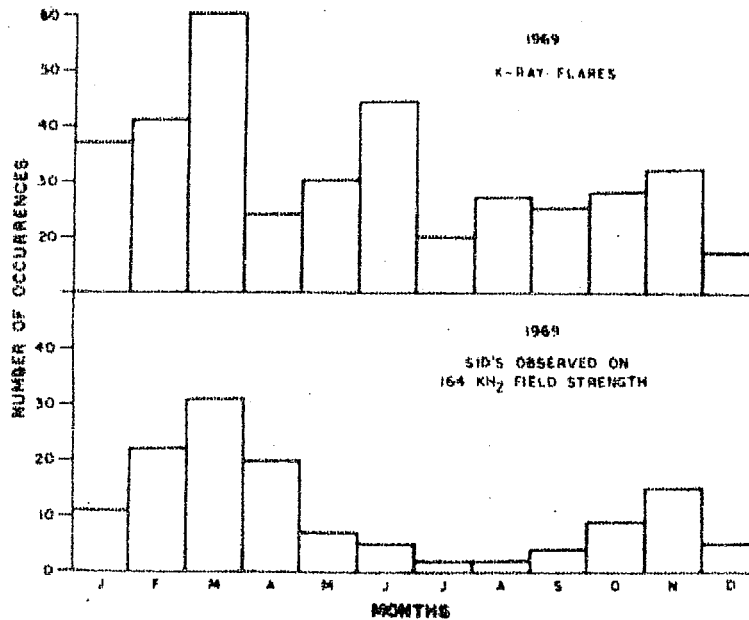


FIGURE 3.11(a)

Histograms representing the number of occurrences of solar X-ray flares and the corresponding flare effects observed in the radio signal intensities.

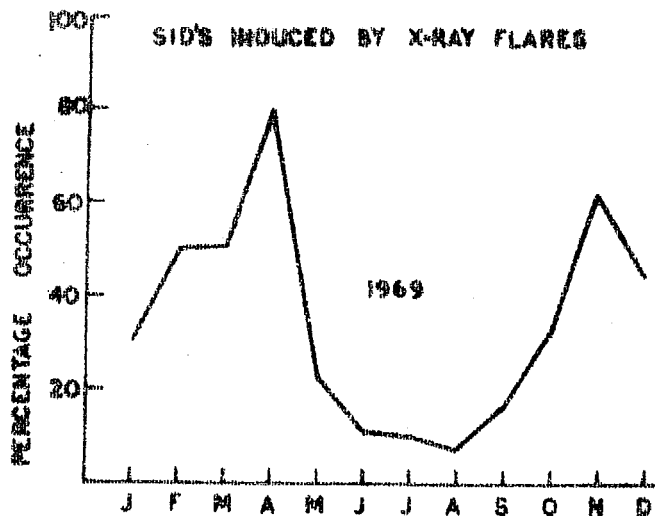
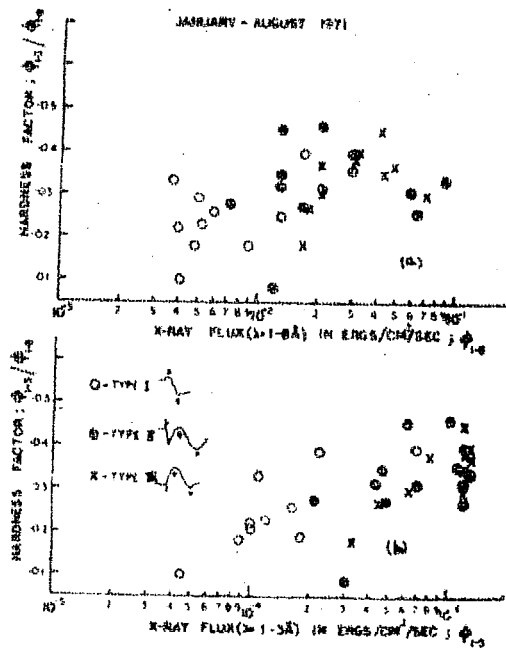


FIGURE 3.11(b)

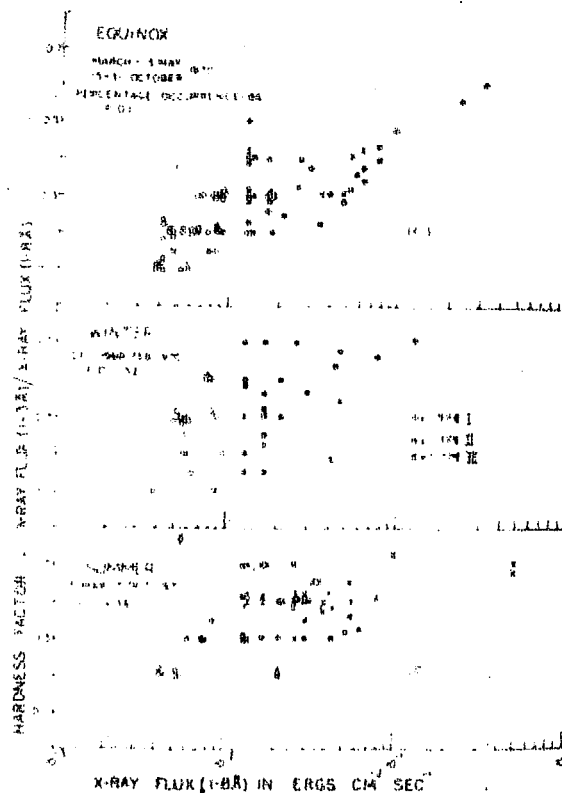
An increase in the hardness factor will mean that the flux of the harder X-rays ( $1-3 \text{ \AA}$ ) has enhanced relatively more than the enhancement in the  $1-8 \text{ \AA}$  band X-rays. The result of our analysis has been given in figure 3.12. In this figure, the hardness factor, as defined above has been plotted with respect to the integrated values of the peak fluxes in the two wavelength bands ( $\lambda = 1-3 \text{ \AA}$  and  $1-8 \text{ \AA}$ ) for each individual case of the SID event observed in the 164 kHz radio amplitude. Hence we have excluded those cases when the X-ray flares did not produce the corresponding effect. The open circles the closed circles and the crosses represent the Type I, Type II and Type III effects discussed earlier. It is interesting to note that in order to observe the Type I changes, the minimum fluxes of  $4 \times 10^{-3} \text{ ergs}/(\text{cm}^2.\text{sec})$  in the  $1-8 \text{ \AA}$  band and  $4 \times 10^{-4} \text{ ergs}/(\text{cm}^2.\text{sec})$  in the  $1-3 \text{ \AA}$  band are necessary. Type II effects are observed for the fluxes greater than about  $10^{-2} \text{ ergs}/(\text{cm}^2.\text{sec})$  in the  $1-8 \text{ \AA}$  band and greater than about  $2 \times 10^{-3} \text{ ergs}/(\text{cm}^2.\text{sec})$  in the  $1-3 \text{ \AA}$  band. Type III effects require same or slightly higher energies needed for Type II changes. It can also be noted that the hardness factor increases with the intensity of the flare, i.e., for stronger X-ray flares the relative increase in the harder X-rays ( $1-3 \text{ \AA}$ ) is more compared to that in the hard X-rays ( $1-8 \text{ \AA}$ ).

Similar analysis has been extended for different seasons. In figure 3.13a,b, and c only the total fluxes



Distribution of the three types of effect observed in the 164 kHz radio intensity at Ahmedabad in relation to the maximum hardness factor in the X-ray flares during January - August 1971.

FIGURE 3.12



Different types of solar flare effects plotted with respect to the X-ray fluxes and maximum hardness factor during different seasons of 1970.

FIGURE 3.13

(  $\lambda = 1-8 \text{ \AA}$  ) have been plotted with respect to the hardness factor - for three seasons. It can be noted that during the equinox large number of Type I and Type II are registered with very few cases of Type III. About 86% of the X-ray events between 0900 - 1500 hr L.T. have been able to produce the corresponding effect in the form of Type I and Type II only. During winter months it can be noticed that only about 52% have been able to produce flare effects. Again we can see the predominant occurrence of Type I and Type II only. A marked difference is observed during summer, with the occurrence of Type III increasing significantly, Also the occurrence of Type I and Type II has noticeably reduced. The number of sudden effects observed is only 36% with respect to the total X-ray flare events suitable for producing effect. Hence it is realised that the X-ray events with comparatively low energies do not produce the corresponding effect in the radio intensities during summer, whereas during equinox the low energy X-ray fluxes become very efficient in producing the effect. Also during summer the initial dip is seen comparatively for less number of events than in winter.

### 3.5 Interpretation of the results on occurrence of solar flare effects in 164 kHz radio strengths

We will attempt to explain the results obtained on the flare effects of 164 kHz field strengths at Ahmedabad by considering only two seasons namely, equinox and summer.



The behaviour during winter is close to that during the equinox. During the equinoctial months as the heights of reflections are around  $76 \pm 2$  km, X-ray events with energies little more than  $4 \times 10^{-3}$  ergs/(cm<sup>2</sup>.sec) in the 1-8 Å wavelength band will be able to produce sufficient ionisation below the reflection level so that the radio waves will be attenuated showing a drop in the intensity. These are registered as Type I changes. If the X-ray fluxes become more than about  $10^{-2}$  ergs/(cm<sup>2</sup>.sec) the waves start getting reflected from a lower height, the reflection coefficient improving with the progress of the flare ultimately reaching a peak value. Then the recovery of the radio intensities will depend upon as how the enhanced ionisation is lost at different levels of the D-region. These give rise to the Type II changes. During summer months the radio waves will be reflected from a lower height of about  $70 \pm 2$  km. The X-ray events with lower energies will not, normally affect heights below 70 km in order to observe the sudden changes of Type I. Because of this reason the percentage occurrence of flare effects in the 164 kHz radio intensities is considerably reduced with respect to the total number of X-ray events suitable for producing such events. Only the X-ray flare events with higher energies are able to produce the corresponding changes, that too mostly in the form of an enhancement of the signal (Type III). The occurrence of the initial drop becomes very much less compared to the equinoctial months.

Hence it can be concluded that during equinox or winter season the ionisation is produced below the level of reflection and then the reflection coefficient value is increased if the X-ray intensities are higher. But during summer months the enhancement of the signal takes place because of increased ionisation near the level of reflection, only in few cases the initial drop of the signal in a small way is also present. In order to have a full understanding of the solar flare effects due to the enhanced X-ray intensity, it will be necessary to know the electron density profiles at close intervals during the progress of the flare. In the next sections the theory of ion-electron pair production by X-rays in the  $1-8 \text{ \AA}$  wavelength band will be discussed in detail. Also, for a particular case of a solar flare the free electron densities at different levels during the course of the event will be estimated by solving the continuity equation.

### 3.6 Electron production by X-rays in the $1-8 \text{ \AA}$ region

Normally to produce a free electron, from an atom or molecule the incident photon should have an energy at least equal to the ionisation potential of the atom or the molecule. In the case of X-rays the energies associated with the  $1-8 \text{ \AA}$  wavelength band are of the order of kilo-electron volts (keV), which are much higher than the ionisation potential for all atmospheric constituents ( $\approx 15 \text{ eV}$ ). When these X-rays interact with the atmospheric constituents of the D-region they produce

ionisation as a result of photo-electric absorption, ie., the incident photon energy is shared between ejected photoelectrons and the residual excited atom. The excited atom, from the inner shell of which one electron has been struck off, produces secondary X-rays which in turn gives the Auger electrons. It has been observed that Nitrogen, Oxygen and Argon produce characteristic K-X-rays at energies 0.39, 0.53 and 3.2 keV, with fluorescent yields at 0.0015, 0.0022 and 0.13 respectively (FINK ET AL., 1966). The cross-section of the electron shells subject to the photo-electric absorption will vary inversely with the photon-energy.

The fraction of monoenergetic X-ray intensity  $dI/I$  absorbed in the height interval between  $h$  and  $h+dh$  is given by, following CHAPMAN (1931a,b).

$$\frac{dI}{I} = - \sum_k \sigma_k N_k(h) \sec \chi dh \quad \dots(3.1)$$

where  $\chi$  = angle between the zenith and the direction of the incident X-ray beam

$\sigma_k$  = absorption cross-section per atom of the  $k^{\text{th}}$  species

$N_k(h)$  = number density of the  $k^{\text{th}}$  species at a height  $h$

we can replace  $\sum_k \sigma_k N_k(h)$  as

$$\sigma P(h) = \sum_k \sigma_k N_k(h) \quad \dots(3.2)$$

where  $\sigma$  = mass absorption coefficient of air in  $\text{cm}^2 \text{g}^{-1}$

substituting for  $\sum_k \sigma_k N_k(h)$  in equation 3.1 and integrating we get

$$I(h) = I_0 \exp ( - \sigma P_0(h) H(h) \sec \chi ) \quad \dots(3.3)$$

where  $I_0$  = incident photon energy and we assume that

$$P = P_0(h) \exp ( - h/H )$$

and  $H(h)$  denotes the scale height at a height  $h$

The electron production rate per unit volume at an altitude  $h$  km is given by

$$q(h) = \frac{\sigma}{Q} P(h) I(h) \text{ cm}^{-3} \text{ sec}^{-1} \quad \dots(3.4)$$

where  $Q$  is the average energy required to produce one ion-electron pair in the atmosphere. This is taken as about 34 eV for X-rays ( SNELL, 1962; SWIFT, 1962). The mass absorption coefficient for air can be adequately represented over

restricted energy ranges by the relation

$$\sigma(E) = AE^{-B} \quad \dots (3.5)$$

where E = energy of photon

A, B = constants

These are obtained from the data of FOROYTHE (1956) and KENKE ET AL. (1967) supplemented at higher energies by those of VICTOREEN (1949). For determining the electron production rate at a particular height, the incident photon spectrum should be known so that equation 3.4 can be integrated for the whole spectrum. Then the calculations are repeated for different heights in the ionosphere to get the height profile of the electron production rate.

After getting the electron production rates due to X-ray flux at different times of the flare, it will be required to estimate the excess free electron densities at various heights during the course of the flare. For this we have to solve the continuity equation:

$$\frac{\partial N(h,t)}{\partial t} = q(h,t) - \psi(h) N^2(h,t) \quad \dots (3.6)$$

where  $N(h,t)$  is electron density at height during the time  $t$  and  $\psi$  is the effective loss rate. Since the changes taking place during a flare are faster compared to the relaxation

time of the ionosphere, the equilibrium condition, equating  $\partial N / \partial t = 0$  will not give the correct electron densities during various times of the flare. Hence the differential equation (3.6) has to be integrated numerically by a method given by RUNGE-KUTTA with the modification of GILL (1951). A possible change in the effective loss rate during the flare will not be considered in our calculations.

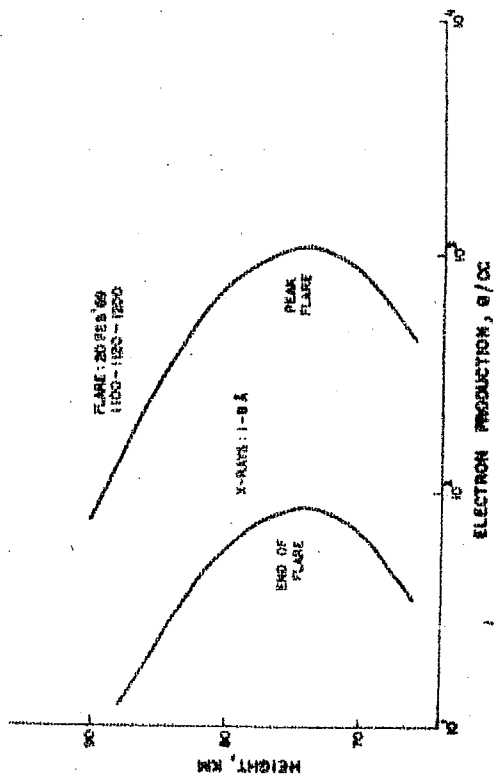
### 3.7 Electron density variations in the D-region during the course of X-ray flares

In this section firstly we present the electron density calculations at various heights of the D-region during a particular flare of 20 February 1969. Figure 3.14 shows the effect of this flare on 164 kHz field-strength, reproduced from the actual records at Ahmedabad. The effect is recognised as the Type II, the intensity of the signal is abnormally low after the peak effect at around 1200 hr signifying high attenuation during that time. This kind of records are quite common with the Type II flare effects when the associated X-ray fluxes in the 1-8 Å wavelength band are higher than about  $6.7 \times 10^{-2}$  ergs/(cm<sup>2</sup>.sec). The object of such calculations will also be to explain the presence of this high absorption of radio waves when the X-ray flare has almost ended. Figure 3.14 also gives the values of the integrated X-ray fluxes for 1-8 Å and .5-3 Å bands. The peak flux in the 1-8 Å band has reached a very high value of about  $9 \times 10^{-2}$  ergs/(cm<sup>2</sup>.sec). The method of computing the electron

production rate has been given in the last section.

The atmospheric densities and scale heights at different levels have been taken from CIRA (1965) for the present calculations. The electron production rates due to the X-rays in the wavelength band  $1-8 \text{ \AA}$  during the flare at different levels for the flare of 20 February 1969 are shown in figure 3.15. The peak electron production is about  $10^3/(\text{cm}^3.\text{sec})$  at the height of about 74 km. The production rates above and below this height are considerably lower. Figure 3.16 shows the height profile of the electron production rate during the peak and end times of the X-ray flare. The maximum ionisation production occurs at heights between 70-75 km. If we compute the electron production by considering the X-ray flux between  $.5-3 \text{ \AA}$  wavelength band it is noticed that the peak of production is shifted down to around 60-65 km, but the quantitative values are much lower than those produced by X-rays in the  $1-8 \text{ \AA}$  band ( figure 3.17). Hence it will be sufficient to consider only the production by  $1-8 \text{ \AA}$  wavelength X-rays to assess the ionisation changes caused during a flare in the lower ionosphere.

The final values of free-electron densities are obtained by numerically integrating the equation (3.6). The values of effective recombination at different heights is used from figure 1.6, whereas the quiet-time electron density profile by NICOLET and AIKIN (1960) is used as the pre-flare condition of



Electron production by X-rays during a flare. FIGURE 3.16

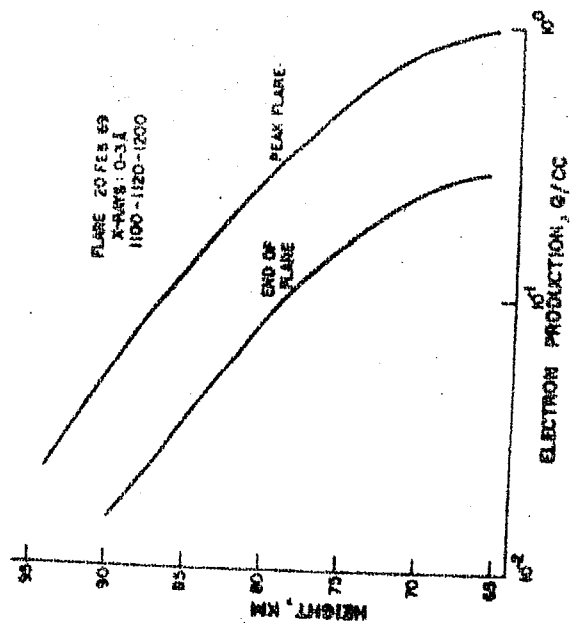


FIGURE 3.17

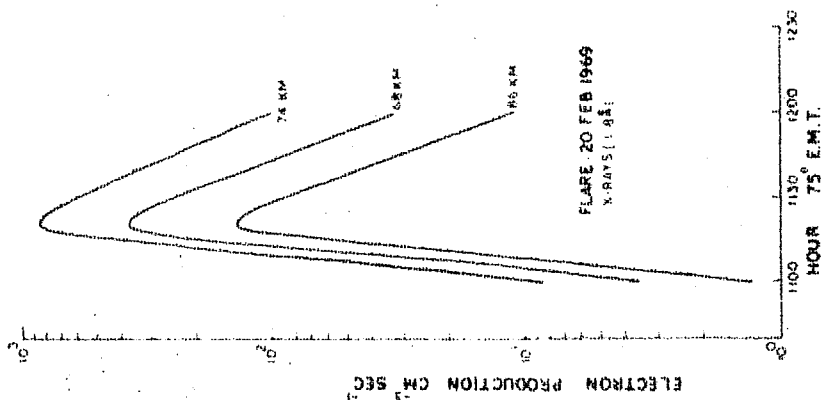


FIGURE 3.15

Electron production rates by X-ray ( $\lambda = 1-8\text{\AA}$ ) during the solar flare of 20 Feb 1969.

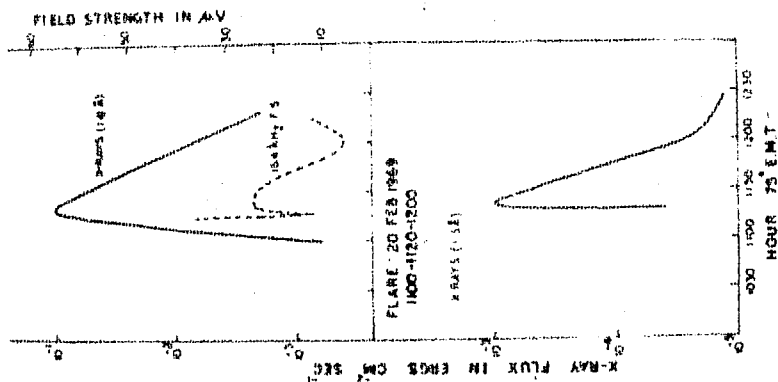


FIGURE 3.14

Integrated X-ray fluxes in the wave-length bands  $1-8\text{\AA}$  and  $0-3\text{\AA}$  during a solar flare of 20 Feb 1969 along with the effect on 164 kHz radio amplitude.



ionisation. In the input data of the computer programme for the numerical integration the values of  $q$  for every half second is given for a step size of integration of 1 sec. The step size cannot be increased as that will not give the steady state solutions. The calculations are repeated for different heights where the values of  $q$  and  $\psi$  are different. The time profiles of electron density for four different heights of 70, 74, 80 and 86 km are shown in figure 3.18. The electron densities represent the total values by considering the excess ionisation during the flare. It can be noticed that the maximum electron density during the peak of the flare will be produced around about 74 km. The peak ionisation for all the levels are reached at the same time, coinciding with the peak X-ray flux time. The post peak period of the effect is quite interesting. As can be noticed from the figure that in lower heights ( $\approx 75$  km) the recovery of the ionisation to the normal conditions is very fast. Hence the lower regions below about 75 km will rapidly regain the ambient electron densities by the end-time of the X-ray flare ( $\approx 1200$  hr L.T.). The loss of excess ionisation at heights above about 75 km is quite slow compared to the losses in the lower levels. It can be seen that electron densities in these levels at 1200 hr is quite high compared to the quiet-condition densities. In fact the electron densities obtain the normal values around 1300 hr L.T. Hence the ionisation at higher levels seems to persist even upto about

1 hour after the end of the X-ray flare has taken place. In light of the above calculations we will now try to explain the corresponding effect observed on 164 kHz radio intensities during this flare. A reflection height during winter of about 78 km before the flare has taken place, is considered for these radio waves. The onset of the flare will produce considerable amount of ionisation below this reflection level and the signal intensity will be attenuated showing a drop in the signal strength, this will also change the height of reflection of these waves to about 70-75 km. The signal intensity reaches a minimum value in about 10 minutes, when the X-ray flux is still increasing producing more ionisation. Now the excess electron densities modify the reflection coefficient of the level of reflection upto the time of peak electron production. The signal intensity shows an enhancement during this time because of the better reflectivity of the layer. Hence the time of maxima of both the signal intensity and electron density match quite well (1120 hr). After this situation is reached, the excess of electron density starts disappearing and the rate of loss of electrons is different at different heights. The reflectivity of the layer slowly deteriorates and the signal intensity starts decreasing, in the meantime the height of reflection also starts shifting up, to attain the normal level. But since the excess ionisation persists in the higher altitudes for longer time there is a possibility that more ionisation would be present below the level of reflection during this period, which may lead to high absorption of the

waves. After reaching a minimum value of absorption the signal recovers completely at around 1300 hr, by this time it is interesting to note that the ionisation in the higher levels also regain their normal values. Hence it is suggested that the end-time of the effect in the radio intensity does not coincide with the end-time of the X-ray flare but coincides with the time by which the excess ionisation is lost at higher levels of the D-region ( 75 - 80 km ). It can be mentioned that during summer there is a better correlation between the end times of flare effects with the end-times of X-ray flares probably because of the initial lower heights of reflection.

The effect of comparatively smaller X-ray flares occurring at large solar zenith angles may not produce any effect on the LF field intensity as the production will have a zenith angle dependence. The electron production rates for different zenith angles taking height as the parameter is shown in figure 3.19. The peak flux of X-rays below  $8 \text{ \AA}$  has been taken as  $4 \times 10^{-3} \text{ ergs}/(\text{cm}^2 \cdot \text{sec})$ . It can be noticed that the zenith angle dependence of production is higher in lower altitudes. This indicates that if the reflection height is lower ( $\approx 70 \text{ km}$ ) the effect of same flare will be less as compared to the case when the height of reflection is more for larger zenith angles. Hence just after sunrise and before sunset upto 2-3 hrs the effect produced by comparatively smaller flares will be less in the intensities of 164 kHz radio waves. For stronger flares the

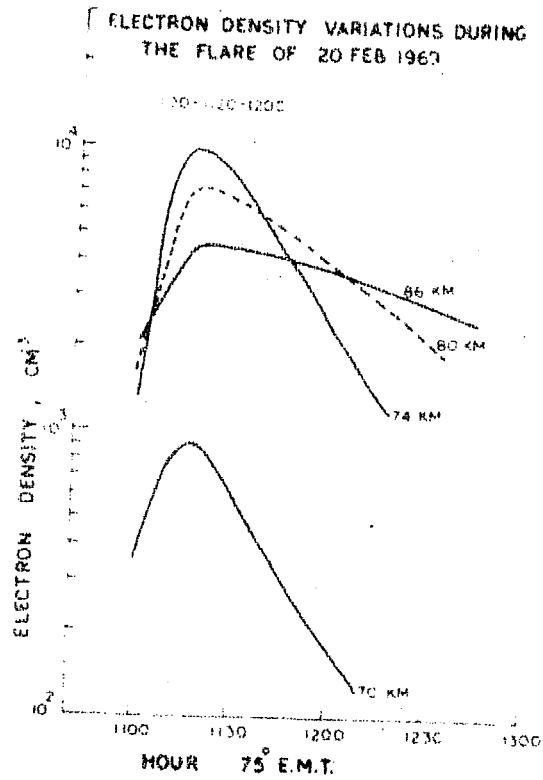


FIGURE 3.18  
Variation of electron density during the period of a solar flare at different heights of 86, 80, 74 and 70 km.

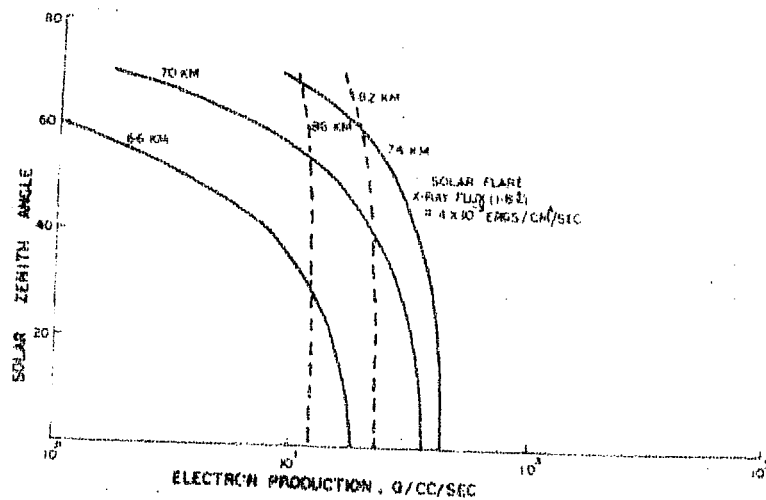


FIGURE 3.19

zenith angle dependence will be quite small compared to the high excess electron densities.

### 3.8 Conclusion

The results presented on the effect of solar flares in the LF radio field intensity can be summarised by way of conclusions as follows:

(1) Three types of effect are observed in the field strength of 164 kHz radio waves during solar flares:

- (a) Type I : which manifest in the form of a drop in the signal intensity
- (b) Type II : which start with a drop followed by an enhancement attaining a peak intensity. The intensity then slowly reduces to a low value from where it starts reviving back to normalcy.
- (c) Type III : which are recorded with an enhancement in the signal intensity ( the initial drop absent ). Rest of the features are similar to Type II.

Type I and Type II are generally observed during non-summer months whereas Type III are observed mainly during the summer-months.

(2) The quickness of the event upto the attainment of the peak intensity during a flare is proportional to the amount of ionisation enhancement in the D-region. Quicker the

initial phases more the possibility of observing other SID's like S.C.N.A. and crochet etc.

(3) Comparatively smaller flares observed on 164 kHz field intensity at Ahmedabad, do not produce the standard crochet effect, but do produce small short-time enhancements in the magnetic field which have been detected at an equatorial station, Kodaikanal.

(4) A direct comparison of the flare effects observed on 164 kHz field strengths at Ahmedabad with the X-ray flare events recorded in satellites shows the following:

- (a) The start time and peak time of the X-ray flare and the sudden changes in the radio signals agree within a few minutes.
- (b) The flare effect on the signal strength persists for a larger time compared to the flare event.
- (c) The details of the X-ray flux variations during a flare are well reflected in the radio intensity changes.
- (d) Tashkent-Ahmedabad or Tashkent-Poona radio paths are more suitable for observing even the small X-ray flares compared to the shorter path of Tashkent-Delhi.

(5) A statistical study on the occurrence of the flare effects of 164 kHz radio intensities at Ahmedabad during 1968-70 show the following:

- (a) Occurrences are maximum during 1000 - 1100 hr L.T.

- (b) Occurrences are maximum during equinoxes and minimum during summer

(6) The X-ray flare events suitable for producing effects show the following:

- (a) During equinoxes and winter about 50-80% of the X-ray flares produce the corresponding effect.
- (b) During summer only about 20-30% of the X-ray flares produce the corresponding effect.

(7) Following are the minimum energies ( average ) in the 1-8 Å wavelength X-rays required to produce the three type of effects:

Type I	:	$4 \times 10^{-3}$ ergs/(cm <sup>2</sup> .sec)
Type II	:	$1 \times 10^{-2}$ ergs/(cm <sup>2</sup> .sec)
Type III	:	$1 \times 10^{-2}$ ergs/(cm <sup>2</sup> .sec)

The hardness factor of the X-ray increases with the intensity of the flare.

(8) The less occurrence of the flare effects during the summer months is interpreted as due to the fact that the small flares, which are quite in abundance, are not able to produce the Type I changes because of low reflection heights of these radio waves during this period.

(9) Calculation of electron densities in the D-region heights during different times of a solar flare, assuming the

production due to X-rays (  $1-8 \text{ \AA}$  ) show that though the X-ray flare ends, its effect in the form of excess ionisation at higher altitudes (  $75 - 80 \text{ km}$  ) for longer time enables the SID effect to be prolonged by about  $1/2 \text{ hr} - 1 \text{ hr}$  for the case of a moderately strong flare.

(10) The effect of smaller flares will be even less at lower altitudes (  $\leq 75 \text{ km}$  ) for larger values of zenith angles which makes type I changes to be almost impossible during the summer months.

### 3.9 Discussion

The effect of the solar flares observed on VLF and LF radio waves at steep and oblique incidences reported by various workers is summarised in Table 3.2. It can be noticed that at low frequencies for oblique incidences a height decrease of about  $4-7 \text{ km}$  is observed depending upon the intensity of the flare, for stronger flares the height decrease is more. The theoretical values of the height changes of about  $5 - 10 \text{ km}$  are included in the table for the  $164 \text{ kHz}$  radio intensities received at Ahmedabad. The amplitudes of the low frequency radio waves at  $70 - 85 \text{ kHz}$  show an enhancement during the flare, whereas at  $164 \text{ kHz}$  received at larger distances the amplitudes show decrease or increase depending upon the season. Hence for  $164 \text{ kHz}$  radio waves the height decrease depends both on the



Table 3.2Summary of the flare effects on VLF and LF waves at steep and oblique incidences

Frequency kHz	Path distance	Height decrease during SID's	Amplitude variations	Reference
16 (Steep incidence)	90 km.	6 - 15 km	Only small decreases in the amplitu- des.	BRACEWELL ET AL. (1951).
70 and 113 (Steep incidence)	100 km.	6 - 15 km	Large decre- ase with rapid onset and slow recovery	WEEKES and STUART (1952a).
16 (Oblique incidence)	535 km	5 - 10 km	Small decre- ase in the amplitude	BAIN ET AL. (1952).
16 (Oblique incidence)	1350 km	-	Small incre- ase in the amplitude	BELROSE (1957).
70-85 (Oblique incidence)	900 km	4 - 7 km	Increase in the amplitude	WEEKS and STUART (1952b).
164 (Oblique incidence)	2100 km	5 - 10 km (theore- tical)	Seasonal variation in the amplitude changes. Increase in summer. Decrease as well as increase in winter and equinoxes.	Present work.

intensity of flare as well as on the season.

The details of the flare-time height variations of LF waves during different seasons are not available from the observations at other stations.

CHILTON ET AL. (1963) have explained the flare effects on VLF radio observations of 18 kHz at oblique incidence on the basis of enhancement of ionisation in the D-region by solar X-rays (  $1-8 \text{ \AA}^{\circ}$  ). The rocket observation for measurement of electron densities during different time of a flare by ROWE ET AL.(1970) are in broad agreement with the electron densities derived from VLF flare effects by MAY (1966). There is a suggestion that even after the end of the flare the ionisation attains the pre-flare values only after 30 - 45 minutes which is again different for different heights. This is in agreement with our calculations showing that the ionisation persists much longer at higher altitudes during a moderately strong flare.

## CHAPTER - IV

### POSSIBILITY OF CONTINUOUS STUDY OF NOCTURNAL D-REGION IONOSPHERE BY LF AND VLF PROPAGATION TECHNIQUE

#### 4.1 Introduction

Sweep frequency ionosonde having a low frequency range between 50 kHz - 2 MHz has been able to provide useful informations about the E-region during the night-time. The electron density in the normal E-region, which is reduced by an order of magnitude during night has been studied at Boulder by WATTS (1967). Since the penetration frequency of the nocturnal E-region lies below the working range of most of the traditional ionosondes, except for special phenomenon like sporadic E, these instruments are insensitive in furnishing details of electron density distribution below about 130 km during night-time. Hence a large scale study of the E-region during night is not possible by simple ground based experiments. However, the electron density profiles of the night-time E-region have been obtained by quite a few rocket experiments (SMITH, 1965; HALL and FOOKS, 1965 ; MECHTLY and SMITH, 1968b etc.). It has been noticed that the observed electron densities in the E-region are higher than what should be predicted theoretically. This discrepancy has been explained by considering electron production due to the night-time sources; like scattered Lyman  $\alpha$  , Lyman  $\beta$  and Meteors.

A continuous study of the nocturnal D-region is even more difficult because of the very low electron densities present below about 85 km. Though rocket experiments provide electron density profiles in the D-region also, their reliability is less compared to those for the E-region. The VLF and LF radio waves, getting reflected from the base of the E-layer ( $\approx 90$  km) during night, should be potentially well suited for providing informations regarding the nocturnal D-region. But the interpretation of the amplitude and phases of these radio waves during night has not been successful enough to substantiate the knowledge of night-time D-region. The results presented in this chapter from the LF propagation measurements during night revive the possibility of continuous monitoring of the nocturnal D-region.

#### 4.2 Observations of electron densities in the nocturnal D-region by rocket borne experiments

There are only a very few D-region electron density estimates during night. In figure 4.1 we have collected some of the N-h profiles available from experimental as well as theoretical considerations. Curve 1 shows the electron density profile obtained by SMITH (1965) at 0435 hr (L.T), 27 October 1961 from Wallops Island by using a rocket langmuir probe experiment. Curve 2 gives the profile at 0050 hr (L.T) of 15 August 1962 from Woomera measured by HALL and FOOKS (1965) using a rocket LF propagation experiment. Curve 3 shows the

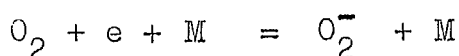
densities at 2210 hr (L.T) on 10 November 1965 from Floria (28°N, dip 62.3°) by using spherical electrostatic analysers in the rocket (SAGALIN and SIMDDY, 1966). Curves 4 and 5 give the electron density profiles measured at Wallops Island and Thumba, using rocket probe experiments (MECHTLY and SMITH, 1968; SUBBARAYA ET AL., 1971). Curve 6 shows the densities estimated by DEEKS (1966) from a series of LF and VLF studies during high sunspot years. Curve 7 gives the theoretical values predicted by OGAWA and TOHAMATSU (1966).

It can be noticed that the electron densities are very low below a height of about 85 km. The nature of the regular variation of electron density with season or solar activity cannot be derived from these curves. Between 85 and 90 km the electron density increases very sharply reaching the values of the E-region. An increase in the negative ion density during night is possibly the reason for low electron densities below 85 km during night.

A comparison of effective loss rates during day and night suggests that the effective loss rates during night below 85 km level are increased considerably because of the increase in  $\lambda$  (negative ion density to electron density ratio). A series of rocket flights conducted by SAGALYN ET AL. (1966) during day-time for measuring electron and negative ion densities suggested that the values of  $\lambda$  would be about 10, 3 and 0.7 at heights of 60, 70 and 75 km respectively. Hence

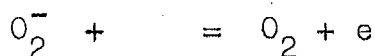
during day-time  $\lambda$  begins to become appreciable only below about 70 km. The corresponding night-time values measured under subsonic conditions with parachute-borne blunt probes in the altitude range 40-80 km (HALE, 1966) show that increases by about a factor of 300 at 70 km and a factor of  $10^3$  over 50 - 65 km. PEDERSON (1965) from the measurement by using Gerdian condensers in descending parachute over Ardoya, Norway showed that  $\lambda$  has a value of 1 at 80 km during day and the same value at heights above 80 km during night. It can be concluded that during night  $\lambda$  becomes an important parameter below 85 km, the values becoming very high below 80 km.

Negative ions are formed mainly due to the three body attachment reactions as follows:

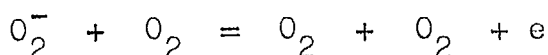


where M is any molecule

During day-time the negative ions are lost because of photo-detachment.



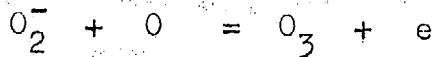
the rate of this reaction is higher compared to the collisional detachment rates of following type of reaction.



during night-time photo detachment is absent and the

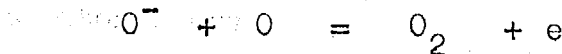
collisional detachment is slow, this results in the increase of negative ion densities.

If we assume the large values of  $3 \times 10^{-10} \text{ cm}^3/\text{sec}$  as the rate coefficient for the following associative detachment process (FERGUSON, 1967):



and also the fast rates of  $7 \times 10^{-10} \text{ cm}^3/\text{sec}$

(PHELPS, 1966) for the following reaction (associative detachment)



then the large negative ion concentrations during night can be explained as due to the rates of the above reactions becoming slower below 80 km because of the depletion in the atomic oxygen concentration after sunset. The photo detachment will become negligible compared to the high rate coefficients of the above mentioned associative detachment reactions during the daytime.

Since the effective loss rates of the electron density will increase for values of greater than 1; during night these coefficients will have larger values compared to those in the daytime specially below about 80 km. There are very few measurements on the effective loss rates for D-region heights during night. In figure 4.2 we present a few night-time

profiles of the effective loss rate in the D-region ionosphere. Curve 1 is based on the theoretical estimates of CRAIN (1961). The profile of curve 2 has been obtained by MCDIARMID and BUDZINSKI (1965) from the angular distribution and energy spectra of electrons associated with the auroral events. From a comparison of N-h profile during a night-time nuclear explosion using rocket probe experiment and production rates (q) from measurement of particle flux, WHITTEN ET AL. (1965) have computed the values of loss functions which are shown in curve 3. We have plotted the curve 4 by combining the recombination coefficient of MOLIER (1960) and  $\lambda$  values of SAGALIN and SMIDDY (1966). It can be noticed that the loss rates are quite high below the height of about 80 km. A good deal of uncertainties are also involved showing a large variability from measurement to measurement. Hence the measurements of electron densities and loss coefficients in the D-region during night-time points out that the presence of free electrons below about 80 km is almost prohibited due to the large enhancement of the negative ion-to-electron density ratio in these heights.

#### 4.3 General pattern of variation of radio intensity at Ahmedabad during night-time

From a study of the low frequency radio data (164 kHz) of Ahmedabad during night-time, two kinds of pattern have



emerged:

(1) Soon after sunset the general level of the signal intensity goes on increasing, reaching a peak near local midnight from where it decreases and maintains almost a constant level upto the sunrise period. This type of variation is generally observed during winter months.

(2) The signal intensity starts increasing after sunset and goes on increasing upto the sunrise time without showing an obvious occurrence of peak intensity in between. This type of effect is seen generally during the summer months (June - September)

Figure 4.3 shows two representative night-time records of 164 kHz field strength at Ahmedabad, one for winter and the other for summer taken during high sunspot years 1969-71. The observation of 22 January 1969 did not have an off period between 0030 - 0430 hr (L.T). It can be noticed that after sunset the field intensity increased upto about 0000 hr L.T. and then decreased slightly. Between 0100 - 0600 hr the signal intensity maintained an average constant level, though there were some short time decreases and increases superimposed on that constant value. The record of 23 July 1971 shows an increase of the signal after sunset, which continues to increase even after midnight. The transmitter had been switched off between about 0030 - 0415 hr, but the

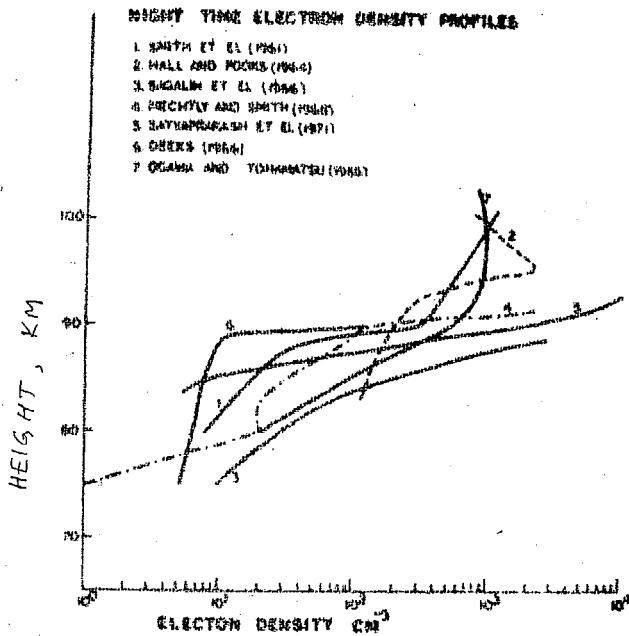


FIGURE 4.1

Few nighttime electron density profiles of the D-region ionosphere obtained from various experimental and theoretical observations.

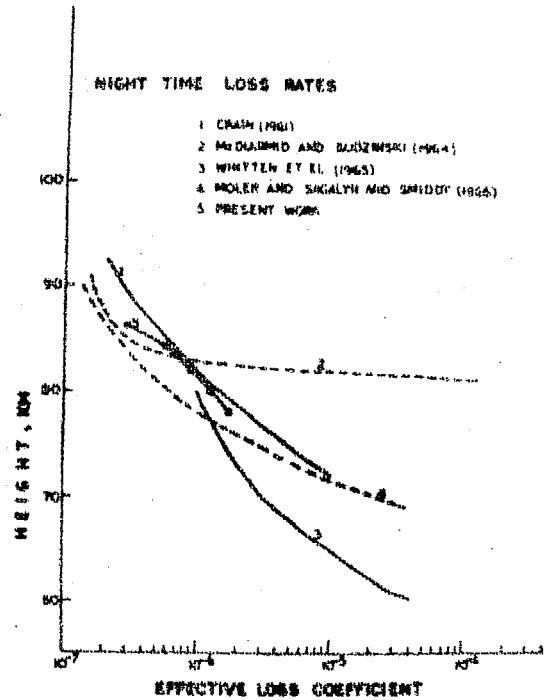


FIGURE 4.2

Effective nighttime loss rates in the D-region ionosphere.

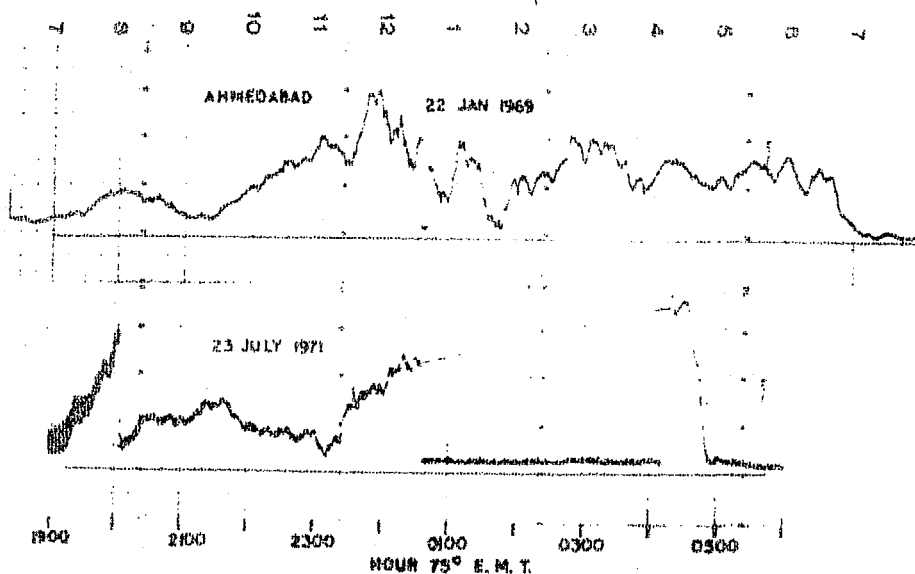


FIGURE 4.3

signal intensity was much higher at 0430 hr compared to the value around midnight. This suggests that the signal intensity would have shown a monotonous increase upto the time of sunrise. The base level of the signal strength variation at Ahmedabad during night is quite clear and should have some fundamental meaning in terms of the night-time D-region processes.

The average half hourly values of radio amplitudes for the months of January and July 1970 are computed and plotted in figure 4.4 ( broken line represents the transmitter off period). We can see that during winter (January 1970), the intensity attains a maximum around midnight and remains almost in that level upto the sunrise time, whereas during summer (July 1970) it shows a steady increase upto the time of sunrise. The amplitudes of the radio signal are lower during summer all through the night.

In order to have some explanation of the above results we should have a knowledge of as how does the electron density vary in the D-region after sunset. To compute this theoretically we solve the continuity equation in the absence of the production function i.e., assuming that there does not exist any source of ionisation for the nocturnal D-region.

Then we have from

$$\frac{dN}{dt} = q - \gamma N^2$$

putting  $q = 0$

$$\partial N / \partial t = - \psi N^2$$

Integrating with the boundary condition of the sunset value of electron density during the time  $t = 0$  we have for a particular height in the ionosphere.

$$N = \left( \psi t + \frac{1}{N_s} \right)^{-1} \quad \dots \quad (4.1)$$

where  $N$  is the electron density  $t$  seconds after the sunset, and  $N_s$  = electron concentration at sunset.

We also assume that  $\psi$  attains the night-time values immediately after sunset. Using the relation (4.1) and taking values from the curve 4 of figure 4.2, the electron density profiles are computed upto about 6 hrs after sunset. These are shown in figure 4.5. It can be noticed that the electron density goes on decreasing and the rate of decrease becomes slower with the progress of time. Hence it is suggested according to the above model that the electron concentration in the D-region should decrease at all heights reaching a minimum value just before the time when the sunrise effect sets in.

The observed low frequency radio intensity variation during summer can be explained on the basis of above calculation. The height of reflection of about 85 - 90 km for these radio waves will be reached within about 1 - 2 hr after sunset, as the

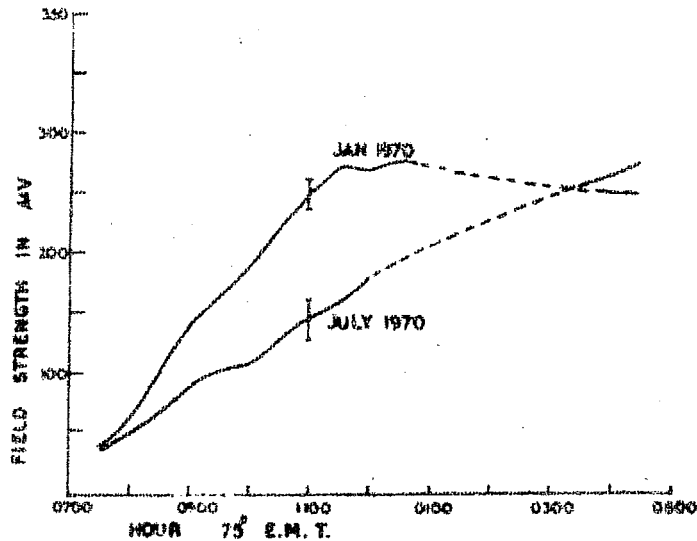
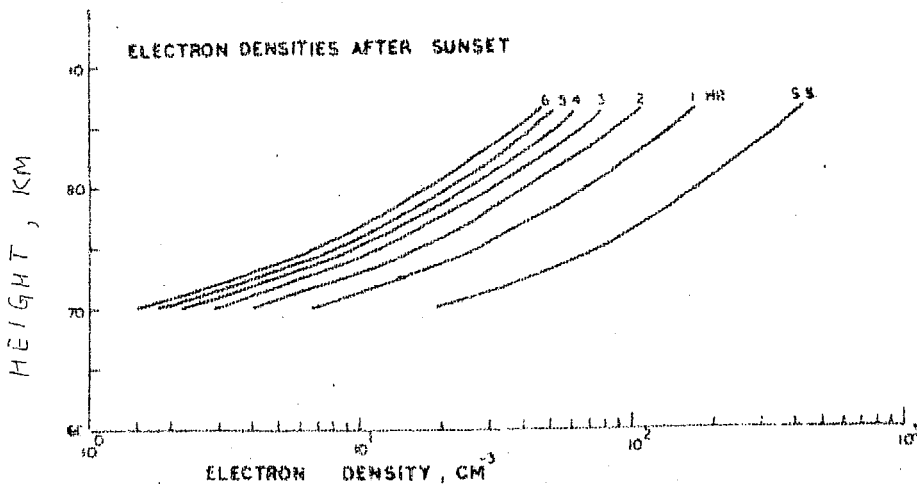


FIGURE 4.4

Average half-hourly values of field strength of 164 kHz radio waves plotted for the months January and July of 1970.



Variation of electron density in the D-region until 6 hours after the sunset period, considering no electron production after sunset.

FIGURE 4.5

changes in the electron densities are fast in this duration. The signal intensity continuously increases because the absorption of these radio waves decreases due to the disappearance of electron concentration below the reflection level. During winter the signal intensity increases after sunset upto about midnight thereafter it persists almost at the same level upto sunrise. This is possible if there is some source of ionisation in the night-time D-region. This source should have a solar control, such as to have maximum strength in the anti-solar direction. The solar Lyman  $\alpha$  scattered from the geocorona can produce ionisation around about 85 km. It is generally believed now that 85% of the night Lyman  $\alpha$  emission originated from scattering of solar Lyman  $\alpha$  by hydrogen in the geocorona; the rest being probably from galactic sources such as emission from gaseous nabulae (TINSLEY, 1969). During summer the night-time electron concentrations are probably high so that the production due to Lyman  $\alpha$  is not sufficient to attenuate the radio waves at any stage during the night. During winter upto about midnight the loss processes are predominant but after midnight the production by Lyman  $\alpha$  becomes sufficient to maintain the electron concentrations between 80 - 90 km.

#### 4.4 Effects observed in 164 kHz radio amplitudes during the transit of a strong X-ray source Sco X-1

##### (a) Discovery of the Sco X-1 effect in the nocturnal D-region

The discovery of galactic X-rays from the region of

the galactic centre by GIACCONI ET AL. (1962) during a rocket experiment devised to observe the albedo X-rays from the moon, opened up a new field in astronomy. This discovery stimulated efforts by several scientific teams in search of other possible X-ray sources at the sametime improving the measurement technique to determine their exact location, angular diameter and spectral character. Since then, more than about sixty sources, mostly of galactic origin, have been discovered. The results of measurement of X-ray fluxes from all sources, carried out so far, reveal that by far the brightest X-ray source as seen from the earth is the X-ray source in the constellation Scorpius, named as Sco X-1.

The idea that the X-rays from these galactic sources can be absorbed in the lower region of the atmosphere to produce ionisation changes in the night-time D-region was followed up by ANANTHAKRISHNAN and RAMANATHAN (1969) and they identified some pronounced minima observed in the night-time field-strength recordings of 164 kHz at Ahmedabad. These minima recurred night after night in the months April to July, the local time of which shifted to earlier hours as the days advanced from April to July. Further examination showed that the times of minima nearly coincided with the times of transit of Sco X-1 across  $72^{\circ}\text{E}$ , which is the meridian of the propagation path of 164 kHz radio waves from Tashkent to Ahmedabad. More detailed study of this observed effect was then undertaken.

Some of the results of the findings have been published (ANANTHAKRISHNAN ET AL., 1970a, 1970b).

(b) Changes in the night-time field strength produced by Sco X-1

The best estimate of the location of Sco X-1 has been made by GURSKY ET AL. (1966a) who give the following coordinates for the source:

Right ascension (RA) :  $16^h 17^m$   
 Declination,  $\delta$  :  $-15^\circ 31'$

A simple calculation for the minimum zenith angle of this X-ray source for the middle point of reflection of 164 kHz radio waves between Tashkent and Ahmedabad ( $32^\circ\text{N}$ ,  $72^\circ\text{E}$ ) can be done from the following relation:

$$\cos \chi = \cos t \cos \phi \cos \delta + \sin \phi \sin \delta \dots (4.2)$$

where  $\chi$  is the zenith angle

$t$  is the hour angle of the source

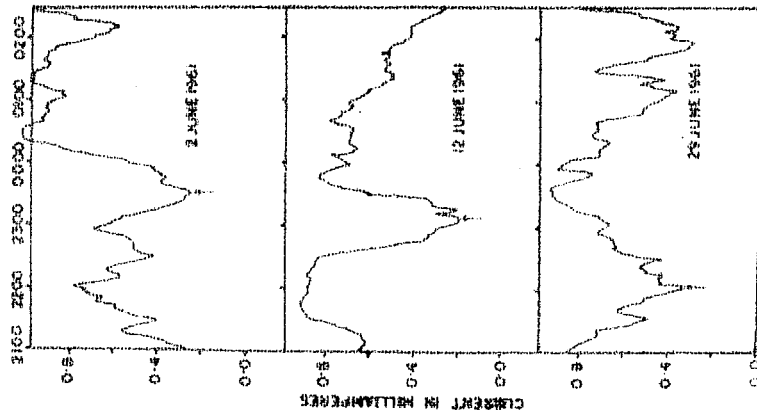
$\phi$  is the latitude

$\delta$  is declination of the source

Using this relation it is seen that Sco X-1 will be at its minimum zenith angle transit across  $72^\circ\text{E}$ ,  $32^\circ\text{N}$  by about 2330 hr L.T. on 1 June. An example of the observed effect in the night radio intensities at Ahmedabad during the transit of Sco X-1 is shown in figure 4.6. It is noticed that

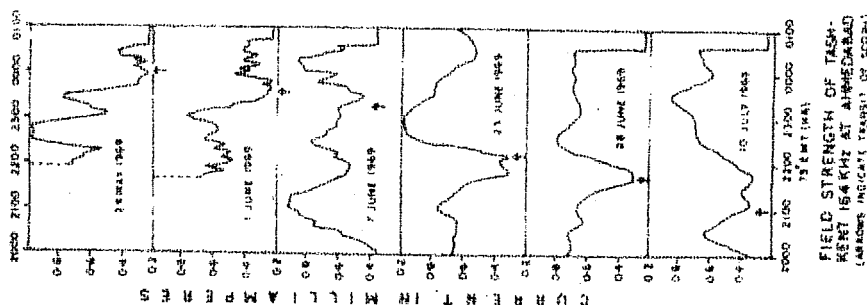


there are significant decreases in the amplitude lasting for about 2 hours associated with the transit of Sco X-1. The sidereal shift of about 1 hr 45 mts between 2 June to 29 June can clearly be seen. In addition to the pronounced minimum during the Sco X-1 transit ( indicated by arrows in the figure), other minima quite sporadic in appearance, are occasionally observed on the records. Another example of the actual records showing the effect of Sco X-1 transit between 24 May - 10 July 1969 is shown in figure 4.7. It can be observed again that the prominent depression in the field intensity takes place around the minimum zenith transit of the source but the total effect lasts for about 2 hrs. Examination of the data between May - June of 1961 and 1969 showed that the prominent depression is present for about 60% nights in May and about 65% nights in June. In figure 4.8 a few selected good records showing this effect from April to July 1961 are plotted alongwith the average transit curves of Sco X-1 across the coordinates  $32^{\circ}\text{N}$  and  $72^{\circ}\text{E}$ . It is noticed that the sidereal shift of about 4 minutes is not strictly observable in two or three days successive records but it can be seen in a general way for a span of about a week. From figure 4.8 it is observed that the signal intensities start decreasing at a point when the zenith angle of Sco X-1 is about  $54^{\circ}$ , the maximum attenuation taking place when the zenith angle reaches a value of  $48^{\circ}$  and the restoration to initial conditions takes place again when the zenith angle is about  $54^{\circ}$ . Thus the effect due to the transit



Night-time field strength records of Tashkent (164 kHz) radio transmissions received at Ahmedabad. Arrows indicate the transit of a X-ray star Sco X-1 during June 1961.

7.5 E.M.T.  
FIELD STRENGTH OF TASHKENT 164 KHz  
OBSERVED AT AHMEDABAD  
ARROWS INDICATE TRANSIT OF SCO X-1



Nighttime field strength records of Tashkent (164 kHz) radio transmissions received at Ahmedabad. Arrows indicate the transit of a X-ray star Sco X-1 during MAY-June 1969.

7.5 E.M.T.  
FIELD STRENGTH OF TASHKENT 164 KHz AT AHMEDABAD  
(ARROWS INDICATE TRANSIT OF SCO X-1)

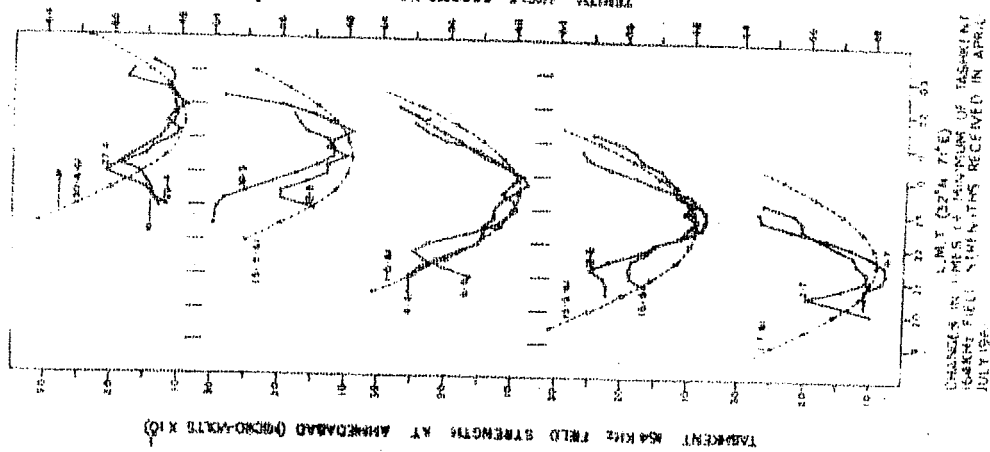
FIGURE 4.6

FIGURE 4.7

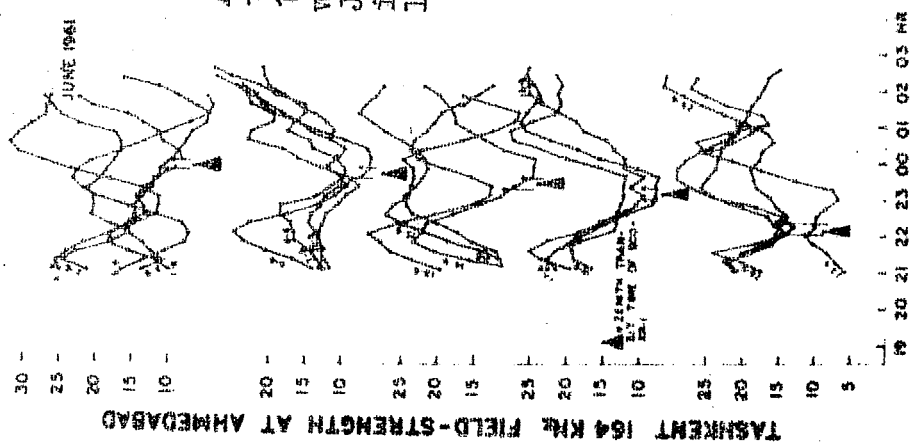
of Sco X-1 lasts for about 2- 2½ hours. During June 1961 the field intensities are plotted in figure 4.9 for all the nights when the Sco X-1 effect is observed. The sidereal shift of the pronounced minimum is followed on an average way from the beginning to the end of the month.

The method of superposed epoch analysis is employed to bring out the average effect more clearly. The transit time is taken as zero epoch and the value of the field strengths at fifteen minute intervals on either side of the transit time are tabulated. These values are then divided by the value of the observed field intensity at the transit time. For the following day the zero epoch is shifted by four minutes and the procedure repeated. The results of this analysis for June 1961 are shown in figure 4.10. The days when the effect is not seen clearly for long time ( about 2 - 3 hrs ) are not considered in this analysis. The low values of the field strength near transit and the higher values on either side bring out clearly the increased absorption of the radio waves during the onset of the X-ray source over the reflection meridian.

As there are occasional decreases in the field intensity, besides the pronounced decrease due to the effect of Sco X-1, it is necessary to study their general behaviour in case they showed any systematic variation. For this purpose all the depressions recorded in the night-time during 1960-62 are studied and the observed time of the minima are tabulated.



Selected records showing the effect of the transit of Sco X-1 on 164 kHz radio signal intensity during the period April-June 1961. Broken line represents the zenith angle variation of Sco X-1 during its transit.



All the night-time records of 164 kHz radio waves during June 1971. Arrows indicate transit line of Sco X-1.

FIGURE 4.8

FIGURE 4.9

The depressions showing widths more than  $1\frac{1}{2}$  hr are separated from the other depressions having width less than about  $1\frac{1}{2}$  hr. Very small depressions lasting upto  $\frac{1}{2}$  an hour have not been considered in this analysis. The results are plotted in figure 4.11, for May - June 1961-62. The straight line in the figure represents the time of meridian transits of Sco X-1 during May-June, across  $72^{\circ}\text{E}$ ,  $32^{\circ}\text{N}$ . The black dots and crosses represent the time of the minima for the large width and small width depressions respectively. It can be noticed that the prominent depressions ( shown by black dots ) cluster around the transit time of Sco X-1, whereas the other minima are randomly distributed. The black dots follow the transit time signifying their production due to Sco X-1 whereas the crosses do not show any systematic trend.

#### 4.5 Effects observed in the 164 kHz radio intensity during the transit of other galactic X-ray sources

To investigate the possible effects produced by other X-ray sources, an examination of all the sources listed by FRIEDMAN (1967) showed that only ones of importance, as far as the present propagation path is concerned, are Tau X-1 and the sources in the Cygnus region (Cyg X-1, Cyg X-2). Hence the X-ray sources Tau X-1, Cyg X-1 and Cyg X-2 and their effects will be considered in this section.

Tau X-1 was discovered by GURSKY ET AL. (1963) in the Crab Nebula. The exact location of the source is as

Relative field strengths  
(normalised) at different  
times before and after  
the transit of Sco X-1  
(June 1961)

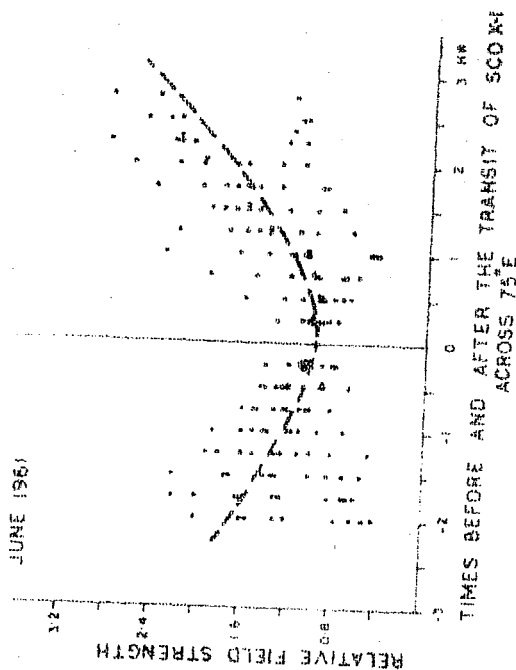


FIGURE 4.10

Time of occurrence of minima  
in the field-strengths of 164  
kHz at Ahmedabad during May-  
June (1960-61). Circles  
represent minima with the  
maximum width greater than  $1\frac{1}{2}$   
hours and crosses with less  
than  $1\frac{1}{2}$  hours.

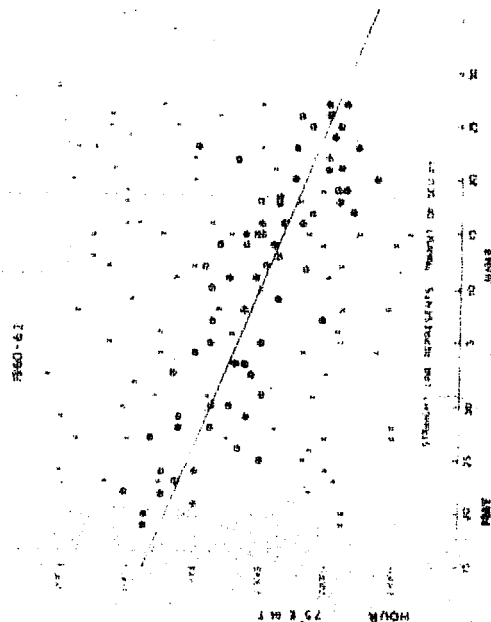


FIGURE 4.11

follows (BOWYER ET AL., 1964; ODA ET AL., 1967)

$$R.A = 5^h 31^m$$

$$\delta = + 22.1^\circ$$

The integrated flux of radiation in the 1-10 keV range is about  $4.3 \times 10^{-8}$  ergs/cm<sup>2</sup> which is about 10 times smaller than the value of  $2.5 \times 10^{-7}$  ergs/cm<sup>2</sup> for Sco X-1.

The locations of Cyg X-1 and Cyg X-2 as listed by FRIEDMAN (1967) are as follows:

Cyg X-1

$$R.A. = 19^h 53^m ; \delta = + 34.5^\circ$$

Cyg X-2

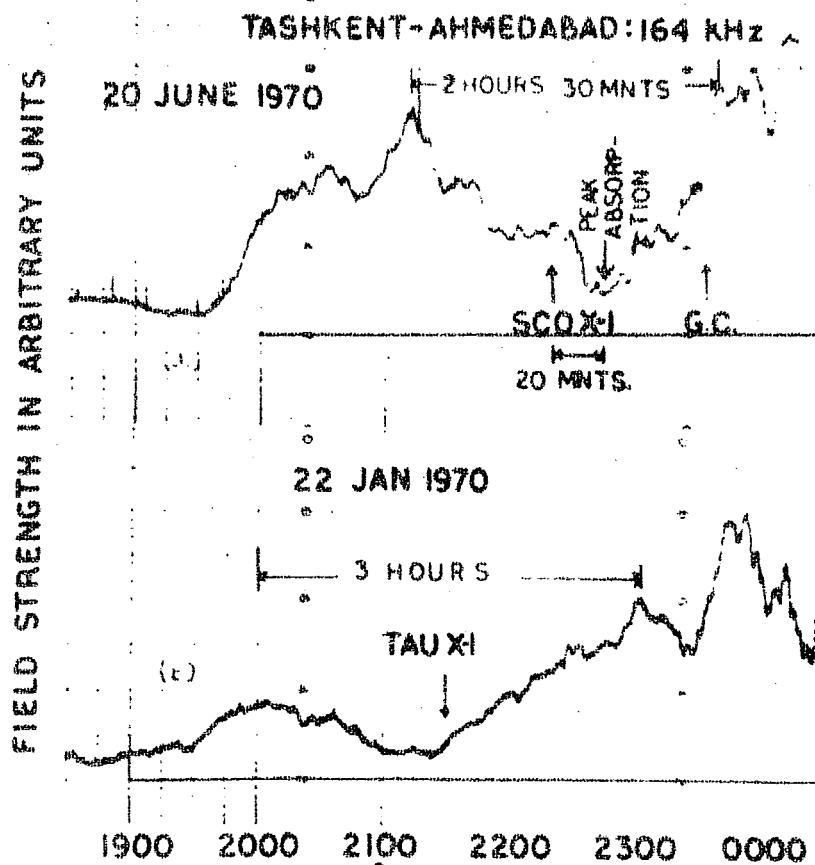
$$R.A. = 21^h 42^m ; \delta = + 38.8^\circ$$

The observations of Cyg X-1 by EYRAM ET AL. (1966) and FISHER ET AL. (1964) suggest that the source reduced in brightness by a factor of three within three months. Cyg X-2 has been observed to have almost equal luminosity with higher intensities in the higher energies (McCRACKEN K.G., 1966). Unlike the X-ray source Sco X-1 and Tau X-1 these sources show large variability in the radiation fluxes.

Though the flux intensities of X-rays from Tau X-1 are about one order of magnitude less compared to that of Sco X-1, Tau X-1 is better situated to produce an effect in the Tashkent - Ahmedabad radio propagation. The minimum zenith

angle is about  $10^\circ$  when Tau X-1 transits across the middle point of reflection for 164 kHz radio waves. A typical example of the amplitude changes during the transit of Tau X-1 for 22 January 1970 is shown in figure 4.12. The effect produced by Sco X-1 on 20 June 1970 is also presented in order to have a comparison of the relative effects. The time of transits for Sco X-1, Galactic Centre (G.C) and Tau X-1 are marked in the figure. Incidentally the two records are also the typical observations during summer and winter nights. For the record of 20 June 1970 the signal starts increasing after sunset and continues to increase except for the depression of about 2 hr 30 mts caused by the passage of Sco X-1 during that time. The field intensity increases after sunset for 22 January 1970 and reaches a peak value around midnight. There is a shallow depression of about 3 hrs, the minimum time of which coincides with the transit time of Tau X-1. This can be expected because the lower flux of this source in comparison with that of Sco X-1 will be partly compensated by its smaller zenith angles at transit. Also it can be noticed that the effect lasts longer in the case of Tau X-1. The effect of Tau X-1 in a general way can be seen from figure 4.13. A superposed epoch analysis similar to that for Sco X-1 is done for Tau X-1 during December 1960 - January 1961. It is noticed that the depressions produced by Tau X-1 in the signal amplitudes are smaller compared to that produced by Sco X-1 ( figures 4.13 and 4.10). There is some

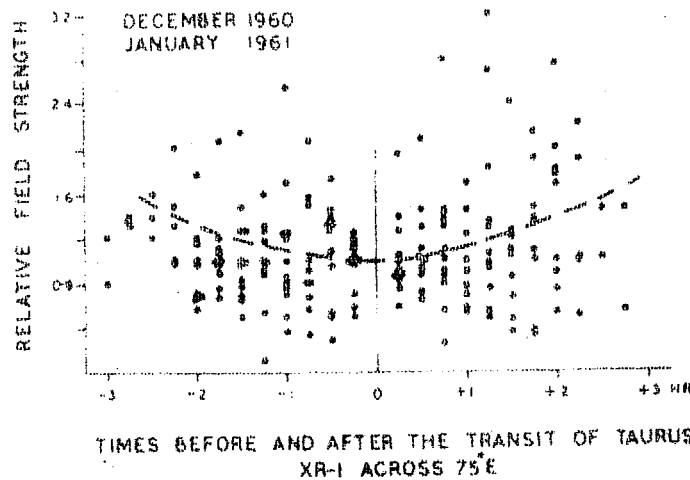




75° E.M.T.

Typical examples of the amplitude variations of 164 kHz radio intensity during the transits of X-ray sources Sco X-1 and Tau X-1.

FIGURE 4.12



Relative normalised field strength at different times before and after the meridian transit of

suggestion that the effect due to Tau X-1 will be observed for longer time as compared to that due to Sco X-1. Similar analysis of the effects produced by Sco X-1 during May - June 1969 and by Tau X-1 during December 1967 - January 1970 have been done and the resultant curves are plotted in figure 4.14. It can be seen that the excess average peak attenuations suffered by the radio waves during the transits of Sco X-1 and Tau X-1 are about 7 decibels and 4 decibels respectively. No definite effect for the X-ray sources, Cyg X-1 and Cyg X-2 have been identified in these radio observations at Ahmedabad.

#### 4.6 Other observational evidence supporting the effect of galactic X-rays on LF and VLF propagation during night

Almost simultaneous with the discovery by ANANTHA-KRISHNAN and RAMANATHAN (1969), EDWARDS ET AL. (1969) observed decrease in the annual variation of the diurnal phase difference during the months of April - May for the 20 kHz signals received at Wellington from Boulder. During the period of April - May a drop in reflection height of about 1 km is observed due to the onset of Sco X-1. The sidereal advance of 2 hrs/month is noticed in the phase anomaly within reasonable errors corresponding to that of the transit of Sco X-1.

KAUFMAN ET AL. (1970) observed a conspicuous night-time phase anomaly on 8 July 1969 in the 17.8 kHz radio waves received at Sao Paulo from N.A.A. (Cuttler, Maine).

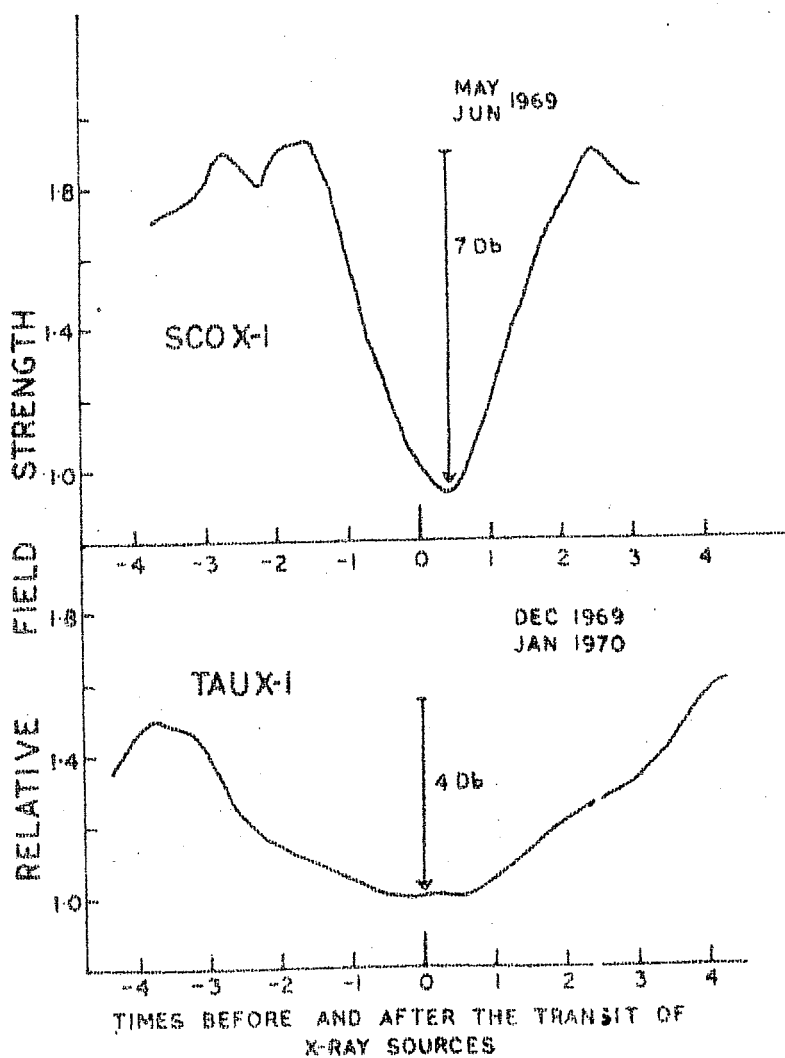


FIGURE 4.14

Average time profile of the 164 kHz field strength variations related to the transit of Sco X-1 and Tau X-1.

CONNER ET AL. (1969) have mentioned the discovery of a strong variable X-ray source near Centaurus ( Cen X-4 ) which appeared between 6 - 9 July 1969. They report that the phase deviation corresponding to the transit of this X-ray source is quite higher than the average night-time variation during July 1969 including the variation of one standard deviation range.

Observations of the VLF transmission NBA ( 18 kHz Balboa, Panama ) made at Tucuman, Argentina, during 1963-64 show a sidereal time variation in the diurnal amplitude change that follows the variation in percent illumination of the propagation path by Sco X-1 during the night-time hours. This has been reported by CHILTON and CRARY (1971). They notice that even-though the diurnal amplitude change can be shown to have a sidereal time variation, the diurnal phase change at Tucuman, Argentina, does not vary much throughout the year and yet remains consistently lower than that observed over a path of the same length from NBA to Boulder, Colorado, in the northern hemisphere. They conclude that the integrated effect of all the X-ray sources illuminating the southern hemisphere is to enhance the ionisation in the southern hemisphere night-time D-region, thus producing smaller diurnal phase change observed at Tucuman compared with that observed on the Boulder recording of the NBA signal over a propagation path of the same length in the northern hemisphere.

The above results alongwith the results presented in the present study suggest the possibility of brighter galactic X-ray sources producing ionisation changes in the night-time D-region which can be detected by the measurements of amplitudes and phases of LF and VLF radio waves reflected from this region during night. Very recently SVENNESSON ET AL. (1972) have observed the effect of Sco X-1, Cen X-2 and Cen X-4 on several of the numerous VLF phase recordings of OMEGA navigation system. The effect due to Tau X-1 has also been detected as a small phase anomaly. They conclude that VLF observations above the frequency of 20 kHz can be more suitable for the continuous monitoring of stellar X-radiation.

#### 4.7 Conclusion

The following conclusions can be drawn from the studies presented in this chapter:

(1) The few measurements of electron density and its effective loss rates in the night-time D-region indicate that the presence of free electrons below about 80 km is almost prohibited due to the rapid attachment of electrons to certain molecules and reactions governing the detachment of negative ions after sunset.

(2) LF radio waves propagating over long distances can provide useful informations about the variations of

night-time D-region.

(3) Average intensity variation of 164 kHz radio waves transmitted from Tashkent and received at Ahmedabad during night, fall under the two following categories:

(a) During winter months the signal amplitude increases after sunset reaching a maximum around local midnight and maintains that level upto sunrise.

(b) During summer the intensity shows a continuous increase from sunset to sunrise.

(4) It is suggested that at low latitudes the electrons produced by scattered Lyman  $\alpha$  intensity in the D-region are effective in maintaining the ionisation during winter whereas during summer because of the already existing high electron densities, the influence of this source is reduced.

(5) Pronounced depressions in the night-time field strength are observed which shift according to the sidereal time advance of the strong X-ray source Sco X-1. The effect of the source seems to last for about 2-3 hours.

(6) Comparatively weaker effect is also observed during the transit of the X-ray source Tau X-1 but its effect persists for a longer time compared to that of Sco X-1.

(7) Variable X-ray sources, like Cyg X-1 and Cyg X-2 though suitable in location for producing an effect do not show a definite influence on the signal intensities of LF radio waves received at Ahmedabad from Tashkent.

(8) On the average, the magnitude of absorption suffered by the LF radio waves are about 7 decibels and 4 decibels due to the effect of Sco X-1 and Tau X-1 respectively.

(9) The results of the effect due to the X-ray sources Sco X-1 and Tau X-1 observed at Ahmedabad combined with the observations at other places demonstrate that the brighter X-ray sources produce changes in the ionisation of D-region sufficient to be detected by LF and VLF measurement techniques.

#### 4.8 Discussion

In interpreting the diurnal phase variation of 15 kHz radio waves for the Rugby - Cambridge path, BELROSE and BOURNE (1966) have suggested the possibility of a nocturnal source of ionisation which is solar controlled having a maximum in the anti-solar direction. From the present study it appears that this source, which is identified as the scattered Lyman  $\alpha$  radiation, is sufficiently strong only after about local midnight of the non-summer months, so far as the effects produced on 164 kHz radio waves are concerned. The observation of the reduction of field intensity by a conside-

rable amount at the transit of Sco X-1 during summer months indicate the possibility that these X-rays produce more ionisation compared to that produced by scattered Lyman between 80 - 90 km during night. One more point is observed that the effect due to the X-ray sources is not clear upto about 1-2 hrs after sunset, probably because of the comparatively higher electron densities in that duration. The effect of Tau X-1 is quite distinct eventhough its flux intensity is an order of magnitude less compared to the source Sco X-1. Sources of approximately the same brightness Cyg X-1 and Cyg X-2 do not produce a clear effect inspite of their favourable locations. This can possibly be explained because Tau X-1 appears overhead in winter while Cyg X-1 and Cyg X-2 appear overhead in summer ( corresponding to  $32^{\circ}\text{N}$ ,  $72^{\circ}\text{E}$ ). In winter the ambient electron densities are lower compared to those in summer during night ( based on the present results ) which makes conditions favourable for Tau X-1 to produce the effect. Besides this, the Cygnus sources have large variability in their fluxes.

Hence the detectability of the effects produced by the galactic X-ray sources will depend upon the particular LF or VLF radio path, the coordinates of the source and the local conditions of the ambient electron densities in the D-region.



## CHAPTER - V

THEORETICAL ESTIMATES OF LF RADIO ATTENUATION DUE TO  
THE IONISATION PRODUCED BY NON-SOLAR X-RAY SOURCES5.1 Introduction

While positive results which have been described in the last chapter regarding the effect of strong nonsolar galactic X-ray sources in causing ionisation variations of nocturnal D-region, some results have also been reported which do not support the effect. The only contradictory observational result is that of BURGESS and JONES (1969). They have not observed any sidereal dependence ( in relation to X-ray sources) in the diurnal phase lag of 10.2 and 13.6 kHz radio waves transmitted from Trinidad (OMEGA) and received at Ottawa during the period 1966-68. The semiannual character of the variation of phase of these radio waves present during night hours has been attributed by them to the semiannual variation of neutral density around 90 km (COOK, 1969). They realise that, theoretically, significant amount of ionisation will be caused by the strong X-ray sources below about 85 km provided the production due to cosmic rays is small ( which depends upon the geomagnetic latitude). But the variations due to the X-ray sources will be masked by the larger semiannual variations making them difficult to be detected by phase measurements of the radio waves.

POPPOFF and WHITTEN (1969) have ruled out the possibility of a measurable enhancement of ionisation by Sco X-1 below about 90 km in the night-time D-region. From theoretical considerations they conclude that the electron densities due to the production of scattered Lyman $\alpha$  radiation will be so high that a comparatively meagre production due to Sco X-1 will perturb the values only by about a few percent. In calculating the production due to Lyman $\alpha$ , they consider the Nitric Oxide (NO) concentrations from the day-time measurements of BARTH (1964). They assume that the NO density will not change after sunset and will not be affected (so far as the calculation of production rates are concerned) because of the variability of the vertical transport processes in the mesosphere (GEISLER and DICKINSON, 1968).

A more detailed examination of the effect of cosmic X-rays in producing D-region ionisation by FRANCEY (1970) shows that the relative importance of the contributions from the discrete galactic sources critically depends on the assumed concentrations of NO in the 80-90 km region. The observability of the effect due to strong celestial X-ray sources depends on the magnitude of their ionisation effect in relation to that from all other causes and in particular to the magnitude of ionisation by Lyman $\alpha$  radiation.

The object of the present chapter is to study the effect of the galactic (non-solar) X-rays in the D-region from the theoretical stand point. Two ways in which the study has

been made are the following:

(a) The electron production rates due to Sco X-1 and Tau X-1 are estimated. The excess electron densities for the equilibrium conditions are computed by using extreme values of the available loss coefficients. These excess electron densities are superimposed on the night-time electron density profiles measured by rockets ( in the absence <sup>of</sup> perturbations). Then the attenuation of 164 kHz radio waves for the Tashkent-Ahmedabad path is computed due to the excess ionisation produced by Sco X-1 and Tau X-1 and compared with the observed values.

(b) The total electron production due to all other sources besides the galactic X-ray sources is estimated and the loss coefficients are calculated by direct comparison of the total production with the experimentally observed electron density profiles. These values of loss coefficients are then used in determining the enhancements in the ambient electron densities by the production due to Sco X-1 and Tau X-1. Again the calculation of attenuation of 164 kHz radio waves is repeated to have a comparison with the observed values. In the subsequent sections the results of the above calculations will be presented. A part of these results have already been published (ANANTHAKRISHNAN ET AL., 1970 ; CHAKRAVARTY, 1971; SHARMA ET AL., 1972).

## 5.2 Electron production rates by Sco X-1 and Tau X-1

In order to calculate the electron production the intensity distributions of the photons in the (  $1-8 \text{ \AA}$  ) region are required. In figure 5.1 we have plotted the spectral distributions of Sco X-1, Tau X-1 and also of sun during solar minimum and maximum conditions. The spectrum of Sco X-1 has been taken from FRIEDMAN (1967) who has summarised the measurements of CHODIL ET AL. (1965); GRADER ET AL. (1966) and HAYAKAWA ET AL. (1966). Spectral variations of Tau X-1 has been taken based on the observation of GRADER ET AL. (1966); CLARK (1965); HAYMES and CRADDOCK (1966, 1967); REIGLER ET AL. (1968); BOLDT ET AL. (1968). The solar spectra are taken from POPPOFF ET AL. (1964). It can be noticed from the figure that the intensity of X-rays above about 3.5 keV are more intense in the case of Sco X-1 compared to that of the quiet sun during sunspot minimum conditions. The fluxes are about one order of magnitude less for Tau X-1 compared to that of Sco X-1.

The electron production rates for Sco X-1 are shown in figure 5.2 for different zenith angles.  $\chi = 48^\circ$  corresponds to the minimum zenith angle of Sco X-1 with respect to the coordinates of the mid-point of reflection of 164 kHz radio waves. It can be noticed that a peak of ionisation is produced around about 80 km which shifts with the increase in the zenith angle. At  $\chi = 60^\circ$  the values of production are about an order of magnitude less than the maximum value.

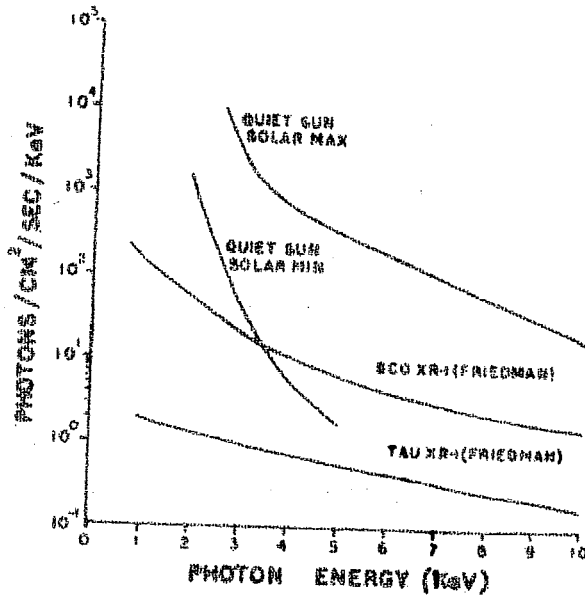
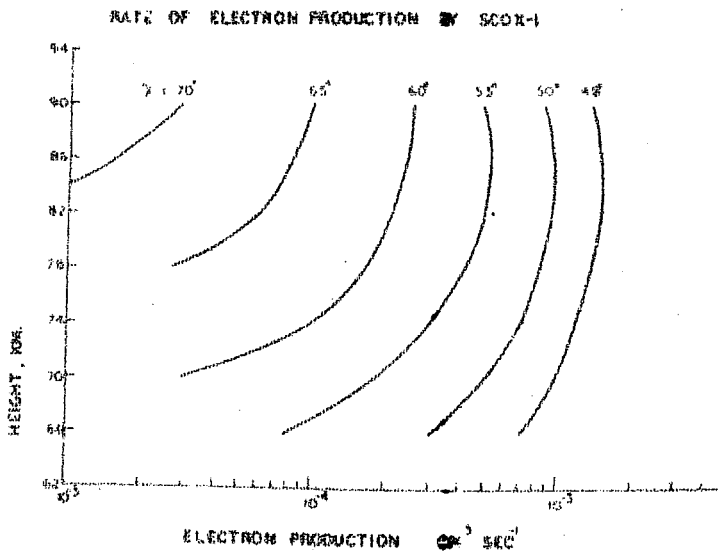


FIGURE 5.1

Photon fluxes of 1 - 10 KeV (X-rays) from the quiet sun under solar minimum condition, from the non-flare sun under solar maximum conditions, and from Sco X-1 and Tau X-1.



Electron production relates at 65 - 90 km due to ScoX-1.

FIGURE 5.2

Based on an examination of all the available results on the absolute flux of Sco X-1 since 1965, RAO ET AL. (1970) have observed the flux to decrease steadily over the period of 1965-68. The spectral distribution of Sco X-1 is generally well approximated to an exponential function:

$$J(E) = K \exp ( -E/kT) \quad \text{..... (5.1)}$$

where E = energy of photon

K = constant

k = Boltzman constant

T = temperature in absolute units

For the spectrum which can be best fitted by the equation (5.1), the values of K and T are available in the literature. Table 5.1 summarises the spectral indices of this source from the observations during the period 1964 to 1968. To determine the effect of the decaying flux intensity of Sco X-1 in the magnitude of production function we repeat the calculations of production for  $\chi = 0^\circ$  based on the spectral indices of table 5.1. The results are shown in figure 5.3. It can be seen that the peak production seems to have varied by about 2 - 3 times in the period 1965-67.

It has also been noticed from these calculations that by changing the air density by about 30% the production values change only by about 5- 10% below 85 km.

Table 5.1Spectral indices of Sco X-1 for different measurements

Experimenter(s)	Flight date	Temperature °K	K	kT(keV)
Fisher et al.	1 October, 1964	$1.6 \times 10^7$	286	1.38
Chodil et al.	12 June, 1965	$4.8 \times 10^7$	31	4.1
Hayakawa et al.	26 July, 1965	$3.8 \times 10^7$	$36 \pm 9$	$3.3 \pm 0.2$
Grader et al.	28 October, 1965	$4.6 \times 10^7$	$28 \pm 1$	3.9
Gursky et al.	28 March, 1966	$5.0 \times 10^7$	$22 \pm 1$	4.3
Chodil et al.	28 July 1966	$5.8 \times 10^7$	$22 \pm 1$	5.0
Gursky et al.	11 October, 1966	$4.8 \times 10^7$	$19 \pm 3$	4.1
Matsouka et al.	6 February, 1967	$5.0 \times 10^7$	$19 \pm 2$	4.3
Chodil et al.	18 May 1967	$8.1 \times 10^7$	$20 \pm 2$	6.9
Rappaport et al.	6 July, 1967	$7.5 \times 10^7$	$8 \pm .5$	6.4
Chodil et al.	29 September, 1967	$4.6 \times 10^7$	18	3.9
Rao et al.	3, 7 Nov 1968	$5.1 \times 10^7$	$55 \pm 5$	$4.4 \pm 0.2$

The production rates for Tau X-1 have been calculated by using the spectrum of figure 5.1. These are shown in figure 5.4 for different values of zenith angle. The maximum value of production is about  $2 \times 10^{-4}/(\text{cm}^3 \cdot \text{sec})$  for the zenith angle of  $10^\circ$  (corresponding to mid-point of reflection). The point to be noticed is that the peak ionisation is produced between about 70 - 75 km which is lower in comparison to that produced by Sco X-1. This is because the Tau X-1 spectrum is harder than that of Sco X-1, thus producing more ionisation in lower heights of the D-region.

### 5.3 Electron densities of the night-time D-region during the passage of Sco X-1 and Tau X-1

The equilibrium condition electron densities for the production rates of Sco X-1 and Tau X-1 can be estimated from equation (3.6) by equating  $\partial N / \partial t = 0$ , so that we have the following relation:

$$N = \left( \alpha / \gamma \right)^{1/2} \quad \dots (5.2)$$

It has been discussed that there is a good deal of uncertainty about the effective loss coefficients of electrons during night. In the present calculations we have taken the curves 2 and 3 of figure 4.2 for the loss coefficient and curve 1 of figure 4.1 for the ambient electron densities. The electron densities at different heights of the ionosphere are computed from three hours before to three hours after the transit



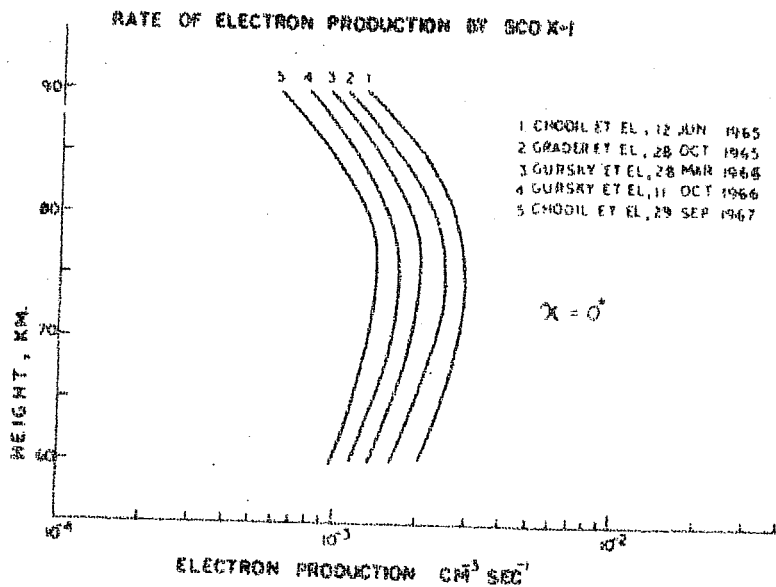
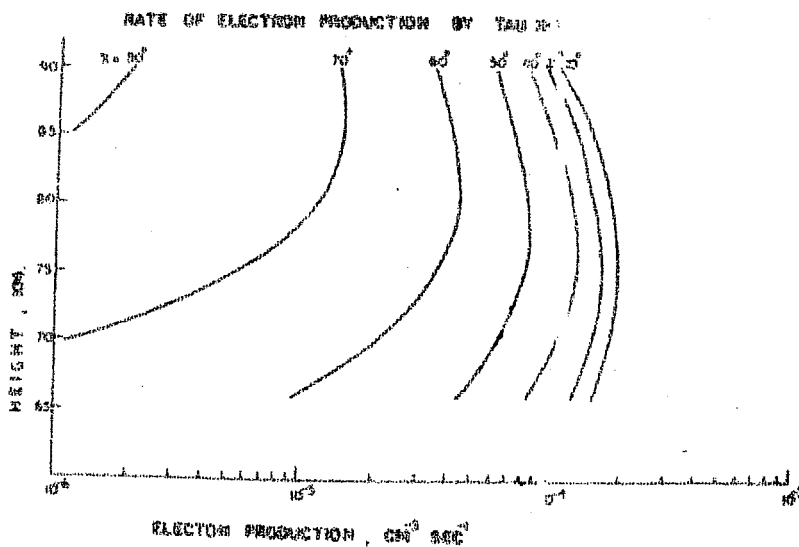


FIGURE 5.3  
 Electron production rates due to Sco X-1 taking into consideration the possible decay of X-ray emission from 1965 to 1967.



Electron production rates at 65 - 90 km due to Tau X-1.

FIGURE 5.4

of the source. Figure 5.5 shows two sets of the values corresponding to the values of curve 3 and curve 2 ( figure 4.2) in the case of Sco X-1. Similar curves for Tau X-1 are presented in figure 5.6. It can be noticed that Sco X-1 produces larger variation in the electron densities at all heights compared to those by Tau X-1.

#### 5.4 Wave-admittance method of Barron and Budden

The method of getting the reflection coefficients of the ionosphere for sharply bounded approximation due to SHEDDY(1968) has been described in Chapter I. For a realistic treatment of long radio waves of frequencies below 1 MHz in the ionosphere, it is necessary to use the full-wave theory. In the case of low frequency wave propagation, part of the upgoing energy of both the ordinary and extraordinary components of the waves is continuously converted into downgoing energy over a range of heights. The received intensity at the ground will be the integrated effect of the partial reflections from various levels in the ionosphere. Hence BOOKER's theory, which refers to reflection at a single level, has to be extended for the real case when the partial reflections from a range of heights are to be considered. The wave admittance method developed by BARRON and BUDDEN (1959) which deals with the problem of such a nature should be used to compute the reflection coefficients. Before describing the theory and the final equations used for

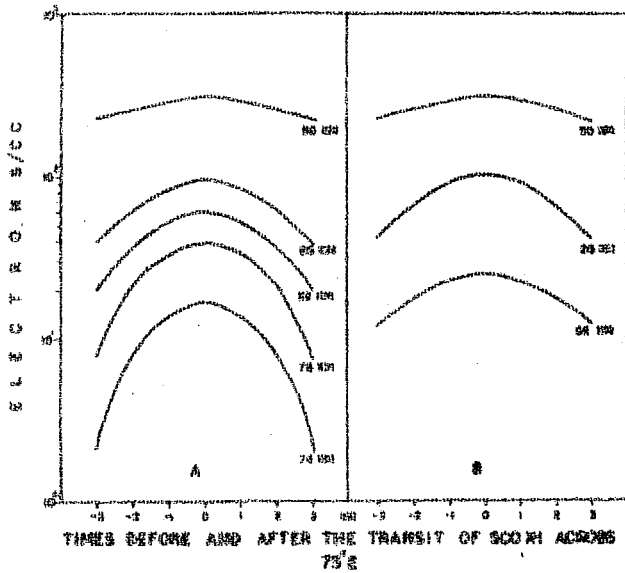


FIGURE 5.5

Time profiles of equilibrium electron density produced by Sco X-1 during night assuming two extreme loss rates of electrons.

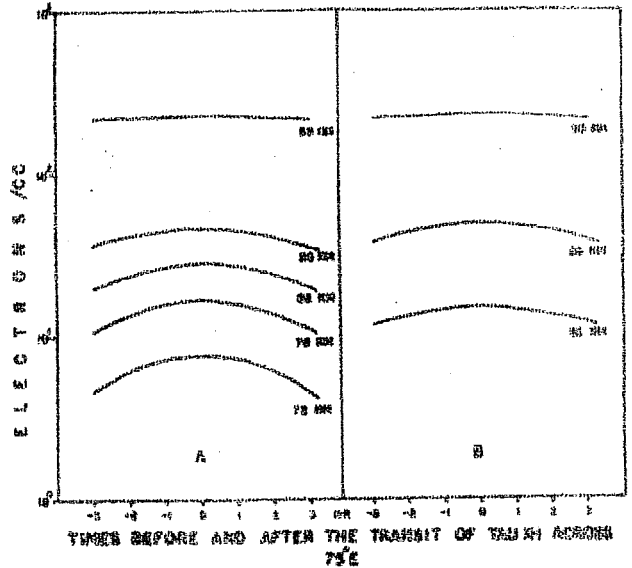


FIGURE 5.6

Time profiles of equilibrium electron density produced by Tau X-1 during night assuming two extreme loss rates of electrons.

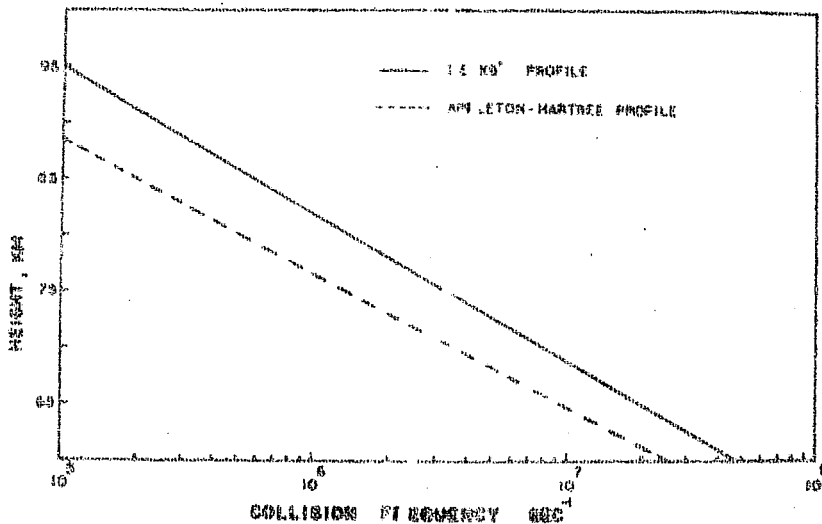


FIGURE 5.7

Collision frequency variation of monoenergetic electrons

the computation, it is convenient to tabulate the symbols appearing in the theory and the subsequent computations. All the quantities are in standard MKS units:

$x, y, z$	Cartesian co-ordinates; $z$ is measured vertically upwards and $x$ is measured horizontally in the plane of incidence, towards the receiver
$\omega$	$2\pi f$ where $f$ is the wave frequency
$c$	velocity of electromagnetic waves in free space
$k$	magnitude of wave vector = $\omega/c = 2\pi/\lambda$ (where $\lambda$ is the wavelength in free space)
$\vec{B}$	Earth's magnetic field
$l, m, n$	Direction cosines of magnetic field vector $\vec{B}$
$e, m$	Charge and mass of the electron
$\epsilon_0, \mu_0$	Electric and magnetic permeabilities of free space
$N$	Number of electrons per unit volume
$\nu$	Effective collision frequency of electrons
$X$	$N_e^2 / \epsilon_0 m \omega^2$
$N$	Electron density per unit volume

$\bar{y}$	$e\bar{B}/m\omega$ ; since $e$ is negative, $\bar{y}$ and $\bar{B}$ oppositely directed
$z$	$y/\omega$
$\theta_i$	Angle between the vertical and the wave normal of the incident wave below the ionosphere
$\theta_r$	Angle of refraction
$\alpha$	Azimuth of magnetic north in the horizontal plane from positive X-axis
$\phi$	Magnetic dip angle
$S, C$	$\sin \theta_i$ , $\cos \theta_i$
$E_x, E_y, E_z$	Components of the electric field vector $E$ of the wave
$H_x, H_y, H_z$	Components of the magnetic field vector $H$ of the wave
$Z_0$	$(\mu_0/\epsilon_0)^{\frac{1}{2}}$ , characteristic impedance of free space
$\mathcal{K}_x, \mathcal{K}_y, \mathcal{K}_z$	$Z_0 (H_x, H_y, H_z)$
$[M]$	Susceptibility matrix

: 160 :

$[T]$  4 x 4 transmission matrix

$[R]$  2 x 2 reflection coefficient matrix

$R_{11}, R_{12}$

$R_{21}, R_{22}$

Components of matrix  $[R]$

$[A]$  Generalised wave admittance matrix for anisotropic medium

$L$  Absorption in decibels

$\vec{E}$  Electric polarisation

$U$   $1 - iZ$

$i$   $\sqrt{-1}$

For the present calculations, the coordinate system chosen is the same as shown in figure 1.10

It is assumed that the ionosphere is horizontally stratified and contains electrons whose motion is influenced by the earth's magnetic field and damped by collisions with neutrals. Then the equation of motion of an electron is written as:

$$e\vec{E} + e \frac{\partial \vec{\pi}}{\partial t} \times \vec{B} = m \frac{\partial^2 \vec{\pi}}{\partial t^2} + m\nu \frac{\partial \vec{\pi}}{\partial t} \quad \dots (5.3)$$

This yields the following matrix equation:

$$\frac{1}{\epsilon_0} \begin{pmatrix} P_x \\ P_y \\ P_z \end{pmatrix} = - \frac{\chi}{U(U^2 - Y^2)} \begin{pmatrix} U^2 - \ell^2 Y^2 & -i n Y U - \ell m Y^2 & i m Y U - \ell n Y^2 \\ i n Y U - \ell m Y^2 & U^2 - n^2 Y^2 & -i \ell Y U - m n Y^2 \\ -i m Y U - \ell n Y^2 & i \ell Y U - m n Y^2 & U^2 - n^2 Y^2 \end{pmatrix} \begin{pmatrix} E_x \\ E_y \\ E_z \end{pmatrix} \quad (5.4)$$

The expression multiplying E is called the susceptibility matrix denoted by  $[M]$ . Equation (5.4) along with the Maxwell's equations for the said coordinate system gives the following matrix differential equation:

$$i \frac{d[A]}{dz} = k \left\{ \begin{pmatrix} A_{11} & A_{12} \\ A_{21} & A_{22} \end{pmatrix} \begin{pmatrix} -T_{11} & T_{12} \\ 0 & 0 \end{pmatrix} + \begin{pmatrix} T_{44} & 0 \\ T_{34} & 0 \end{pmatrix} \begin{pmatrix} A_{11} & A_{12} \\ A_{21} & A_{22} \end{pmatrix} \right. \\ \left. + \begin{pmatrix} A_{11} & A_{12} \\ A_{21} & A_{22} \end{pmatrix} \begin{pmatrix} -T_{14} & 0 \\ 0 & 1 \end{pmatrix} \begin{pmatrix} A_{11} & A_{12} \\ A_{21} & A_{22} \end{pmatrix} + \begin{pmatrix} T_{41} & -T_{42} \\ T_{31} & -T_{32} \end{pmatrix} \right\} \quad \dots(5.5)$$

where  $T_{ij}$ 's denote the following matrix

$$[T] = \begin{pmatrix} \frac{-S M_{zx}}{1 + M_{zz}} & \frac{S M_{zy}}{1 + M_{zz}} & 0 & \frac{C^2 + M_{zz}}{1 + M_{zz}} \\ 0 & 0 & 1 & 0 \\ \frac{M_{yz} M_{zx}}{1 + M_{zz}} - M_{yx} & \frac{C^2 + M_{yy}}{1 + M_{zz}} - \frac{M_{yz} M_{zy}}{1 + M_{zz}} & 0 & \frac{S M_{yz}}{1 + M_{zz}} \\ 1 + M_{yx} & \frac{M_{xz} M_{zx}}{1 + M_{zz}} & \frac{M_{xz} M_{zy}}{1 + M_{zz}} - M_{xy} & - \frac{S M_{xz}}{1 + M_{zz}} \end{pmatrix} \quad \dots(5.6)$$

Where  $M_{ij}$ 's are the components of the susceptibility matrix given in equation (5.4) and the dependent variable (A) is the wave admittance matrix given by

$$[A] = \begin{pmatrix} \mathcal{H}_y^{(1)} & \mathcal{H}_y^{(2)} \\ \mathcal{H}_x^{(1)} & \mathcal{H}_x^{(2)} \end{pmatrix} \begin{pmatrix} E_x^{(1)} & E_x^{(2)} \\ E_y^{(1)} & E_y^{(2)} \end{pmatrix}^{-1} \quad \dots(5.7)$$

the superscripts (1) and (2) denote the upgoing and downgoing waves. The components of (T) matrix are functions of electron density and collision frequency and hence vary with height. The value of wave admittance matrix at any particular height of the ionosphere enables us to determine what fraction of the amplitude ratios of the incident magnetic and electric wave fields will be reflected from and transmitted into the ionosphere. In order to get the value of the ratios of H/E which gives the measure of the wave admittance of the radio waves leaving the ionosphere after reflection we have to integrate the differential equation (5.5) step by step downwards through the ionosphere (with N and  $\nu$  as parameters) to a defined lower level below the ionosphere. The final value of the wave admittance matrix gives the reflection coefficients of the ionosphere from the following relation:

$$[R] = \begin{pmatrix} R_{||} & R_{\perp} \\ R_{||} & R_{\perp} \end{pmatrix} = 2 \begin{pmatrix} -CA_{11}-1 & A_{12} \\ A_{21} & 1-A_{22}/C \end{pmatrix}^{-1} \begin{pmatrix} 1 & 0 \\ 0 & -1 \end{pmatrix} \quad \dots(5.8)$$



The absorption  $L$  of the radio waves in decibels is related to the final value of any component of  $R$  by the following formula:

$$L = -20 \log R \quad \dots (5.9)$$

To start the integration of differential equation (5.5), initial values of the wave admittance matrix  $[A]$  are required at a particular height. Shetty's method is used to obtain the initial solutions. The initial values of  $[A]$  can be obtained from the initial values of  $R$  using the following relationship.

$$[A] = \begin{pmatrix} -\left(\frac{1 R_{11} + 1}{2 R \text{ POLY}} + 1\right) / c & -\frac{11 R_{11}}{2 R \text{ POLY}} \\ -\frac{1 R_{11}}{2 R \text{ POLY}} & -\left(\frac{(11 R_{11} - 1)}{2 R \text{ POLY}} - 1\right) c \end{pmatrix} \quad \dots (5.10)$$

Where  $R \text{ Poly}$  represents reflection from a polytropic atmosphere.

#### 5.5 Calculation of the attenuation suffered by LF radio waves passing through the excess ionisation produced by Sco X-1 and Tau X-1

##### (a) Initial values of $[R]$ for 164 kHz radio waves

The initial values of the reflection coefficients at a height of 90 km are computed, as the waves during night will be reflected from a region below this altitude.

Besides calculating the initial value of  $[R]$ , an attempt has been made to calculate the reflection coefficients for a range of heights giving at each height the values of electron density, collision frequency and the angle of incidence. Other quantities in the input data ie., dip angle, azimuth, magnetic field etc. are kept unchanged for each set. The collision frequency profile used for the analysis is taken from DEEK's paper (1966) and is shown in figure 5.7. This profile is also in good agreement with that derived from the theoretical calculations of SEN and WYLLER (1960). The electron density profile for a normal night has been taken from SMITH's rocket observations of 27 October 1961 at Wallops Island. The equilibrium electron density profiles during the meridional transit (across  $71^{\circ}E$ ) for Sco X-1 and Tau X-1 along with the normal profile have been included in figure 5.8. The electron densities produced by the X-ray sources have been calculated down to 78 km; below this height, the values of loss coefficients are very high and uncertain. Hence in our calculations it is assumed that the electron density below 75 km will not change appreciably from the normal value during the transit of Sco X-1 and Tau X-1. The calculation of reflection coefficient at various heights is repeated for the electron density profiles during the transit of Sco X-1 and Tau X-1. The amplitude of  $||R||$  is plotted for the height range 78 to 95 km for the electron density curves in the normal night as well as for nights when the atmosphere is

illuminated by Sco X-1 and Tau X-1. From figure 5.9, it can be seen that on a normal night, the value of the reflection coefficient is less than 0.2 upto 85 km and that there is a sharp increase in the value of the reflection coefficient between 85 and 87 km. It is expected that most of the energy of 164 kHz radio waves during a normal night will be reflected from the height region 85 to 90 km in the ionosphere. The value of the reflection coefficient at lower heights between 85 to 78 km increases from about 0.20 to 0.45 and 0.60 when electron production by Sco X-1 and Tau X-1 is considered ( see dashed lines in figure 5.9 ). Hence it can be concluded that most of the additional intensity of reflected radio waves (164 kHz) during the transit of Sco X-1 and Tau X-1, will come from the height range of 80-85 km. Therefore due to the electron densities produced by Sco X-1 and Tau X-1 a change in the phase of the radio waves corresponding to the height change of about 1-2 km should be observed. The absorption of the radio waves corresponding to the changes in the reflection coefficients by the electron production of Sco X-1 and Tau X-1 will be of the order of 4-5 and 2-3 decibels respectively. These results of absorption are somewhat smaller than the values of absorption of 164 kHz radio waves actually observed at Ahmedabad during the transits of Sco X-1 and Tau X-1. It may be mentioned that though an estimate of the phase change can be made by using the sharply bound model of the ionosphere, one has to resort to full wave calculations for

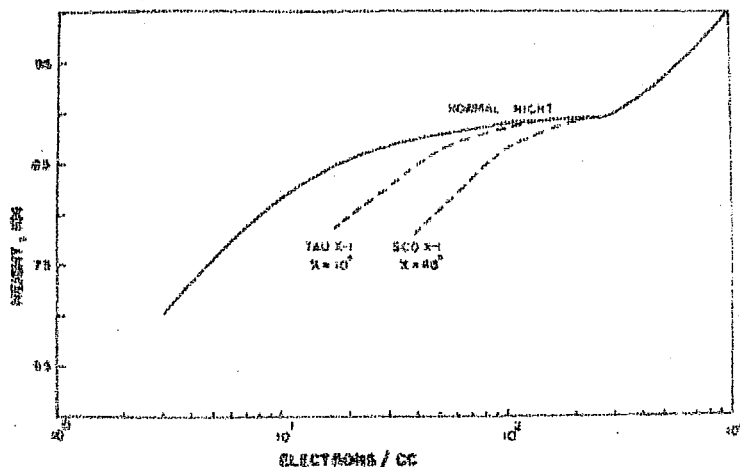


FIGURE 5.8

The electron density profile for a normal night in the D-region is shown as continuous line (based on Smith's rocket observations at Wallops Island). The two broken lines show the equilibrium electron density profiles during the transit across  $71^\circ\text{E}$  of Sco X-1 and Tau X-1 respectively.

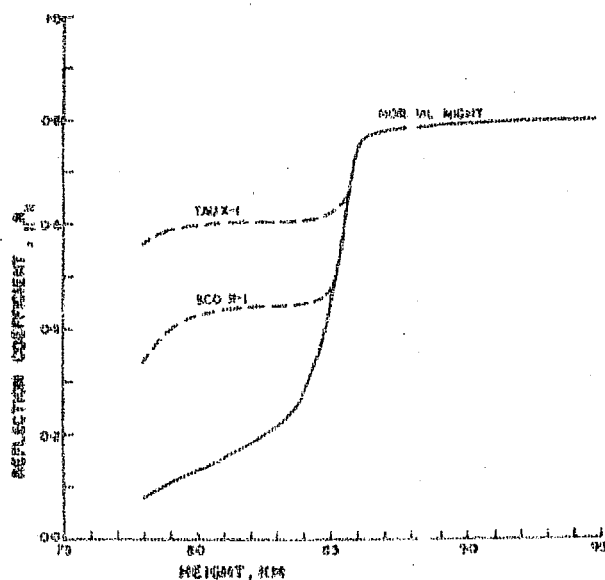


FIGURE 5.9

The variation of the amplitude of reflection coefficient ( $R_{11}$ ) with height for the above three electron density profiles

determining the absorption produced by the electron density profiles of Sco X-1 and Tau X-1.

(b) Final values of  $[R]$  by full-wave theory

A modified Runge Kutta method due to GILL (1951) has been used for the numerical integration down through the real ionosphere starting with the initial solutions already obtained in the last section. The initial values of wave admittance matrix  $[A]$  are obtained from the initial values of  $[R]$  by using equation (5.10). It has been suggested by Budden that the step size of the integration of the four differential equations (5.5) should be roughly about  $\lambda/50$ . This step-size should be about .04 km for 164 kHz radio waves. The smaller the step size, the longer is the time taken in the computer for integration. Since the real and imaginary components of the derivatives are to be integrated separately, hence it finally comes to integrating eight simultaneous differential equations to get the final complex value of wave admittance. It has been checked that the step size can be conveniently reduced to a value of 0.1 km without much deviation in the results.

The values of electron density and collision frequency starting from 90 km down to 70 km are given in the input data at intervals of 1 km. Linear interpolation is used to get the values of electron density and

collision frequency at an interval of .05 km, needed in the Runge-Kutta integration for a step size of .1 km. The final reflection coefficient values are obtained for the electron density profiles of the normal night and of the ones shown in figures 5.10 and 5.11. Figure 5.10 shows the electron density profiles before and after 1, 2 and 3 hrs from the transit time ( $\chi = 48^\circ$ ) of Sco X-1. Figure 5.11 shows similar profiles for Tau X-1. The increased absorption of radio waves due to the transit of Sco X-1 and Tau X-1 can be calculated by subtracting the value of absorption due to the normal electron density profile. Similarly the absorption after or before 1, 2 and 3 hrs of transit of Sco X-1 and Tau X-1 are estimated. It is noted that the coefficients  $_{||}R_{||}$  and  $_{\perp}R_{\perp}$  are approximately the same in magnitude, which is also true for the coefficients  $_{||}R_{\perp}$  and  $_{\perp}R_{||}$ . Figure 5.12 shows the values of attenuation calculated from the reflection coefficient  $_{||}R_{||}$  or  $_{\perp}R_{\perp}$  for Sco X-1 and Tau X-1 at, before and after 1, 2 and 3 hrs from their transits. Also included in the diagram are the average observed values of absorption calculated from the field-strength records of 164 kHz radio waves at Ahmedabad for the period May - June 1961. It can be seen from the Figure that the trend of the calculated values compare well with those of the observed ones. For Sco X-1 the calculated value of absorption for the time of transit is about 12 dB compared to about 7 dB for that of the observed. The corresponding values are about 6 dB and 4 dB

for Tau X-1. It can be noted from the figure that before and after two hours of the transit of Sco X-1 the value of absorption is lower than the corresponding value due to Tau X-1. Hence the effect due to Tau X-1 though much smaller in magnitude compared to Sco X-1, will be observed for a longer time. The flatness of the curve due to Tau X-1 is observed both experimentally as well as theoretically. Figure 5.13 shows the values of attenuation calculated from the other two reflection coefficients " $R_1$ " or " $R_2$ ". The values of absorption are about 14 dB and 8 dB for Sco X-1 and Tau X-1 respectively.

The possible explanation of the difference between the calculated and observed values of attenuation are as follows:

(1) The equilibrium electron densities are calculated from the equation:

$$\partial N / \partial t = Q - \gamma N^2 = 0$$

In order to get the electron densities at various times of the transit of the X-ray source, we have to know the value of  $N$  at different times during the passage of the source and at different levels. There is a good deal of uncertainty about the quantitative values.

(2) The contribution from all the four different polarisations of the reflected waves will add upto more observed intensity which will mean less absorption compared to the

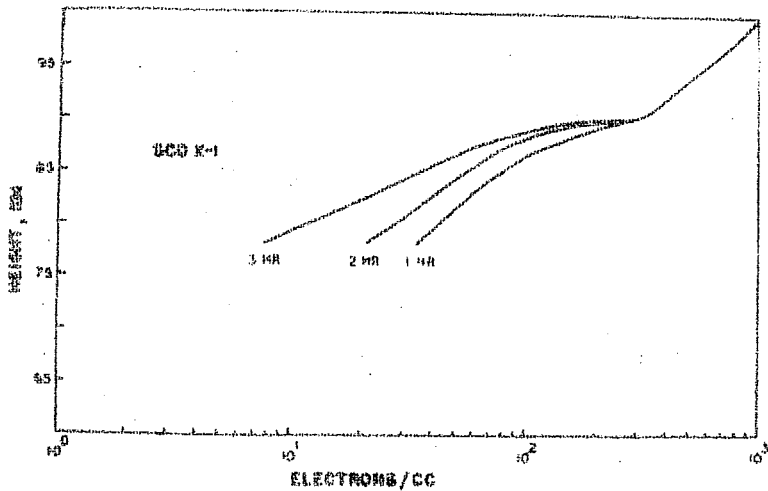


FIGURE 5.10

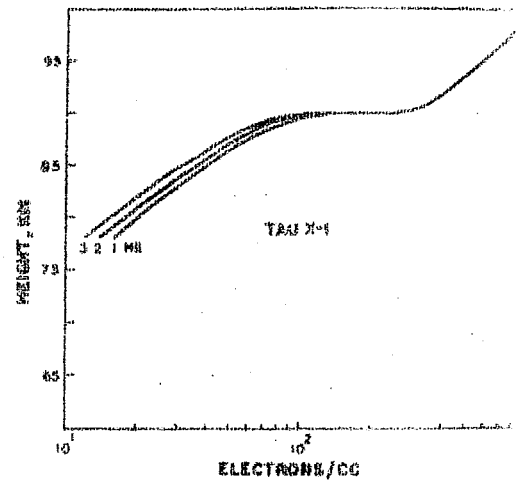


FIGURE 5.11

The curves show the electron density profiles in the D-region after the 1st, 2nd and 3rd hour of the transit of Sco X-1 and Tau X-1 across 71°E.

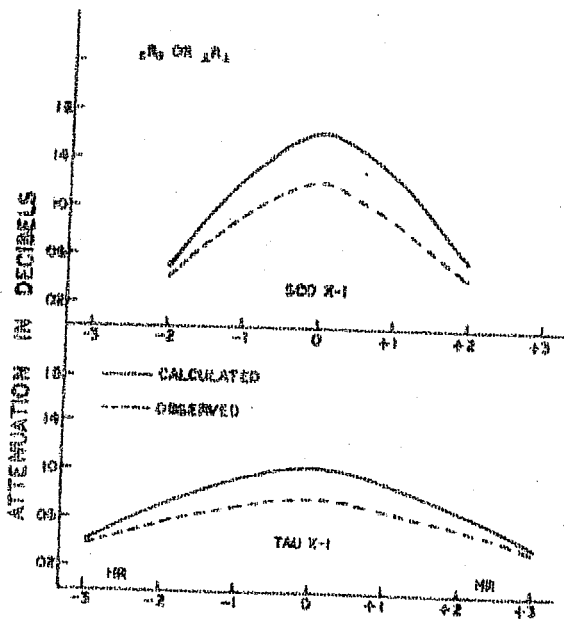


FIGURE 5.12

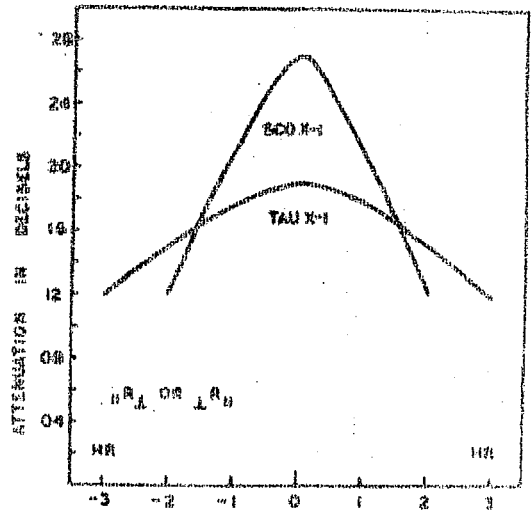


FIGURE 5.13

The calculated (Budden's wave admittance method) and observed time variation of the absorption of 164 kHz radio

Calculated (Budden's wave-admittance method) time variation of the attenuation of 164 kHz radio



calculated values of absorption individually for the four components. The fractional contribution of each component will depend upon the antenna orientation.

(3) Full wave theory used have assumed a single mid-point reflection from the ionosphere. Multiple reflection of atleast second and third-hop propagation should also be taken into account. These additional modes would increase the intensity and hence reduce the calculated values of absorption.

The calculated and observed attenuation of the radio waves will match perfectly if the electron density profile after one hour of Sco X-1 transit ( figure 5.10 ) is taken as the peak ionisation produced by Sco X-1. Then comparing the excess electron densities with the maximum production rates during the equilibrium condition the effective loss rates of night-time D-region can be estimated. The results are shown in Table 5.2. These values are also plotted in figure 4.2.

#### 5.6 Review of all possible night-time ionizing sources and their production rates in the D-region

It has been seen in the previous chapter that the detection of the effect due to galactic X-ray sources depends upon the ambient electron density which varies with season and also possibly with solar activity. Hence in this section we critically examine the ionisation rates by all the possible agencies contributing to the ambient electron density of night-time D-region.

Table 5.2

Effective loss rates in the night-time D-region from  
LF absorption due to the ionisation produced by Sco X-1

Height	Total electron density/ cc/sec.	Ambient electron density/ cc/sec.	Electron density due to Sco X-1/ cc/sec.	Production rate by Sco X-1/ cc/sec.	Effective loss rate	Effective loss rates (obs. (Medaaimid and Budznisky)
78	34.0	6.4	27.6	$1.4 \times 10^{-3}$	$1.8 \times 10^{-6}$	$10^{-4}$
80	41.0	8.0	33.0	$1.5 \times 10^{-3}$	$1.3 \times 10^{-6}$	-
82	50.0	10.0	40.0	$1.5 \times 10^{-3}$	$9.3 \times 10^{-7}$	$5 \times 10^{-6}$
84	66.0	15.0	51.0	$1.5 \times 10^{-3}$	$6.0 \times 10^{-7}$	-
86	90.0	22.0	68.0	$1.5 \times 10^{-3}$	$3.0 \times 10^{-7}$	$2.0 \times 10^{-7}$

These ionizing sources in the nocturnal D-region are now identified to be (i) diffuse cosmic background X-rays (ii) galactic cosmic radiation and (iii) scattered Lyman  $\alpha$  radiation. In addition to these sources the possibility of soft electron fluxes producing ionisation in the D-region has been reported by TULINOV ET AL. (1969) and POTEIRA and ZMUDA (1970). These electron fluxes precipitate from the Van Allen belts (THOMAS, 1971 and AIKIN, 1971). But because of the inconclusive nature of the evidence on the importance of these fluxes as a night-time source of electrons in the D-region, especially for lower latitudes, they are not considered in the present study.

(a) The diffuse cosmic X-rays

The galactic X-ray sources are observed against a diffuse X-ray background of celestial origin which is isotropic in character (GOULD, 1969). The fluxes in the 1- 10 keV of these background X-rays have been quite accurately measured by rocket borne experiments (BOLDT ET AL., 1969; GORENSTEIN ET AL., 1969 and PRAKASHRAO ET AL., 1971). These X-rays will be a constant source of electron production in the D-region, independent of time and season. The electron production rates have been calculated by assuming a spectral distribution of the following type (KASTURIRANGAN and RAO, 1972).

$$J(E) = 13.6 E^{-1.7} \text{ photons cm}^{-2} \text{ sec}^{-1} \text{ keV}^{-1} \quad \dots (5.11)$$

(b) Galactic cosmic rays

The electron production due to galactic cosmic rays has already been discussed in chapter I. The electron production rates by cosmic rays at geomagnetic latitude  $23^\circ$  in the 60 - 100 km range is shown in figure 5.14. The shaded area represents the extent of variation resulting from the solar modulation effects of the cosmic radiation and the seasonal variation of the atmospheric densities.

(c) Scattered Lyman $\alpha$  Radiation

The scattered Lyman $\alpha$  radiation from the hydrogen of solar geocorona is believed to be the most important nighttime source of ionisation in the D-region. The correct estimate of the production of ionisation by Lyman $\alpha$  radiation requires an accurate knowledge of the nighttime Lyman $\alpha$  intensity as well as the concentration of the ionisable constituent nitric oxide.

The satellite data on Lyman $\alpha$  intensity by the space-crafts OGO III, OGI IV and OSO IV from 20 KR at noon down to 1.1 KR at midnight (MEIER, 1970). Over a solar cycle a change by almost a factor of two in the Lyman $\alpha$  intensity has been suggested by HINTEREGGER (1965). For the present calculation Lyman $\alpha$  intensities of 1.1 KR or  $1.5 \times 10^{-3}$  ergs/cm<sup>2</sup>/sec/sr for the solar minimum period and 2.2 KR or  $3 \times 10^{-3}$  ergs/cm<sup>2</sup>/sec/sr for the solar maximum period are assumed outside the absorption

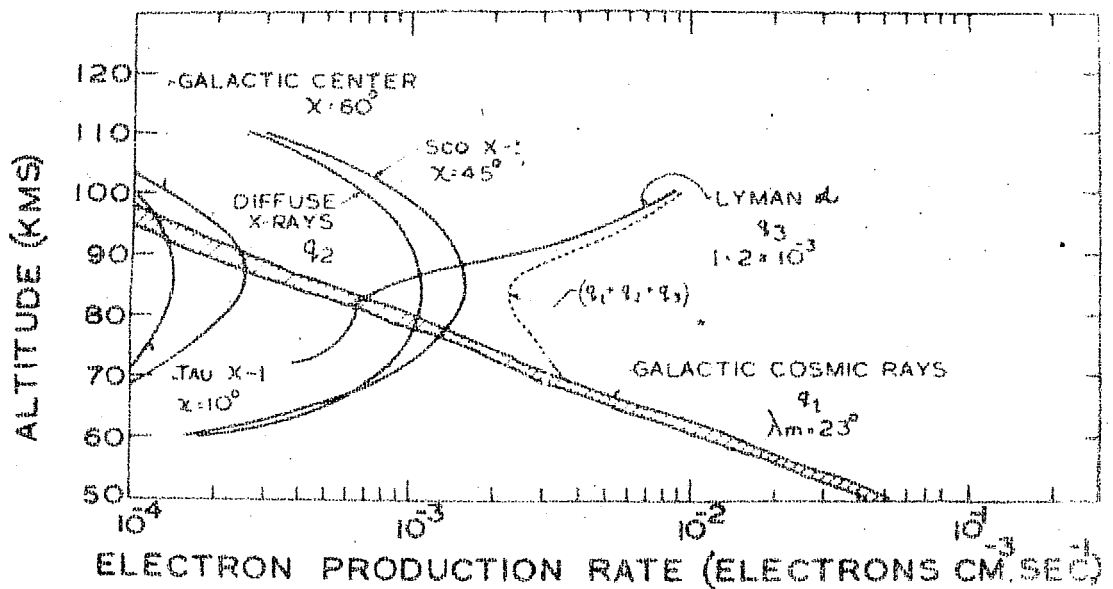
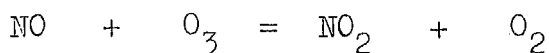


FIGURE 5.14

The altitude profile of the electron production rates due to stable background agencies viz., galactic cosmic rays, diffuse cosmic X-rays and scattered Lyman  $\alpha$ . Also shown are the transient effects arising from the passage of Sco X-1, galactic centre and Tau X-1. The total ambient effect of all the stable sources has been shown by the dotted line.

region in the atmosphere. While ionising the constituent NO, Lyman  $\alpha$  gets attenuated due to absorption by molecular oxygen. Below 120 km all atmospheric models (CIRA, 1965; JACCHIA, 1970; US standard 1966) predict the same concentrations of molecular oxygen. The direct experimental observations of molecular oxygen are found to be in good agreement with the CIRA model (BRANNON and HOFFMAN, 1971; CARVER ET AL., 1964; WILDMAN ET AL., 1969 and SUBBRAYA ET AL., 1971). A diurnal variation of the order of 20% has been calculated from the existing measurements (WEEKS and SMITH, 1968) on the density of molecular oxygen.

The main difficulty in the estimation of the Lyman  $\alpha$  ionisation results from the uncertainties involved in the NO concentration. Various experimental evaluation of NO density have already been discussed in chapter I. It has been suggested that the NO density does not have a significant diurnal variation in the altitude range 70 - 150 km (STROBEL, 1971), even though the possibility of a depletion in NO density in the D-region heights after sunset cannot be ruled out owing to the increase in ozone concentration. The following reaction results in the loss of NO density:



It has been noticed that the rate of production due to Lyman  $\alpha$  changes at the most by about 25% when molecular oxygen concentrations of different models are considered. Though Meira's

values of NO concentration appear to be quite reliable, the uncertainties involved specially in the height range of our interest ( 80 - 90 km ) cannot be overlooked. The proper assessment of the effect of stellar X-rays critically depends upon the NO density in this height range. Moreover, if we use the NO densities given by Meira, the electron production rate becomes so high that it makes the X-ray effect almost improbable. NO densities estimated from ionospheric and photochemical methods always show about order of magnitude less values between 80 - 90 km heights. We have extrapolated these values assuming similar height variation as observed by Meira. Table 5.3 summarises the NO densities estimated by different methods at heights around 75 km. It can be noted that the mean value of NO density at about 75 km will be  $\sim 2 \times 10^6$  per c.c. agreeing fairly with most of the observations. In our calculations we have used a similar profile of Meira but with the value of NO density normalised to  $2 \times 10^6$  per c.c. at 75 km. It can be noticed from figure 5.14 that the production rates by Lyman  $\alpha$  are comparable to those by the background cosmic X-rays and by the X-rays from Sco X-1.

5.7 Enhancement in the electron densities caused by Sco X-1  
Tau X-1 and the Galactic Centre (G.C.) over the background  
ionisation and the corresponding absorption of LF radio  
waves

The ambient production rates calculated in the last section are compared with the nighttime electron density profiles of SUBBARAYA ET AL. (1971), DEEKS (1966) to calculate the effective

Table 5.3

Summary of the Nitric Oxide densities measured  
at heights around 75 km.

Height (Kms)	NO concen- tration (cm <sup>-3</sup> )	Method of estimate	Reference
70	$8 \times 10^5$	From Solar cycle variation in electron density	Mitra (1966)
75	$2 \times 10^6$	From diurnal variation in electron density	Mitra (1968)
75	$2 \times 10^6$	From NO <sup>+</sup> , O <sub>2</sub> <sup>+</sup> measurements	Mitra (1968)
75	$1.8 \times 10^6$	From laboratory measurements of rate coefficients	Kistiakowsky and Vilpi (1957)
75	$2 \times 10^6$	-do-	Mavorayannis and Winckler (1961)
75	$3.5 \times 10^6$	-do-	Clyne and Thrush (1959)
75	$3 \times 10^7$	NO Air glow by rocket	Meira (1971)
80	$1 \times 10^6$	Zenith angle variation in absorption	Parthasarathy and Larfald (1965)
80	$6 \times 10^7$	NO Air glow by rocket	Barth (1966)
80	$1.7 \times 10^7$	-do-	Meira (1971)
84 -100	$10^6$	From NO <sup>+</sup> , O <sub>2</sub> <sup>+</sup> measurements	Wagner (1966)
85	$6 \times 10^7$	NO Air glow by rocket	Barth (1966)
85	$1.3 \times 10^7$	-do-	Meira (1971)



loss rates ( 4 ) as a function of altitude. The electron density enhancements due to X-rays from Sco X-1, galactic Centre (R.A.=  $17^h 45^m$ ) and Tau X-1 sources at  $45^\circ$ ,  $60^\circ$  and  $10^\circ$  zenith angles, corresponding to meridional transit over Gulmarg ( the middle point of 164 kHz radio waves lies above Gulmarg for Tashkent - Ahmedabad circuit) are computed by using the already estimated values and the total production rates. It is interesting to note that eventhough the resultant absolute electron density increase arising from the transit of these sources, depends on the assumed value of ambient electron density, the percentage value of the effect is independent of the same. This is because the background ionisation is normalised to the measured electron densities and the relative electron density increases due to the X-ray sources are computed from such a comparison. Table 5.4 gives the enhancements at different altitudes for different sources alongwith the ambient electron densities.

The calculation of the peak absorption of 164 kHz radio waves due to the irradiation of the ionosphere by the X-rays from cosmic X-ray sources are done by following the method discussed earlier for the reflection coefficient (  $||R||$  ). Table 5.5 gives the values so obtained alongwith the average observed values of absorption for Sco X-1, Galactic centre and Tau X-1. The Galactic centre transits 1 hr 25 mts after the

Table 5.4

Enhancement of electron densities at different altitudes  
due to galactic X-ray sources

Height (kms)	Ambient production rate ( $q_1+q_2+q_3$ ) $\text{cm}^{-3} \text{sec}^{-1}$	Electron density increases due to Sco X-1 and galactic center				Electron density increases due to Tau X-1		
		Ambient electron density Subbaraya et al. and Deeks (Summer) $=N_e \text{ cm}^{-3}$	$q(h)$	$N$		Ambient electron density Deeks (Winter) $N_e \text{ cm}^{-3}$	$q(h)$ Tau X-1 $\text{cm}^{-3} \text{sec}^{-1}$	$N$ Tau X-1 $\text{cm}^{-3}$
			Sco X-1 $\text{cm}^{-3} \text{sec}^{-1}$	G.C. $\text{cm}^{-3} \text{sec}^{-1}$	Sco X-1 $\text{cm}^{-3}$	G.C. $\text{cm}^{-3}$		
75.0	$2.996 \times 10^{-3}$	6.4	$1.210 \times 10^{-3}$	$1.65 \times 10^{-4}$	1.184	0.175	$1.15 \times 10^{-4}$	0.133
77.5	$2.675 \times 10^{-3}$	7.0	$1.365 \times 10^{-3}$	$1.95 \times 10^{-4}$	1.603	0.251	$1.25 \times 10^{-4}$	0.223
80.0	$2.413 \times 10^{-3}$	7.0	$1.500 \times 10^{-3}$	$2.20 \times 10^{-4}$	1.915	0.313	$1.36 \times 10^{-4}$	0.263
82.5	$2.287 \times 10^{-3}$	7.0	$1.565 \times 10^{-3}$	$2.42 \times 10^{-4}$	2.085	0.361	$1.43 \times 10^{-4}$	0.470
85.0	$2.284 \times 10^{-3}$	10.0	$1.600 \times 10^{-3}$	$2.55 \times 10^{-4}$	3.040	0.540	$1.42 \times 10^{-4}$	18.300
87.5	$2.674 \times 10^{-3}$	$2.0 \times 10^3$	$1.580 \times 10^{-3}$	$2.60 \times 10^{-4}$	523.0	95.0	$1.40 \times 10^{-4}$	18.100
90.0	$3.458 \times 10^{-3}$	$8.0 \times 10^3$	$1.480 \times 10^{-3}$	$2.45 \times 10^{-4}$	1560.0	278.0	$1.35 \times 10^{-4}$	9.700

Table 5.5

Comparison of the observed and computed magnitudes  
of absorption suffered by 164 kHz radio waves during  
the zenith transits of galactic X-ray sources

Source	Calculated excess peak absorption (dB)	Observed excess peak absorption (dB)
Sco X-1	4.2	-
Galactic Center	1.5	-
Sco X-1 + Galactic Center	4.4	7
Tau X-1	1.2	4

transit of Sco X-1 hence the effects produced by them is not observed individually ( figure 4.12). From figure 4.14 it can be noted that the composite effect is seen as a shift in the time of peak absorption by about 20 - 30 mts, subsequent to the time of transit of Sco X-1. The calculated peak absorption for the resultant effect is 4.4 dB ( table 5.5) and compares favourably with the observed absorption. In the case of Tau X-1, the agreement between the calculated and observed peak absorption values is less striking.

#### 5.8 Summary and conclusion

The results obtained in this chapter can be summarised as follows:

(1) The maximum values of production of ion-electron pairs in the D-region due to the X-rays from Sco X-1 and Tau X-1 are about  $2 \times 10^{-3}$  and  $2 \times 10^{-4} \text{ cm}^{-3} \text{ sec}^{-1}$  at the maximum zenith transits across  $32^\circ\text{N}$  and  $72^\circ\text{E}$  ( middle point of the reflection of 164 kHz radio waves from Tashkent to Ahmedabad).

(2) The electron densities in the D-region below about 90 km are considerably enhanced over the ambient conditions during the passage of Sco X-1 and Tau X-1.

(3) From the equilibrium condition electron densities using a sharply bounded model it is observed that a phase change corresponding to a height change of about 1-2 km will be observed

in the 164 kHz radio waves during the time of the irradiation by the X-rays from Sco X-1 and Tau X-1.

(4) The full-wave calculations using the method of BARRON and BUDDEN (1959) show that the attenuation of the amplitude of the radio signal under equilibrium condition electron densities produced by Sco X-1 and Tau X-1 are about 12 and 7 decibels respectively. By matching the electron density profiles to get the observed values of absorption from the full wave calculation the effective loss rates of the night-time D-region have been estimated.

(5) All the night-time sources capable of producing ionisation in the D-region have been reviewed and their production rates estimated. It follows that the proper assessment of ionisation due to scattered Lyman $\alpha$  radiation is difficult because of the uncertainties involved in the measured NO densities between 80 - 90 km height range. However assuming the NO densities obtained from the ionospheric and photochemical methods as closer to reality, the electron production rates due to Lyman $\alpha$  come out to be of the same order as those produced by the background galactic X-rays and by the X-rays from Sco X-1.

(6) From the calculation of total production rates the effective loss coefficients for different heights in the D-region are estimated by direct comparison with the measured

electron density profiles representative of the ambient night-time conditions. These are then used to get the maximum ionisation enhancement due to Sco X-1, galactic centre and Tau X-1. It is found that the Sco X-1 produces an increment of about 30% over and above the normal values whereas Galactic Centre and Tau X-1 produce only meagre enhancements.

(7) The effect of the galactic X-ray sources persist for about 2 - 3 hrs on either side of the time corresponding to the peak effect, the extent of spread depending upon the declination of the source as well as the intensity of its fluxes. Also the effect of all the sources clustered in intervals of an hour or so in right ascension is seen as a composite one. The peak absorption due to Sco X-1 shows a shift of about 30 minutes in the forward direction because of the overlapping effect of the galactic centre making its transit about 1 hr 25 mts after the transit of Sco X-1.

## 5.9 Discussion

It seems that the evidence regarding the detection of ionospheric effect due to the strong galactic X-ray sources is quite acceptable both from observational as well as theoretical stand point. There is a reasonable agreement between the nature of the observed effect and that predicted by theoretical considerations. The main uncertainty in studying the night-time D-region ionosphere lies in the improper knowledge of nitric oxide

concentration. There is not a single direct measurement of night-time NO concentration, which leads to unjustified guessing from the daytime concentrations. Assuming the daytime NO concentrations, the production rates due to Lyman  $\alpha$  radiation becomes so high that their comparison with measured electron density profiles yield the effective loss coefficients 1-2 orders of magnitude higher than those estimated from other observations which means that in order to account for the measured electron density and effective loss rate profiles, the contribution to the ambient production rates by Lyman  $\alpha$  should be about 1 - 2 orders of magnitude less than what is estimated by assuming daytime NO concentrations. This in turn fixes a considerably lower nighttime value of NO concentration in the D-region ionosphere ( 70 - 90 km ). Two rocket experiments conducted to measure nocturnal electron density in the D-region with and without the irradiation by strong X-ray source would finally confirm the effect evidenced strongly from ground based observations.

By making suitable circuits for LF and VLF radio propagation, it should be possible to study the variation of the intensity of strong X-ray sources on an average long term basis. Also there is possibility for the detection of rare celestial events like X-ray flares in the stars or supernova from their sudden effects in the LF and VLF propagation especially during

night. Besides the high utility of technique in the study of X-ray astronomy, it can provide useful informations about the various physical processes in the nighttime D-region which have remained hitherto undiscovered.



CHAPTER - VI

LUNAR TIDES IN THE D-REGION IONOSPHERE

6.1 Introduction

Lunar tides in the F-region of the ionosphere have been extensively studied using different parameters namely, the critical frequency of the layer ( $f_oF_2$ ), minimum virtual height ( $h'F$ ) and the height of peak ionisation ( $h_mF_2$ ) (MARTYN, 1947, 1948; APPLETON and BEYNON, 1948; McNISH and GAUTIER, 1949). The latitudinal distribution of the amplitude of lunar semi-monthly oscillation (corresponding to midday values of  $f_oF_2$ ) shows two peaks, one in a narrow belt within  $\pm 3^\circ$  magnetic latitude and the other a broader maximum centred around the magnetic latitude of  $\pm 20^\circ$ . The phase (time of maximum deviation) of the tide changes from about 4 lunar hour to about 10 lunar hour between low and high latitudes, the reversal taking place at about  $\pm 11^\circ$  magnetic latitude (OSBORNE, 1952; BROWN, 1956; KOTADIA and RAMANATHAN, 1956; RASTOGI, 1961).

Determination of lunar tidal effects in the normal E-region have been difficult owing to the presence of sporadic E layer. Results obtained after separating the effect due to the sporadic E layer do not project a clear picture of the latitudinal variation of the amplitude and phase of the lunar

variation in  $h'E$  and  $f_oE$  (APPLETON and WEEKS, 1939; MARTYN, 1948; ZAGULYAYEVA ET AL., 1967; ROUGERIE, 1961). From a study of lunar tides using the  $f_oE$  values over 14 years at Ibadan, BROWN (1967) has concluded that the phase and amplitude of the lunar oscillations undergo large seasonal variation which makes the interpretation of the average annual effect difficult. There are comparatively very few observation of lunar tidal effects in the D-region ionosphere. Information about the tidal oscillations at these heights are derived either from the absorption measurements of the medium frequency radio waves, phase measurements of VLF radio propagation or from the minimum frequency recorded in the ionograms ( $f_{min}$ ).

APPLETON and BEYNON (1949) for the first time detected the existence of lunar semi-monthly tide in the noon absorption values at a high latitude station, Slough. The amplitude of the tide was found to be .26 dB occurring at 10.9 lunar hour. Later, the computations of the tide for other high latitude stations, Pennsylvania (MITRA, 1955), Freiburg (BOSSOLASCO and ELENA, 1960) and Boulder (BRADY and CROMBIE, 1963), confirmed the phase of oscillation to be about 10 lunar hour. SKINNER and WRIGHT (1964) and RASTOGI (1969) found that for the equatorial stations Ibadan and Colombo the phase of the tide was about 3 lunar hour suggesting the possibility of the phase reversal taking place between high and low latitudes. A systematic study of lunar variations in the lower ionosphere has not been possible due to

the limitation of available data on ionospheric absorption.

Although the exact nature of the relation between the index of absorption and  $f_{\min}$  is not known still to a good approximation the variations in  $f_{\min}$  represent the relative changes in ionospheric absorption. Large number of stations tabulate the hourly values of  $f_{\min}$ , which can be made use of in deducing the lunar oscillations in the D-region. An attempt has been made in the present study to compare the lunar tides in absorption and in  $f_{\min}$  to estimate if further study of  $f_{\min}$  could give world-wide pattern of lunar tide at lower ionosphere.

In this chapter we describe the results of the computations of lunar tide in the ionospheric absorption at equatorial stations Colombo (period 1957-59 and 1964-68) and Singapore ( period 1951-55) and at a mid-latitude station Kokubunji ( period 1957-68). Also the results of the lunar tide in  $f_{\min}$  for the stations Huancayo, Chimbote, Talara and Panama during IGY-IGC period are described. The results of the findings have already been published (CHAKRAVARTY and RASTOGI, 1969, 1970a, 1970b, 1972).

## 6.2 Data and method of analysis

For Colombo, noon absorption values (L's) on the frequencies 2.0, 2.2 and 2.6 MHz for the period 1964-68 and on the frequencies 2.55 and 2.85 MHz for the period 1957-59 have

been utilised. For Singapore, noon L values on frequencies 2.0, 2.4 and 2.6 MHz for the period April 1951 - May 1955 have been considered for the analysis.

At Kokubunji (Japan), for studying the lunar effects in the D-region of the ionosphere, the absorption data at the lowest available frequency of 2.4 MHz has been analysed in preference to the data corresponding to other frequencies due to two main reasons following a study by YASUDA (1963). The reasons are as follows:

(1) The contribution of the deviative absorption due to E and F layers increase with the increase in the frequency, therefore, the measurements of absorption at low frequency (2.4 MHz) signify the contribution mainly due to the non-deviative absorption of the D-region.

(2) The effect of the occurrence of  $E_s$  layer on the absorption is found to be minimum for the frequency of 2.4 MHz.

Hence at Kokubunji we have used the noon absorption values only at 2.4 MHz during the period of 12 years (1957-68).

To derive the lunar tidal oscillation when the data is available for a fixed solar hour, the method given by Van' Der Stock (CHAPMAN and BARTELS, 1940) is generally used. Let us denote the daily values of the ionospheric parameter as  $L_j$  for a particular hour. In order to remove the effect caused by

sun, the monthly averages of these values are computed ( $\bar{L}_j$ ). These are then subtracted from the individual daily values to obtain the deviations from the monthly means ( $\Delta L_j = L_j - \bar{L}_j$ ).

The synodic period of moon, called one lunar month is equivalent to 29.5306 solar days. The phase changes of the moon during a lunation is represented by lunar age ( $\nu$ ). The lunar age has values from 0-24 lunar hour or  $0^\circ - 360^\circ$  from one new moon to the next in course of a lunation. From one solar day to the next the lunar age;  $\nu$ , increases by 0.81272 hour. The values of  $\nu$  have been published by SUGUIRA and FANSELAU (1966) for the years 1850 to 2050. For lunar tidal analysis either these values can be directly used or they can be generated from simple relations for any particular day (MALIN and CHAPMAN, 1970).

The deviations ( $\Delta L_j$ 's) obtained are now grouped according to lunar age (00, 01, 02, ..... 21, 22 and 23 hr) and their average value determined ( $\overline{\Delta L_j}$ ) for all the lunar ages (0 - 23 hr). Hence the plot between these average values with lunar age gives the variation due to lunar gravitation forces, having a semi-monthly periodicity. To get the lunar variations during different seasons the whole data is divided according to the following:

- (i) D-months ( winter solstice ) - November, December, January and February
- (ii) E-months (Equinoxes ) - March, April, September and October

- (iii) J-months ( Summer solstice) - May, June, July and August.

The average deviations corresponding to the lunar ages from 0 to 23 hour are then harmonically analysed for two harmonics according to the following equation.

$$M_n = \sum_{n=1}^2 x_n \sin (n\mathcal{V} + P_n) \quad \dots (6.1)$$

where  $x_n$  and  $P_n$  are the amplitudes and phase angles corresponding to the  $n^{\text{th}}$  harmonic. The determination of the probable errors in the amplitude and phase of the tide is important in order to justify the significance of the results. Let us denote  $N_{\mathcal{V}}$  as the total number of deviations for a particular value of lunar age  $\mathcal{V}$ , then the variance of the average value of the deviations  $\sigma_{\mathcal{V}}^2$  is calculated as follows:

$$\sigma_{\mathcal{V}}^2 = \frac{1}{N_{\mathcal{V}}} \left\{ \sum_{j=1}^N (\Delta L_j)^2 - \left( \overline{\Delta L_{\mathcal{V}}} \right)^2 \right\} \quad \dots (6.2)$$

The weighted mean variance,  $\sigma^2$ , for all the lunar ages 00 - 23, is then computed from the following relation:

$$\sigma^2 = \frac{1}{24} \sum_{\mathcal{V}=1}^{24} (\sigma_{\mathcal{V}})^2 \quad \dots (6.3)$$

$$\sigma^2 = \frac{1}{24} \sum_{\nu=1}^{24} (\sigma_{\nu})^2 \quad \dots (6.3)$$

The probable error (P.E) in the amplitude of lunar, variation at a fixed solar hour is then estimated from the following equation (RASTOGI, 1962):

$$\text{P.E.} = \underline{0.275} \sigma \quad \dots (6.4)$$

For determining lunar tidal oscillations in the D-region parameters special care has to be taken for the values affected by solar disturbances. Inclusion of the days with abnormally high values during solar flares; makes the estimation of the average solar monthly component unrealistic and subsequently giving erroneous results regarding lunar tides. In the present study we have excluded all the values of absorption parameter ( $L$  or  $f_{\min}$ ) affected during moderate to strong solar flares.

In deriving the variation of ionospheric absorption with respect to the phase of the moon some authors have taken the moving mean of 7 days or 14 days to estimate the effects due to solar flares etc. In such cases as has been shown by DEACON (1966) strong transference of random variation into the required semi-monthly lunar variation will take place. Hence, though the 7 or 14 days running mean will smoothen the lunar variations

but the results about its phase and amplitude can be misleading. For finding the lunar variation of ionospheric absorption, it is more advantageous to remove the abnormal values ( which are solely caused by sun) rather than taking small running means to smoothen the variations.

### 6.3 Lunar tide in the D-region absorption at Singapore

The lunar variations at Singapore have been derived from the three frequencies 2.0, 2.4 and 2.6 MHz. It is observed that for any particular season the lunar effects for the three frequencies are not significantly different. Hence, seasonal curves are derived by averaging the individual curves for the three frequencies. Figure 6.1 shows the resultant curves for the three seasons averaged for the  $\lambda$  values from 0 to 11 and 12 - 23 hr, representing only the semi-monthly variation. Table 6.1 gives the values of amplitude and time of maximum absorption obtained from the harmonic analysis. The continuous curves in figure 6.1 show the built up curves derived from the second harmonic.

The amplitudes of lunar tide are 0.86, 0.48 and 0.55 dB for D, E and J-months respectively. The annual average lunar variations has the amplitude of 0.57 dB. Thus the amplitude of tide in D-months is more than that in E or J-months similar to the seasonal variation of lunar tides in D-region absorption at Colombo (RASTOGI, 1969). The lunar time of maximum absorption



Table 6.1

Summary of lunar semi-monthly oscillations in the  
D-region absorption of radio waves of the ionosphere

Stations	Geog. Lat.	Geomag Lat.	Ampl. (dB)	Time of max. E. Hr.	References
Slough	52°N	50°N	0.26	10.9	Appleton and Beynon (1949)
Pennsylvania	40°N	56°N	0.39	9.6	Mitra (1955)
Freiburg	48°N	46°N	0.86	10.6	Bossolasco and Elena (1960)
Ibadan	7°N	3°S	0.35	2.7	Skinner and Wright (1964)
Colombo	7°N	3°S	0.38	3.3	Rastogi (1969)
<u>Singapore</u>	1.3°N	9°S			
Annual			0.57	8.0	Present work
D-months			0.86	9.6	
E-months			0.48	6.9	
J-months			0.55	8.8	

varies with season between 6.9 and 9.6 hours, the annual average oscillation having the phase of 8.0 lunar hours.

The lunar tide in  $f_oF_2$  at Singapore has a phase around 04 lunar hour (OSBORNE 1952, RASTOGI 1961). From the results presented, it is noted that the lunar tides in the D and F regions of the ionosphere over Singapore have almost opposite phase. The tidal behaviour in the F-region for Singapore (magnetic latitude  $9^\circ$ ) lying close to the transition region of  $\pm 11^\circ$  magnetic equator, is equatorial in nature, while the variation in the D-region is of the high latitude type. Therefore, the reversal of the phase of the tides in the D-region may be taking place at slightly lower latitudes compared to that for the tides in the F-region. More observations of absorption at low latitude stations are necessary to determine the transition region of the lunar tides in the D-region.

#### 6.4 Solar cycle variation of lunar tides in ionospheric absorption at Colombo

Figure 6.2 shows the variation of average  $\Delta L$  at Colombo as the function of  $\lambda_o$ , separately for the three seasons of IGY/IGC. During any season lunar oscillations are seen to be almost identical for the two frequencies. Table 6.2 gives the amplitudes and phases (times of maximum positive deviation) of lunar monthly ( $M_1$ ) and lunar semi-monthly ( $M_2$ ) oscillations derived from the curves averaged for both the frequencies.

# SINGAPORE

2.0 2.4 AND 2.6 MHz

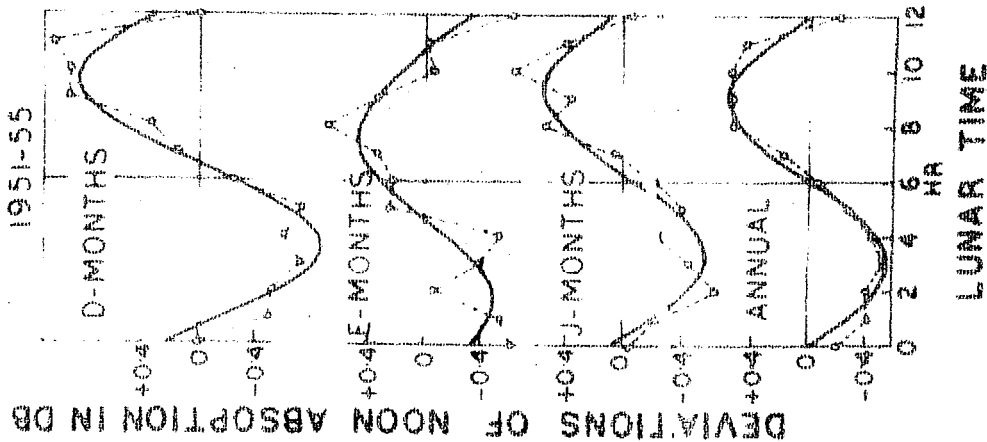


FIGURE 6.1

Average variation of the noon value of the D-region absorption of radio waves at Singapore with lunar time for different seasons of the year.

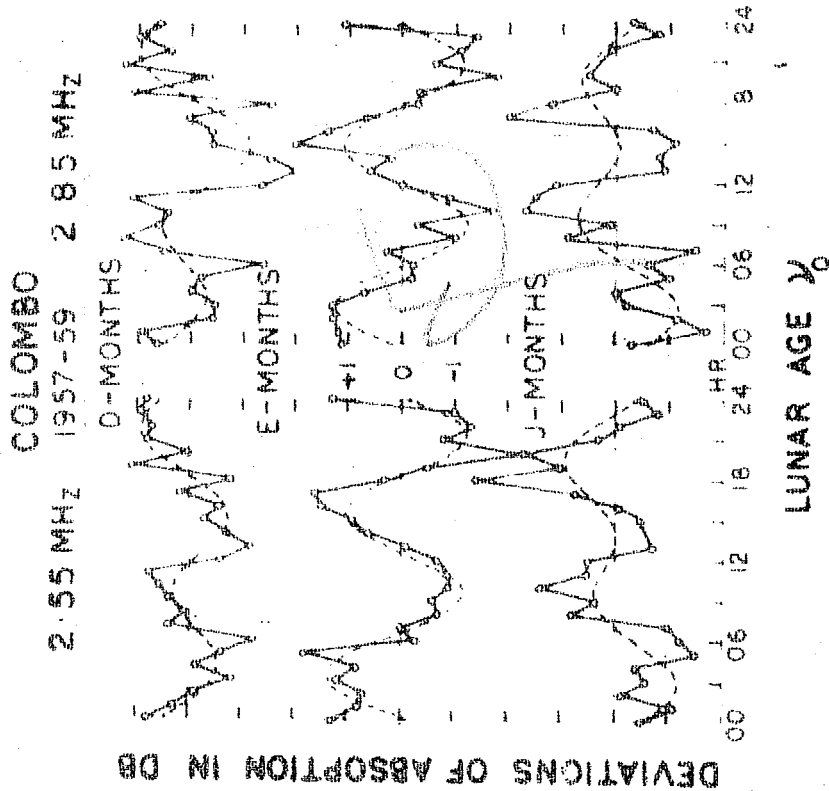


FIGURE 6.2

The variation of mid-day absorption of the radio waves at Colombo with the lunar age for different seasons of the year.

Table 6.2

Harmonic coefficients of seasonal lunar variations  
at Colombo

Season	Period	Frequencies (MHz)	Ampl. $P_1$ (dB)	Time of max. $t_1$ (L.hr.)	Ampl $P_2$ (dB)	Time of max. $t_2$ (L.hr.) <sup>2</sup>
D-months	1964-68	2.0, 2.2 & 2.6	-	-	0.78	2.0
	1957-59	2.55 & 2.85	0.38	23.4	0.67	2.5
E-months	1964-68	2.0, 2.2 & 2.6	-	-	0.42	4.6
	1957-59	2.55 & 2.85	0.13	21.3	1.17	8.9
J-months	1964-68	2.0, 2.2 & 2.6	-	-	0.38	4.9
	1957-59	2.55 & 2.85	0.57	8.0	0.61	3.7

During the E-months the tide is predominantly semi-monthly in character, the amplitude ( $P_2$ ) being about 1.2 dB, with the time of maximum positive deviation ( $t_2$ ) at 8.9 lunar hours. From a comparison with the corresponding values for the period 1964-68 (table 6.2) it can be noted that the amplitude ( $P_2$ ) has increased by a factor of three while the phase ( $t_2$ ) of the tide has changed by 4.3 lunar hour. During the D-months the amplitude and phase of the  $M_2$  tide are similar to that observed for the period 1964-68. During the J-months the variations are rather irregular giving the amplitudes of  $M_1$  and  $M_2$  tides almost of the same magnitude. Thus the lunar tidal amplitudes in the D-region absorption at Colombo during E and J-months are larger during the years of high solar activity than during the low sunspot years. During the high sunspot years the phase of the tide experiences large variation with seasons such that the oscillations would cancel each other when averaged over the whole year, giving insignificant harmonic coefficients.

#### 6.5 Lunar effects in ionospheric absorption at Kokubunji during 1957-68

Figure 6.3 shows the final curves of lunar variations during the three seasons and for the whole year for the high and low sunspot years. Also the lunar variations combined for the two epochs, ie. during the period 1957-67 are included in the figure. In all the curves the variations for the  $\nu'_0$  values between 0 - 11 and 12 - 23 hrs have been averaged to show only

the semi-monthly oscillations. Table 6.3 gives the amplitudes and phases of three  $M_2$  tides for each season during different periods, obtained from the results of harmonic analysis. The probable errors for the amplitudes are also included in the table.

It can be seen from the figure that at any particular season the nature of the variation is almost identical for high and low sunspot years. The phase of the  $M_2$  tide undergoes large seasonal changes during both the epochs. Because of these phase variations the annual average curves are reduced to random and irregular oscillations from which no conclusion about the  $M_2$  tide can be drawn. It can be noted from table 6.3 that during E-months the phase of the tide is almost opposite to that during D and J months. During any season the phase of the tide is opposite to that observed at Colombo for the high sunspot years, which is in confirmity with the phase reversal of the tide between low and high latitudes. Owing to the seasonal phase variations it is suggested that the lunar tides in the D-region should be computed separately for three seasons and not for the whole year to avoid any wrong interpretation of the results. Also as the phase of the tide changes by about 2-3 hrs between low and high sunspot years (table 6.3), a comparative study of the nature of the tide for various stations should only be made if analysis accounts roughly for the same period of data.

Table 6.3

Harmonic coefficients of the seasonal lunar semi-monthly variations at Kokubunji for different periods

Period	Season	Amplitude (dB)	Time of max. (L.hr)
1957 - 62	D-months	.84 $\pm$ .28	7.0
	E-months	.55 $\pm$ .28	2.6
	J-months	.92 $\pm$ .24	10.6
1963 - 67	D-months	.34 $\pm$ .25	9.3
	E-months	.45 $\pm$ .23	4.2
	J-months	.45 $\pm$ .20	1.3
1957 - 67	D-months	.46 $\pm$ .19	7.2
	E-months	.31 $\pm$ .18	2.1
	J-months	.54 $\pm$ .16	11.45

34  
 98  
 123  
 3 40

148  
 3  
 4.9

The amplitudes of the  $M_2$  tide during D and J months of high sunspot years are about two times compared to those of the low sunspot years. The amplitude of the tide remains almost constant during E months of both the epochs. For the whole period ( 1956 - 67 ) the amplitudes are comparable to those during the low sunspot years. This shows that the phase variation of the tide between high and low sunspot years almost compensates for the larger amplitude of the tide during the high sunspot years.

In order to understand the phase variation of the lunar semi-monthly oscillations with season more closely the whole data ( 1957 - 68 ) has been utilised to compute the  $M_2$  tide for each calendar month of the year. By doing so we assume that the comparatively smaller solar cycle variation of the phase will not make any serious alteration to the nature of these  $M_2$  tides for different months. The lunar semi-monthly curves for each month have been shown in figure 6.4. It can be noted that the nature of these variations around E-months are almost opposite to the variations in the rest of the year. Figure 6.5 and table 6.4 show the variation of the amplitudes and phases of these  $M_2$  oscillations with respect to different months of the year. It can easily be noticed that though the amplitude of the tide varies from 0.35 to 0.99 dB, there is no regularity in its variation. It can be mentioned that the probable errors of these amplitudes have quite large values,



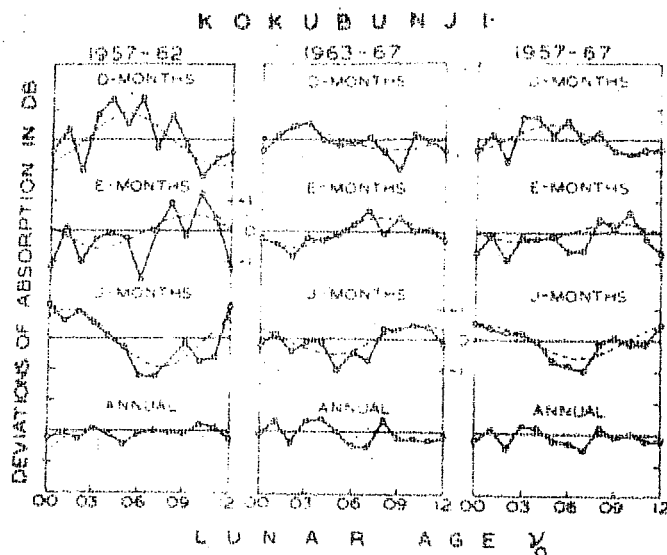
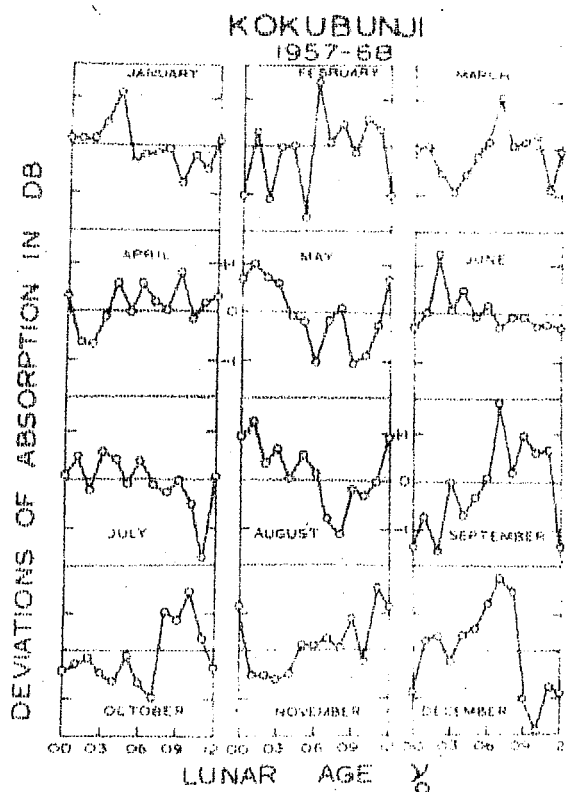


FIGURE 6.3

Seasonal and annual variation of average deviation with lunar age for the high sunspot years (1957 - 62), the low sunspot years (1963 - 67) and for the period 1957 - 68.



Monthly variation of average deviations with lunar age

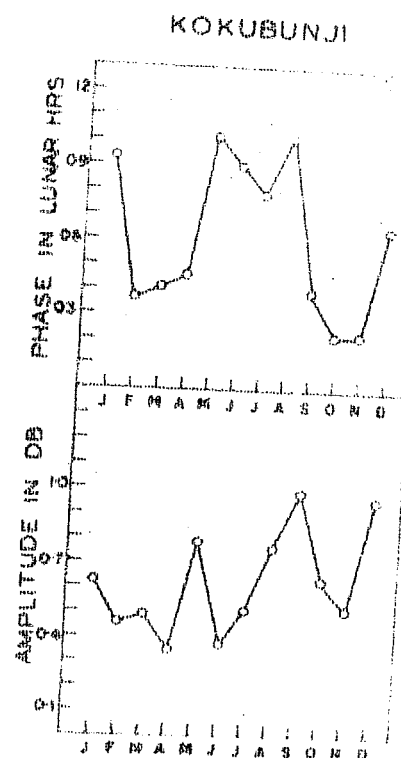


FIGURE 6.5

Table 6.4

Harmonic coefficients of lunar semi-monthly  
variations for different months of the year  
at Kokubunji

Month	Amplitude (dB)	Time of max. (L. hr)
January	.63	9.3
February	.46	3.7
March	.49	4.1
April	.35	4.6
May	.78	10.2
June	.37	9.0
July	.51	7.9
August	.76	10.2
September	.99	4.0
October	.63	2.2
November	.51	2.3
December	.96	6.6

and hence they are not as significant as the amplitudes of the tide during the three seasons. Hence before concluding about their monthly variation, large amount of data would be necessary for reducing the errors.

The phase of the tide shows a semi-annual variation being about 2- 5 lunar hours during or close to the E-months and between 7 - 10 hours during the rest of the months (figure 6.5). The phases of these oscillations have probable errors within the limit of 30% and hence they can be considered significant.

#### 6.6 Lunar tides in $f_{\min}$ close to the magnetic equator during IGY-IGC

In order to intercompare the lunar tides in ionospheric absorption and in  $f_{\min}$ , the lunar variation over the whole lunar month in L at Colombo and in  $f_{\min}$  at Huancayo and Panama for the three seasons of IGY/IGC period are shown in figure 6.6. Lunar oscillations in  $f_{\min}$  for the low latitude stations Huancayo, Chimbote and Talara are found to be almost identical (figure 6.7). The smooth dotted lines show the curves built up of the first two harmonics. The coefficients of the first and second harmonics have been given in Table 6.5.

It can be seen that for a particular season the nature of the tidal oscillation in  $f_{\min}$  at Huancayo is strikingly similar to the absorption tide at Colombo. The

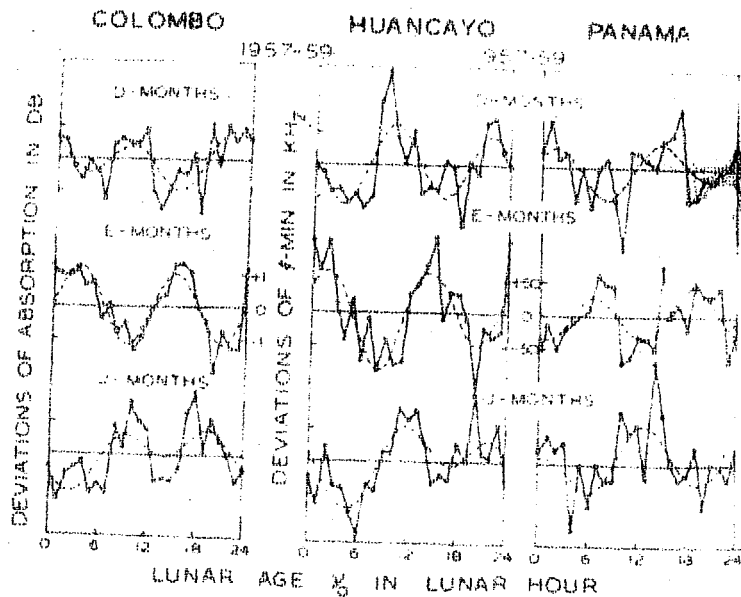
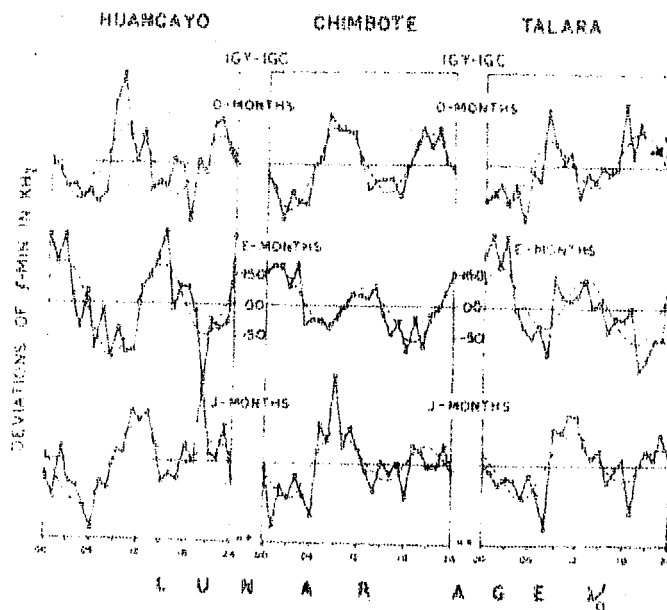


FIGURE 6.6

Variation of mid-day absorption at Colombo and of mid-day fmin at Huancayo and Panama with lunar age for different seasons.



The variation of midday fmin values at Huancayo, Chimbote and Talara with the lunar age for different seasons of the year. FIGURE 6.7

Table 6.5

Summary of seasonal lunar variations in ionospheric  
absorption and in f-min

Season	Station	Mag.lat.	Amplitude $P_1$	Phase $t_1$ (L.hr)	Amplitude $P_2$	Phase $t_2$ (L.hr)
D-months	Colombo	3.2°S	0.38 dB	23.4	0.67 dB	2.5
	Huancayo	0.6°S	10.6 kHz	12.2	54.4 kHz	2.2
	Chimbote	2.2°N	16.1 "	11.4	58.8 "	2.9
	Talara	6.6°N	21.8 "	6.9	43.4 "	3.7
	Panama	20.6°N	16.9 "	4.8	32.4 "	9.8
E-months	Colombo	-	0.13 dB	21.3	1.17 dB	8.9
	Huancayo	-	18.3 kHz	3.9	67.9 kHz	9.8
	Chimbote	-	21.8 "	10.2	41.8 "	11.0
	Talara	-	21.8 "	17.9	53.2 "	10.6
	Panama	-	6.2 "	4.4	36.3 "	5.3
J-months	Colombo	-	0.57 dB	8.0	0.61 dB	3.7
	Huancayo	-	36.1 kHz	8.1	41.3 kHz	1.1
	Chimbote	-	19.5 "	11.3	39.8 "	2.8
	Talara	-	21.4 "	9.5	40.0 "	0.5
	Panama	-	24.9 "	7.5	35.7 "	9.7

phase reversal between D and E months, already discussed for Colombo (IGY-IGC period) is also shown by the  $f_{\min}$  tide at Huancayo. From table 6.5, it is clearly seen that the phase of the tide in  $f_{\min}$  at Huancayo, Chimbote and Talara are similar to that observed for absorption tide at Colombo during any of the seasons. The annual mean curve is very irregular in all these cases and hence omitted from the figure. These seasonal phase variations seem to be a prominent feature of the tide in the lower ionosphere specially during the high sunspot years.

The lunar oscillations at Panama are of opposite kind compared to Huancayo or Colombo in each season. This confirms the phase reversal of the tide in absorption between equatorial and tropical latitudes. It is worth mentioning that no such change-over in phase could be studied by determining only the annual tide for each case, owing to seasonal variation of phase.

In all the stations it is seen that during the E-months the oscillation is purely semi-monthly in nature and during the J-months the monthly oscillation is almost equally predominant as the semi-monthly oscillation. During the D-months though the oscillations are mainly semi-monthly in character there is appreciable amplitude for the monthly tide also.

From table 6.5 by looking at the amplitudes of  $M_2$  tide for the stations Huancayo, Chimbote and Talara the conclusion can be drawn that the D-region tidal amplitudes are not enhanced

over the magnetic equator unlike the enhancement of lunar tide in  $f_oF_2$  (RASTOGI, 1962, 1963) and in the horizontal component of magnetic field  $H$  (RASTOGI, 1965). Thus the lunar oscillations in the D-region do not seem to be affected by the presence of the equatorial electrojet currents.

As a check to any possible effect of the electrojet in the D-region near the equator, sudden enhancements of  $f_{min}$  due to solar flares have been tabulated from the  $f$ -plots of the stations Huancayo, Chimbote, Chiclayo and Talara for the IGY period. For any particular event, the  $f_{min}$  is divided by the corresponding values at Huancayo. The average ratios of  $f_{min}$  at these stations normalised to that at Huancayo are shown in figure 6.8. The variation of  $H$  due to magnetic crochet at these stations for the same period are also included in the diagram after RASTOGI ET AL. (1964). It is clearly seen that the ratio of  $f_{min}$  does not change significantly with latitude whereas within same latitudes  $H$  ratio has decreased from 1.0 to 0.2. In conclusion the changes in  $f_{min}$  due to either by solar flares or due to tides do not show any enhancement over the magnetic equator.

For determining the phase variation of the lunar tide in the equatorial stations during different calendar months the  $f_{min}$  data at the three stations Huancayo, Chimbote and Talara are combined. This is justified because of the striking

similarity in the variation of lunar tides at these stations. Figure 6.9 shows the variation of the time of maximum positive displacement of  $M_2$  oscillation for each month of the year, being about 10 lunar hr during either of the equinoxes and around 01 lunar hr during the solstices showing a semiannual variation of the phase. This kind of phase variation is opposite to that observed at Kokubunji.

#### 6.7 Variation of normal absorption and the amplitude of semimonthly tide in absorption with the magnetic latitude

To evaluate the variation of ionospheric absorptions with the dip latitude the absorption at  $\chi = 0$  and  $R_z = 0$  is computed for different stations. Ionospheric absorption increases with the increase in sunspot numbers according to the well known relationship:

$$L = L_0 ( 1 + bR_z ) \quad \dots\dots(6.5)$$

where  $R_z$  is the sunspot number and  $b$  is a constant.

In order to get the value of absorption at  $R_z = 0$ , the daily noon values of absorption for each month are plotted ( in y - axis ) with respect to the sunspot numbers, the intercept in the y - axis gives the value of absorption at  $R_z = 0$ . The average value of this intercept for the whole year is computed to eliminate the seasonal variation.



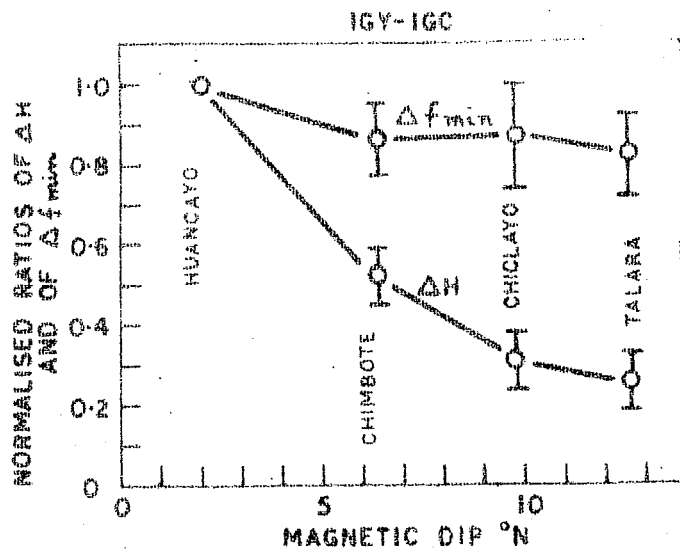


FIGURE 6.8

Latitudinal variation of the sudden changes in horizontal force  $H$  and  $f_{min}$  during solar flares normalised to that at Huancayo.

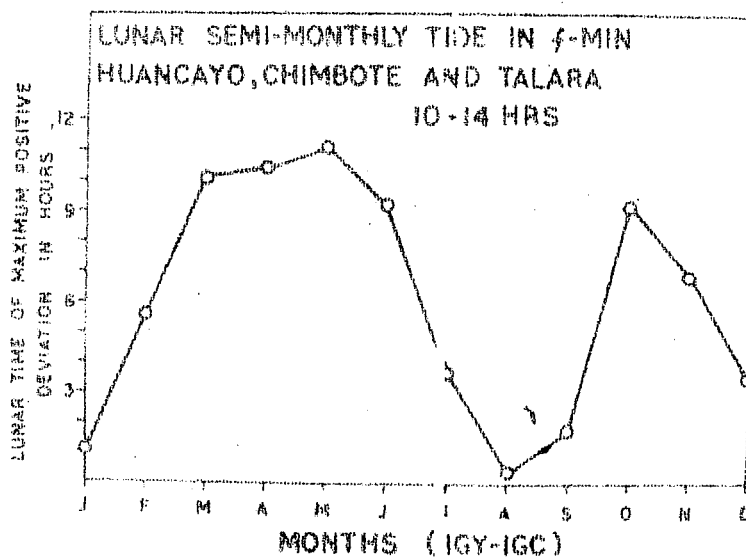


FIGURE 6.9

The annual variation of the phase of the lunar semi-monthly tide averaged for the three equatorial stations Huancayo, Chimbote and Talara.

In figure 6.10 the normal absorption values on 2.0 MHz at  $X = 0$  and  $R_z = 0$ , have been plotted against the dip angles of the stations (GNANALINGAM, 1969). The curve shows the maximum of absorption around  $20^\circ$  dip latitude. For comparison the amplitudes of the semi-monthly lunar oscillation have also been plotted for the stations where the data has been analysed for computation of lunar tides. Table 6.6 gives the amplitudes of the lunar semi-monthly oscillations for different stations during the periods mentioned alongwith the references. In the figure the open circles correspond to the observation during the high sunspot years and the solid circles correspond to the observation during low sunspot years. It can be seen that if we consider the amplitudes of the lunar tide during the low sunspot years the points fall on the solid curve fairly well. The points corresponding to the analysis during high sunspot years seem to deviate from the general trend during the low sunspot years. During the high sunspot years the amplitude of the tide increases and so the points do not fall on the curve plotted in the figure. For the period of low sunspot years it can be noticed that the maximum amplitude of the tide happens to be around  $20^\circ$  dip which is quite similar to the normal variation of absorption with dip latitude. But this type of variation is different from the results of the lunar tide in  $f_oF_2$  where the amplitude also shows a maximum near the electrojet.

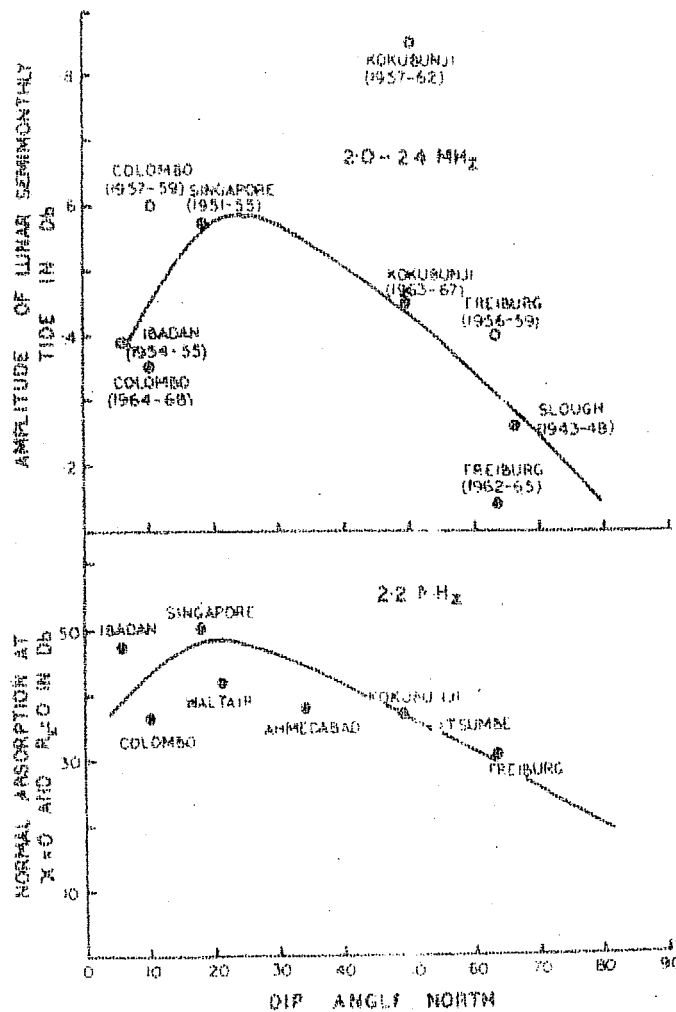


FIGURE 6.10

Variation of the average amplitude of lunar semi-monthly oscillation and the normal absorption with the dip angle.

Table 6.6Summary of the amplitude of lunar semi-monthly  
oscillation in ionospheric absorption

Station	Dip. angle	Period.	Amplitude of M <sub>2</sub> oscillation (dB)	Reference
Ibadan	6° N	1954-55	.39	Skinner and Wright (1964)
Colombo	10° N	1957-59	.60	Present work
Colombo	10° N	1964-68	.35	Rastogi (1969)
Singapore	18° N	1951-55	.57	Present work
Kokubunji	49° N	1957-62	.85	Present work ✓
Kokubunji	49° N	1963-67	.45	Present work ✓
Freiburg	64° N	1956-59	.40	Kotadia and Patel (1969)
Freiburg	64° N	1962-65	.14	Kotadia and Patel (1969)
Slough	66° N	1962-65	.26	Appleton and Beynon (1949)

## 6.8 Conclusion

Following conclusions can be listed based on the study of lunar tides in the D-region:

(1) The average phase of the lunar tide in ionospheric absorption is about 2 - 3 lunar hr at equatorial latitude and 9 - 10 lunar hr at high latitudes. The transition takes place at a latitude less than  $9^\circ$  during low sunspot years.

(2) At Colombo the phase of the lunar tide undergoes a large seasonal variation during high sunspot years. The phase during equinoxes is opposite to that during the solstices. The amplitudes of the oscillation in general show enhancements with the increase in sunspot activity.

(3) Lunar tide in absorption at Kokubunji is opposite in character compared to the tide at an equatorial station, Colombo. The phase of the tide shows large variation with season and smaller variation with solar activity. The amplitude of the tide is enhanced considerably during the high solar activity period.

(4) The lunar tides in  $f_{\min}$  are identical in all respects to those in ionospheric absorption.

(5) The amplitude of D-region tide does not show any marked enhancement close to the magnetic equator, indicating the

absence of equatorial electrojet effects in the D-region variations.

(6) The phase of the lunar tide in the D-region shows semi-annual variations which are exactly opposite to each other for equatorial and middle latitude stations, especially during high sunspot years.

(7) During the low sunspot years, the amplitude of the tide in absorption as well as the normal absorption values ( $R_z = 0$ ,  $X = 0$ ) exhibit a maximum around  $20^\circ$  magnetic latitude.

#### 6.9 Discussion

The phase of the lunar tide in atmospheric pressure is about 10 lunar hours on the surface of the earth (SIEBERT, 1951), which compares with the phase of the lunar tide in ionospheric absorption at a mid-latitude station, Kokubunji. However, the phase reversal during the equinoctial period for the tide in absorption at Kokubunji does not correspond to a similar change over of phase in the pressure tide. For the equatorial stations the situation is reversed, ie., the phase of the tide in absorption and pressure compare well during the equinoxes. The information about the lunar tide in the atmospheric pressure at ionospheric heights is completely lacking because of the unavailability of the relevant pressure data. In order to establish that the ionospheric absorption tide is due to the changes in the

neutral density, the corresponding behaviour of the pressure tide around D-region heights should be known. There is a similarity between the seasonal phase variation of the  $f_oE$  tide (BROWN, 1967) and the tide in absorption near the equator which indicates that the variations are mainly due to the changes in electron densities in the E and D-regions rather than the changes in the collision frequency.

In the F-region, though there is a seasonal change in the phase of the tide in  $f_oF_2$  by about 04 lunar hour (RASTOGI, 1963), the variation is not semi-annual in character. Also, the lunar tides in the F-region parameters have been shown to covary with the corresponding geomagnetic tide near the equator (SHARMA and RASTOGI, 1970). Hence the lunar tides in the lower regions of the ionosphere are quite different from the tides in the surface pressure, F-region ionosphere and geomagnetic field in the sense of their characteristic seasonal phase variation.

It can be expected that the neutral density in the D-region under the influence of the gravitational tides of moon modifies or perturbs the electron density carrying it alongwith it. The variation of this electron density results in the lunar tide of ionospheric absorption. The semianual phase variation of the tidal oscillation in the lower ionosphere may have some bearing on the similar variations of temperature around these heights observed by GREENHOW and NEUFELD( 1961) and KOCHNASKI (1963).

# REFERENCES

- |                                                                         |       |                                                                    |
|-------------------------------------------------------------------------|-------|--------------------------------------------------------------------|
| Aikin, A.C.                                                             | 1971  | COSPAR Symp, Urbana; Illinois, USA.                                |
| Aikin, A.C.,<br>Kane, J.A., and<br>Troim, J.                            | 1964  | J. Geophys. Res., <u>69</u> , 4621.                                |
| Alurkar, S.K.                                                           | 1963  | Ph.D. thesis (Gujarat University).                                 |
| Alurkar, S.K.                                                           | 1965  | Ind. J. Pure and Appl. Phys.,<br><u>3</u> (2), 58.                 |
| Ananthakrishnan, S.                                                     | 1967  | Ph.D. thesis (Gujarat University).                                 |
| Ananthakrishnan, S.                                                     | 1970  | Brazilian J. Phys.                                                 |
| Ananthakrishnan, S., and<br>Chakravarty, S.C.                           | 1969  | Proc. III Equat. Aero. Symp.,<br>Ahmedabad, India, Vol.I-A, p.251. |
| Ananthakrishnan, S.,<br>Chakravarty, S.C., and<br>Ramanathan, K.R.      | 1970a | L. Gratton (ed.) Non-solar<br>X- and Gamma-Ray Astronomy, p.46.    |
| Ananthakrishnan, S.,<br>Chakravarty, S.C., and<br>Ramanathan, K.R.      | 1970b | Proc. Ind. Acad. Sci., <u>71A</u> , 69.                            |
| Ananthakrishnan, S., and<br>Ramanathan, K.R.                            | 1967  | Proc. Ind. Acad. Sci., <u>66</u> , 60.                             |
| Ananthakrishnan, S., and<br>Ramanathan, K.R.                            | 1969  | Nature, <u>223</u> , 488.                                          |
| Appleton, E.V., and<br>Beynon, W.I.G.                                   | 1948  | Nature, <u>162</u> , 486.                                          |
| Appleton, E.V., and<br>Beynon, W.I.G.                                   | 1949  | Nature, <u>164</u> , 486.                                          |
| Appleton, E.V., and<br>Weeks, K.                                        | 1939  | Proc. Roy. Soc., <u>A171</u> , 171.                                |
| Bain, W.C.                                                              | 1953  | J. Atmos. Terr. Phys., <u>3</u> , 141.                             |
| Bain, W.C.,<br>Bracewell, R.N.,<br>Straker, T.W., and<br>Westcott, C.H. | 1952  | Proc. Inst. Elect. Engrs.,<br><u>99</u> , 250.                     |



- |                                                                 |      |                                                                                           |
|-----------------------------------------------------------------|------|-------------------------------------------------------------------------------------------|
| Barrington, R.L.,<br>Landmark, B., and<br>Thrane, E.V.          | 1962 | Electron density profiles in<br>the ionosphere and exosphere,<br>Pergamon press, p.21.    |
| Barron, D.W., and<br>Budden, K.G.                               | 1959 | Proc. Roy. Soc., <u>A249</u> , 387.                                                       |
| Barth, C.A.                                                     | 1964 | J. Geophys. Res., <u>69</u> , 3301.                                                       |
| Barth, C.A.                                                     | 1966 | Annal. de Geophys., <u>22</u> , 198.                                                      |
| Belrose, J.S., and<br>Bourne, I.A.                              | 1967 | Ground based radio wave<br>propagation studies of the<br>lower ionosphere, Vol.I, p.79.   |
| Belrose, J.S.,<br>Bourne, I.A., and<br>Hewitt, L.W.             | 1966 | Proc. Third NATO advanced<br>study institute, North Holland<br>Publishing Co., Amsterdam. |
| Belrose, J.S., and<br>Centiner, E.                              | 1962 | Nature, <u>195</u> , 688.                                                                 |
| Beynon, W.J.G., and<br>Jones, E.S.O.                            | 1965 | J. Atmos. Terr. Phys., <u>27</u> , 761.                                                   |
| Bhattacharyya, J.C., and<br>Balakrishnan, T.K.                  | 1967 | J. Atmos. Terr. Phys., <u>29</u> , 1573.                                                  |
| Boldt, E.A.,<br>Desai, U.D., and<br>Holt, S.S.                  | 1969 | Astrophys. J., <u>156</u> , 427.                                                          |
| Booker, H.G.                                                    | 1939 | Phil. Trans., <u>A237</u> , 411.                                                          |
| Bossolasco, M., and<br>Elena, A.                                | 1960 | Geofis. Pura. Appl., <u>46</u> , 167.                                                     |
| Bourdeau, R.E.,<br>Aikin, A.C., and<br>Donley, J. L.            | 1966 | J. Geophys. Res., <u>71</u> , 727.                                                        |
| Bowhill, S.A., and<br>Smith, L.G.                               | 1966 | Space Res. <u>VII</u> , 511.                                                              |
| Bowyer, S.,<br>Byram, E.T.,<br>Chubb, T.A., and<br>Friedman, H. | 1964 | Science, <u>147</u> , 394.                                                                |

- |                                                                                          |      |                                                          |
|------------------------------------------------------------------------------------------|------|----------------------------------------------------------|
| Bracewell, R.N.                                                                          | 1952 | Proc. Inst. Elec. Engrs., <u>99</u> , 217.               |
| Bracewell, R.N., and<br>Bain, W.C.                                                       | 1952 | J. Atmos. Terr. Phys., <u>2</u> , 216.                   |
| Bracewell, R.N.,<br>Budden, K.G.,<br>Ratcliffe, J.A.,<br>Straker, T.W., and<br>Weeks, K. | 1951 | Proc. Inst. Elect. Engrs., <u>98</u> , 221.              |
| Brady, A.H., and<br>Crombie, D.D.                                                        | 1963 | J. Geophys. Res., <u>68</u> , 5437.                      |
| Bramnon, P.J., and<br>Hoffman, T.M.                                                      | 1971 | J. Geophys. Res., <u>76</u> , 4630.                      |
| Branscomb, L.M.                                                                          | 1964 | Annal. de Geophys., <u>20</u> , 88.                      |
| Branscomb, L.M.,<br>Burch, D.S.,<br>Smith, S.J., and<br>Geltman, S.                      | 1958 | Phys. Rev., <u>111</u> , 504.                            |
| Brown, R.A.                                                                              | 1956 | J. Atmos. Terr. Phys., <u>9</u> , 144.                   |
| Brown, R.A.                                                                              | 1967 | J. Atmos. Terr. Phys., <u>29</u> , 1087.                 |
| Budden, K.G.                                                                             | 1955 | Proc. Roy. Soc., <u>A227</u> , 516.                      |
| Burgess, B., and<br>Jones, T.B.                                                          | 1969 | Nature, <u>224</u> , 680.                                |
| Burnside, W.S., and<br>Penton, A.W.                                                      | 1904 | The theory of equation<br>(Dublin Univ. Press, Dublin ). |
| Byram, E.T.,<br>Chubb, T.A., and<br>Friedman, H.                                         | 1966 | Science, <u>152</u> , 66.                                |
| Carver, J.H.,<br>Horton, B.H., and<br>Burger, F.G.                                       | 1966 | J. Geophys. Res., <u>71</u> , 4189.                      |
| Carver, J.H.,<br>Mitchell, P., and<br>Murray, E.L.                                       | 1964 | J. Geophys. Res., <u>69</u> , 3755.                      |
| Chakravarty, S.C.                                                                        | 1971 | Proc. Ind. Acad. Sci., <u>A74</u> , 99.                  |

- Chakravarty, S.C., and Ramanathan, K.R. 1972 Proc. Ind. Acad. Sci., A75, 249.
- Chakravarty, S.C., and Rastogi, R.G. 1969 Nature, 223, 939.
- Chakravarty, S.C., and Rastogi, R.G. 1970a J. Atmos. Terr. Phys., 32, 945.
- Chakravarty, S.C., and Rastogi, R.G. 1970b Ind. Jour. Pure Appl. Phys., 8, 541.
- Chakravarty, S.C., and Rastogi, R.G. 1972 Ind. Jour. Radio and Space Phys., I(2), 158.
- Chamberlain, J.W. 1961 Physics of the Aurora and Airglow, Academic press, New York and London.
- Chapman, S. 1931a Proc. Phys. Soc., 43, 26.
- Chapman, S. 1931b Proc. Phys. Soc., 43, 483.
- Chilton, C.J., Steele, F.K., and Norton, R.B. 1963 J. Geophys. Res., 68, 5421.
- Chodil, G.R., Jopson, R.C., Mark, H., Seward, F.D., and Swift, C.D. 1965 Phys. Rev. Lett., 15, 605.
- Chodil, G., Mark, H., Rodrigues, R., Seward, F.D., and Swift, C.D. 1967 Astrophys. J., 150, 57.
- Chodil, G., Mark, H., Rodrigues, R., Seward, F.D., Swift, C.D., Turiel, I., Hiltner, W.A., Wallerstein, G., and Mannery, E.J. 1968 Astrophys., J., 154, 645.
- Chubb, T.A., Friedman, H., and Kreplin, R.W. 1960a J. Geophys. Res., 65, 1831.

- Chubb, T.A.,  
Friedman, H.,  
Kreplin, R.W.,  
Nicholo, W.A.,  
Unzicker, A.E., and  
Votaw, M.J. 1960b IGY Bull. 42, Trans. Ann.  
Geophys. Union 41(4), 717.
- CIRA 1965 North Holland Publication.
- Clark, G. 1965 Phys. Rev. Lett., 14, 91.
- Clyne, M.A.A., and  
Thrush, B.A. 1959 Proc. Phys. Soc., A261, 159.
- Conner, J.P.,  
Evans, W.D., and  
Belian, R.D. 1969 Astrophys. J. Lett., 157, L157.
- Cook, G.E. 1969 Nature, 222, 969.
- Crain, C.M. 1961 J. Geophys. Res., 66, 1117.
- Crombie, D.D. 1961 J. Res. N.B.S., 65D(5), 455.
- Curran, R.K. 1962 Phys. Rev., 125, 910.
- Deacon, E.L. 1966 J. Atmos. Sci., 23, 131.
- Deeks, D.G. 1966 Proc. Roy. Soc., 291, 413.
- de Lisle, J.M. 1967 Radio Sci., 2(6), 653.
- Dieminger, W.,  
Rose, G.,  
Schwentek, H., and  
Widdel, H.U. 1967 Space Res., VII, 228.
- Edlen, B. 1960 J. Chem. Phys., 33, 98.
- Edwards, P.J.,  
Burt, W.J., and  
Knox, F. 1969 Nature, 222, 1052.
- Farragher, A.L.,  
Page, F.M., and  
Wheeler, R.C. 1964 Disc. Faraday Soc., 37, 203.
- Ferguson, E.E.,  
Freshenfeld, F.C., and  
Schmeltekopf, A.L. 1967 Space Res., VII, 135.

- Fink, R.W.,  
Jopson, R.C.,  
Mark, H., and  
Swift, C.D. 1966 Rev. Mod. Phys., 38, 513.
- Fisher, P.C.,  
Johnson, H.M.,  
Jordan, W.C.,  
Meyerott, A.J., and  
Action, L.W. 1966 Astrophys. J., 143, 203.
- Foroythe, W.E. 1956 Smithsonian Physical Tables,  
p.705.
- Francey, R.J. 1970 J. Geophys. Res., 75, 4849.
- Freshenfeld, F.C.,  
Schmeltekopf, A.L.,  
Schiff, H.I., and  
Ferguson, E.E. 1967 Planet. Space Sci., 15, 373.
- Friedman, H. 1961 Annal. de Geophys., 17, 245.
- Friedman, H. 1967 Ann. Rev. Nucl. Sci., 17, 317.
- Friedman, H.,  
Chubb, T.A.,  
Kupperian, J.E.,  
Kreplin, R.W. Jr., and  
Lindsay, J.C. 1958 Annal. de Geophys., 14, 232.
- Gardner, J.A., and  
Pawsey, J.L. 1953 J. Atmos. Terr. Phys., 3, 321.
- Geisler, J.E., and  
Dickinson, R.E. 1968 J. Atmos. Terr. Phys., 30, 1505.
- Giacconi, R.,  
Gursky, H.,  
Paolini, P.R., and  
Rossi, B. 1962 Phys. Rev. Lett., 9, 439.
- Gill, S. 1951 Proc. Camb. Phil. Soc., 47, 96.
- Gnanalingam, S. 1969 Proc. III International Symp.  
Equat. Aeron., Vol. I, p.47.
- Gorenstein, P.,  
Kellog, E.M., and  
Gursky, H. 1969 Astrophys. J., 156, 515.

- Gould, R.J. 1967 Amer. J. Phys., 35, 376.
- Grader, R.J.,  
Hill, R.W.,  
Seward, F.D., and  
Toor, A. 1966 Science, 152, 1499.
- Greenhow, J.S., and  
Neufeld, E.L. 1961 Quart. J. Roy. Met. Soc.,  
75, 228.
- Gregory, J.B. 1965 2nd Conf. Direct. Aeron.  
Measurements in the Lower  
Ionosphere, Urbana,  
Illinois.
- Gursky, H.,  
Gorenstein, P., and  
Giacconi, R. 1967 Astrophys. J. (Lett), 150, L50.
- Gursky, H.,  
Giacconi, R.,  
Gorenstein, P.,  
Waters, J.R.,  
Oda, M.,  
Bradt, M.,  
Garmin, G., and  
Sreekantan, B.V. 1966 Astrophys. J., 146, 311.
- Gursky, H.,  
Giacconi, R.,  
Paolini, F., and  
Rossi, B. 1963 Phys. Rev. Lett., 11, 530.
- Hale, L.C. 1965 J. Geophys. Res., 70, 2241.
- Hall, J.E., and  
Fooks, J. 1967 Planet. Space Sci., 15, 1717.
- Hall, J.E., and  
Fooks, J. 1965 Planet. Space Sci., 13, 1013.
- Hayakawa, S.,  
Matsuoka, M., and  
Sugimoto, D. 1966 Space Sci. Rev., 5, 109.
- Hayakawa, S.,  
Matsuoka, M., and  
Yamashita, K. 1966 Report on Ionosphere and  
Space Res. in Japan, 20, 480.

- Haymes, R.C., and  
Craddock, J.R. 1966 J. Geophys. Res., 71, 3261.
- Henke, B.L.,  
Elgin, R.L.,  
Lent, R.E., and  
Ledingham, R.B. 1967 Norelco Rep., 14, 112.
- Hesstvedt, E. 1968 Geophys. Pub., 27, 1.
- Hinteregger, H. 1965 Space Sci. Rev., 4, 461.
- Hopkins, H.G., and  
Reynolds, L.G. 1954 Proc. Inst. Elect. Engrs., III, 101,  
21.
- Hultqvist, B. 1966 Annal. de Geophys., 22, 235.
- Hunt, B.G. 1965 J. Atmosph. Terr. Phys., 27, 133.
- Hunter, D.M., and  
McElroy, M.B. 1968 J. Geophys. Res., 73, 2421.
- Inn, E.C.Y., and  
Tanaka, Y. 1959 Advan. Chem. Ser., 21, 263.
- Jacchia, L.G. 1970 Smithsonian Astrophys. Observ.  
Space Rep. 313.
- Johler, J.R., and  
Walters, L.C. 1960 J. Res. N.B.S., 64D, 455.
- Kane, J.A. 1969 Planet. Space Sci., 17, 609.
- Kasturirangan, K., and  
Rao, U.R. 1972 Astrophys. Space Sci. ( in press )
- Kaufmann, P.,  
Pass de Barros, M.H., and  
Vianna, E.N. 1970 Nature, 228, 1080.
- Kochanski, A. 1963 J. Geophys. Res., 68, 213.
- Kotadia, K.M., and  
Patel, B.M. 1969 J. Atmosph. Terr. Phys., 31, 621.
- Kotadia, K.M., and  
Ramanathan, K.R. 1956 Proc. Ind. Acad. Sci., 43, 394.
- Kreplin, R.W. 1961 Annal. de Geophys., 17, 151.

- Kreplin, R.W.,  
Chubb, T.A., and  
Friedman, H. 1962 J. Geophys. Res., 67, 2231.
- Kreplin, R.W.,  
Van Allen, J.A., and  
Teske, R.G. 1970 Solar X-ray data for three 1968  
flares NSSDC 70-75.
- Kristiakowsky, G.B., and  
Volpi, G.C. 1957 J. Chem. Phys., 27, 114.
- Lauter, E.A. 1966 Proc. Summer School on lower  
ionosphere Reih II, Heft I.
- Lauter, E.A. 1959 Kleinhenbacher ber 6, 21.
- Lauter, E.A. 1966 Annal. de Geophys., 22, 289.
- Malin, S.R.C., and  
Chapman, S. 1970 Geophys. J. Royl. Astr. Soc.,  
19, 15.
- Martyn, D.F. 1947 Proc. Roy. Soc., A190, 273.
- Martyn, D.F. 1948 Proc. Roy. Soc., A194, 429.
- Matsouka, M.,  
Oda, M.,  
Ogawara, Y.,  
Hayakawa, S., and  
Kato, T. 1968 Can. J. Phys., 46, 466.
- May, B.R. 1966 J. Atmos. Terr. Phys., 28, 553.
- Mavorayannis, C., and  
Winckler, C.A. 1961 Chemical Reactions in the  
lower and upper atmosphere,  
Interscience Publishers, 287.
- McCracken, K.G. 1966 Science, 154, 1000.
- Mediarimid, I.B., and  
Budzinsky, E.E. 1964 Can. J. Phys., 42, 2048.
- McNish, A.G., and  
Gautier, T.N. 1949 J. Geophys. Res., 54, 303.
- Meier, R.R. 1970 Space Res. X, 572.
- Meira, L.G. Jr. 1971 J. Geophys. Res., 76, 202.



- Mechtly, E.H., and Smith, L.G. 1968a J. Atmos. Terr. Phys., 30, 363.
- Mechtly, E.H., and Smith, L.G. 1968b J. Atmos. Terr. Phys., 30, 1555.
- Mitra, A.P. 1955 J. Atmos. Terr. Phys., 7, 99.
- Mitra, A.P. 1966 J. Atmos. Terr. Phys., 28, 945.
- Mitra, A.P. 1969 Space Res., IX, 418.
- Mitra, A.P. 1968 J. Atmos. Terr. Phys., 30, 1065.
- Moler, W.F. 1960 J. Geophys. Res., 65, 1459.
- Nestorov, G., and Taubenheim, J. 1965 Bull. Geophys. Inst. Bulgr. Acad. Sci., 7, 37.
- Neupert, W.M. 1963 The Physics of solar flare, NASA, 49.
- Nicolet, M. 1945 Mem. Inst. Meteor. Belg., 19, 83.
- Nicolet, M., and Aikin, A.C. 1960 J. Geophys. Res., 15, 1469.
- Oda, M., Clark, G., Garmire, G., Wada, M., Giacconi, R., Gursky, M., and Walters, J. 1965 Nature, 205, 554.
- Osborne, B.W. 1952 Nature, 169, 661.
- Parthasarathy, R., and Larfald, G.M. 1965 University of Alaska Report.
- Pederson, A. 1964 Rep. 13, Uppsala Ionospheric Observatory, Uppsala.
- Pearce, J.B. 1969 J. Geophys. Res., 74, 853.
- Phelps, A.V., and Pack, J.L. 1961 Phys. Rev. Letter, 6, 11.
- Piggot, W.R., and Thrane, E.V. 1966 J. Atmos. Terr. Phys., 28, 467.

- Poppoff, I.G., and Whitten, R.C. 1969 Nature, 224, 1187.
- Poppoff, I.G., Whitten, R.C., and Edmonds, R.S. 1964 J. Geophys. Res., 69, 4081.
- Potnera, T.A., and Zmuda, A.J. 1970 J. Geophys. Res., 75, 7161.
- Prakashrao, A.S., Sharma, D.P., Jayanthi, U.B., and Rao, U.R. 1971 Astrophys. Space Sci., 10, 150.
- Ramanathan, K.R. 1970 NASA Report UAG-12, Part I, p.92.
- Rao, U.R., Chitnis, E.V., Prakashrao, A.S., and Jayanthi, U.B. 1970 L. Gratton (ed.) Non-solar X- and Gamma-ray Astronomy, p.88.
- Rappaport, S., Brandt, H.V., Naranan, S., and Spada, G. 1969 Nature, 221, 428.
- Rastogi, R.G. 1961 J. Atmos. Terr. Phys., 22, 290.
- Rastogi, R.G. 1962 J. Res. (NBS), 66D, 601.
- Rastogi, R.G. 1963a J. Geophys. Res., 68, 2445.
- Rastogi, R.G. 1963b Nature, 200, 1083.
- Rastogi, R.G. 1965 Z. Geophysik, 31, 27.
- Rastogi, R.G. 1969 J. Atmos. Terr. Phys., 31, 759.
- Rastogi, R.G., and Chakravarty, S.C. 1969 Proc. III International Symp. Equat. Aerom. Vol. II, p.384.
- Rastogi, R.G., Kaushika, N.D., and Trivedi, N.B. 1964 J. Atmos. Terr. Phys., 27, 663.
- Rawer, K. 1952 The Ionosphere, Frederick Ungar Publishing Co., New York, p.96.
- Reid, G.C. 1961 J. Geophys. Res., 66, 4071.

- Reid, G.C. 1970 J. Geophys. Res., 75, 2551.
- Reigler, G.R.,  
Boldt, E., and  
Serlemitsos, P. 1968 Astrophys. J. Lett., 153, 1659.
- Rougerie, P. 1961 Annal. de Geophys., 17, 145.
- Rowe, J.H.,  
Ferraro, A.H.,  
Lee, H.S.,  
Kreplin, R.W., and  
Mitra, A.P. 1970 J. Atmos. Terr. Phys., 32, 1659.
- Sagalin, R.C., and  
Smiddy, M. 1966 Space Res. IV, 371.
- Sagalin, R.C.,  
Smiddy, H., and  
Pullivan, W.P. 1966 Space Res. VII, 449.
- Satyaprakash,  
Subbaraya, B.H., and  
Gupta, S.P. 1971 J. Atmos. Terr. Phys., 33, 129.
- Sechrist, C.F., Jr. 1968 J. Atmos. Terr. Phys., 30, 371.
- Sen, H.K., and  
Wyller, A.A. 1960 J. Geophys. Res., 65, 3931.
- Sharma, D.P.,  
Jain, A.K.,  
Chakravarty, S.C.,  
Kasturirangan, K.,  
Ramanathan, K.R., and  
Rao, U.R. 1972 Astrophys. Space Sci. ( in press )
- Sharma, R.P., and  
Rastogi, R.G. 1970 Pure Appl. Geophys. (PAGLOF),  
80 (III), 288.
- Sheddy, C.H. 1968 Radio Sci., 3 (8), 792.
- Shirke, J.S., and  
Alurkar, S.K. 1963 Proc. Ind. Acad. Sci., 57, 49.
- Siebert, M. 1961 Advances in Geophys., 7, 105.
- Skinner, N.J., and  
Wright, R.W. 1964 J. Atmos. Terr. Phys., 26, 1221.

- Smiddy, M., and Sagalin, R.C. 1967 Space Res., VII, 428.
- Smith, L.G. 1961 Science Report No.3, University of New England.
- Smith, L.G. 1965 G.C.A. Tech. Report, 65-22-N.
- Snell, A.H. 1962 Nuclear Instruments and their uses, Vol.1.
- Somayajulu, Y.V., and Aikin, A.C. 1969 Space Res. XI
- Spencer, N.W., Bogges, R.L., and Taeush, D.R. 1964 J. Geophys. Res., 69, 1369.
- Straker, T.W. 1955 Proc. Inst. Elec. Engrs., Monogr. 114.
- Strobel, D.F. 1971 J. Geophys. Res., 75, 2441.
- Stroud, W., and Nordberg, W. 1963 IGY Rocket Report 7, 73.
- Subbaraya, B.B., Satyaprakash, and Gupta, S.P. 1971 Ind. J. Pure Appl. Phys., 9, 626.
- Subbaraya, B.H., Satyaprakash, and Pareek, P.N. 1972 J. Atmos. Terr. Phys. ( in press ).
- Sugaira, M., and Fanselau, G. 1966 God. Space Flight Centre, rep. (X-612-66-401).
- Svennesson, J., Reder, F., and Grouchley, J. 1972 J. Atmos. Terr. Phys., 34, 49.
- Swider, W., Jr. 1964 Planet. Space Sci., 12, 761.
- Swift, D.W. 1962 J. Atmos. Terr. Phys., 23, 29.
- Thomas, L. 1971 J. Atmos. Terr. Phys., 33, 157.
- Thome, G., and Wagner, L. 1967 Ann. Arbor, Michigaon.

- Tinseley, B.A. 1969 J. Geophys. Res., 74, 2327.
- Tulinov, N.F.,  
Shibaeva, L.V., and  
Jakovleva, S.G. 1969 Space Res. IX, 231.
- U.S. Standard Atmosphere  
Supplements 1966 ESSA, NASA.
- Velinov, P. 1966 C.r. Acad. Bulg. Sci., 19, 109.
- Velinov, P. 1968 J. Atmos. Terr. Phys., 30, 1891.
- Victoreen, J.A. 1949 J. Appl. Phys., 20, 1141.
- Viertel, W.A., and  
Lechrist, C.F. Jr. 1969 Aeron. Rep. No.33, Univ. of  
Illinois.
- Vigroux, E. 1953 Annales de Geophys., 8, 709.
- Wagner, Ch.V. 1966 J. Atmos. Terr. Phys., 28, 607.
- Wait, J.R. 1963 J. Geophys. Res., 68, 43.
- Watanabe, K. 1958 Advances Geophys. Res., 73, 4835.
- Watt, L.D. 1967a VLF Radio Engineering,  
Pergamon Press, p.425.
- Watt, L.D. 1967b VLF Radio Engineering,  
Pergamon Press, p.185.
- Watts, J.M. 1958 J. Geophys. Res., 63, 717.
- Webber, W.R. 1962 J. Geophys. Res., 67, 5091.
- Weeks, L.H., and  
Smith, L.G. 1968 J. Geophys. Res., 73, 4835.
- Weeks, K., and  
Stuart, R.D. 1952a Proc. Inst. Elec. Engrs., 99, 29.
- Weeks, K., and  
Stuart, R.D. 1952b Proc. Inst. Elec. Engrs., 99, 38.
- Whitten, R.C., and  
Poppoff, I.G. 1962 J. Geophys. Res., 67, 1183.

- Whitten, R.C., and  
Poppoff, I.G. 1965 Physics of the Lower Ionosphere,  
Prentice Hall Inc. N.J.
- Wildman, P.J.L.,  
Kerley, M.J.,  
Edmonds, R.S., and  
Berming, N.F. 1969 J. Atmos. Terr. Phys., 31, 951.
- Wood, R.M., and  
D'Orazio, L.A. 1965 J. Phys. Chem., 69, 2562.
- Yasuda, J. 1963 J. Radio Res. Labs. (Japan), 10, 213.
- Young, J.M.,  
Corruthers, G.R.,  
Helm, H.C.,  
Johnson, C.Y., and  
Patterson, N.P. 1968 Science, 160, 990.
- Zagulayayeva, V.A.,  
Martynova, K.V.,  
Prilezhayeva, N.A., and  
Fatkullin, M.N. 1967 Geomagn. Aeron., 7, 813.